IDENTIFICATION OF PROTEIN MARKERS OF DRUG-INDUCED NEPHROTOXICITY BY MALDI MS: IN VIVO DISCOVERY OF UBIQUITIN-T

BY

KRISTEN HERRING

Dissertation

Submitted to the Faculty of the

Graduate School of Vanderbilt University

in partial fulfillment of the requirements

for the degree of

DOCTOR OF PHILOSOPHY

In

Biochemistry

May, 2009

Nashville, Tennessee

Approved:

Professor Richard M. Caprioli
Professor Richard Armstrong
Professor Billy Hudson
Professor Daniel Liebler
Professor Lawrence Marnett

-To those who dare to dream

Faithful is he who has called you and he will do it.

I Thess 5:24

This work is dedicated to my parents who always told me I could do it.

ACKNOWLEDGEMENTS

This has been quite a journey for me and it would not have been possible without the support and guidance from so many people. First I would like to thank my advisor Dr. Richard Caprioli for allowing me the opportunity to work in his laboratory and grow both as a scientist and an individual. Thanks also to my committee members Drs. Richard Armstrong, Dan Liebler, Larry Marnett, and Billy Hudson for their assistance and patience as I found my way as well as encouraging me to meet the challenge set before me. I am especially grateful for the guidance given by Dr. Hudson whether as an idea or just an encouraging word.

To the members of the Caprioli lab and Mass Spectrometry Research Center both past and current, thank you for your support and assistance through the years. I would like to think that we did more than collaborate on great science-some great friendships were built as well. You have given me countless hilarious stories to recount, as I am sure I have added a few to your collection as well. I can't thank you enough for your support in my various extracurricular activities. Hopefully I have inspired you to get involved in some way in your local community.

I must thank a few people who were instrumental in accomplishing the work presented herein. Dr. Kristin Burnum for her assistance in the initial ubiquitin cleavage experiments, Sara Frappier and Dr. Joey Latham for their assistance with the animal dosing, Dr. Junhai Yang for the synthesis of fluorescent ubiquitin, Salisha Hill and Dr. David Friedman for assistance with the MS/MS fragmentation of Ub-t, Shawn at the Vanderbilt Imaging Core for his assistance with the fluorescence experiments, Dr. Shannon Cornett for his assistance with image processing, Dr. Deming Mi for his

assistance with the statistical analysis, and all members of the lab who contributed any data they had with m/z 8451 in it. This work truly would not have been possible without you. I must also acknowledge funding support from GM58008-09 and DOD W81XWH-05-1-0179.

While at Vanderbilt I have met some amazing people. Thank you so much to my classmates Drs. Omari Bandele and Karissa McCall-Culbreath as well as future Drs. Kenneth Martin and Randolph Roberts. We all came in together, struggled together, bonded together, celebrated together, and though we will not leave together I know we will always maintain contact. I don't know if I could have made it through IGP without you. Thanks for being such great teachers!

To my family, thank you for supporting and believing in me even when it seemed as though I didn't believe in myself. I am deeply appreciative for the sacrifices you have made and I hope that I have made you proud, not only in my academic accomplishments but in the person I have become.

TABLE OF CONTENTS

LIST OF TABLES

Table Page

LIST OF FIGURES

Figure Page

TECHNOLOGICAL ABBREVIATIONS

HPLC, high performance liquid chromatography

MALDI, Matrix Assisted Laser Desorption Ionization

MS, Mass Spectrometry

OCT, Optimum cutting temperature

SA, sinapinic acid

CHCA, α-cyano-4-hydroxycinnamic acid

DHB, dihydroxybenzoic acid

H&E, hematoxylin and eosin

TLC, thin layer chromatography

RP-LC, reversed-phase liquid chromatography

ACN, acetonitrile

ESI, electrospray ionization

FT-ICR, Fourier Transform Ion Cyclotron Resonance

SAM, Significance Analysis of Microarrays

FDR, False Discovery Rate

LCQ, Linear capacity trap

PBS, Phosphate buffered saline

BIOLOGICAL ABBREVATIONS

ATP, Adenosine Triphosphate

APF-1, ATP-dependent Proteolysis Factor 1

UBIP, ubiquitous immunopoietic polypeptide

CATB, cathepsin B

CATL, cathepsin L

NAG, N-acetly glucosaminidase

GGT, γ-glutamyl transferase

BUN, blood urea nitrogen

ccRCC, clear cell renal cell carcinoma

Ub-t, Ubiquitin-t

CHAPTER I

INTRODUCTION

Overview

This chapter will introduce the drug discovery process as well as the pitfalls associated with it. Techniques employed to address biological problems associated with drug discovery are introduced with an emphasis placed on proteomics. In particular, direct tissue MALDI MS is described as well as sample preparation methods associated with this technique. Finally, an overview of the work contained in this thesis is presented.

Drug Discovery

The drug discovery process is a laborious task for the researcher and an expensive endeavor for the pharmaceutical industry. It has been proposed that it can take up to 15 years and $800 million to see a drug from bench to bedside [1]. Continued development of drug candidates tends to bottleneck at the pre-clinical or clinical trial stage because a molecule can behave differently *in vivo* than it does *in vitro*. Possible side effects of drugs are not seen until they are introduced into a living organism. It is here that toxicity becomes a problem. Kidneys are particularly susceptible to toxins because of their role in filtering the blood. Monitored indicators of nephrotoxicity, such as changes in serum creatinine levels or cellular morphology, often are not detected until the onset of toxic nephropathy [2]. Nephrotoxcity will be further discussed in chapter II. If mechanisms

of toxicity were more thoroughly understood, then more precautions could be taken at the front end of the process thereby saving time and money. Several 'omics techniques have been used to assess effects of drug treatment, thereby shedding insight into mechanisms of toxicity. Biological changes associated with drug treatment can be monitored at the genomic (DNA and mRNA expression profiling), proteomic (protein profiling in tissues and surrounding biofluids) and metabolomic levels (monitoring endogenous metabolites in tissues and surrounding biofluids). The differences in the strategies have been described as examining what could happen (genomics), what is happening (proteomics) and what has happened (metabonomics) [3]. To truly ascertain and understand what is causing the toxicity, it is important to know what is happening. For this reason the work in this thesis utilized proteomics techniques to assess toxicity.

Proteomic Techniques

Proteomics has the advantage of utilizing various techniques in a high-throughput manner to identify a protein and its function. One of the most commonly used methods involves 2D gels. Tissue or cell extracts are separated first by their isoelectric point and then further separated by molecular weight on a 1D gel. A spot corresponding to the protein of interest is then excised and digested with an enzyme, typically trypsin, and then analyzed by mass spectrometry to identify the protein. Quantification can be done in this same manner with the aid of fluorescent cyanine dyes known as Cy3 and Cy5 [4]. Two protein extracts are labeled with the dyes, mixed and then run on the same gel. The difference in the intensity of the corresponding dyes as determined by fluorescence can be visualized and the relative amounts of proteins determined in a process called 2D-

difference gel electrophoresis (DIGE). There are several limitations associated with this technology including sensitivity and types of proteins visualized. Typically the most abundant proteins are indentified in this type of analysis [5]. Additionally, if the protein of interest does not enter the gel (insoluable or larger molecular weight proteins) or easily exits the gel as is the case with smaller molecular weight proteins, identification will not be achieved [6].

Multidimensional liquid separation techniques coupled to mass spectrometry are also used to identify proteins in a biological system. This process is termed multidimensional protein identification technology (MudPIT) [7]. In MudPIT analysis extracts are first enzymatically digested and then separated based on hydrophobicity or charge on a packed column followed by on-line mass spectrometry analysis. Quantification can be done with the use of isotopically labeled standards or reagents [8, 9]. This technique referred to as "shot-gun analysis," attempts to identify everything in a sample without any separation prior to digestion. This then can become a limitation if the protein of interest is not abundant enough to generate peptides to get a confident identification.

A limitation of both techniques is the need for homogenization and extensive sample preparation. The spatial integrity of the tissue as well as any corresponding information is lost with these methods. Great insight can be gained by not only knowing the identification of a protein but the localization as well. Direct tissue analysis by MALDI MS allows for the investigation of disease while maintaining the spatial integrity of the tissue with minimal sample preparation. This technique is described further below.

Direct Tissue Analysis by MALDI MS

Background

MALDI MS, introduced in the late 1980s [10, 11], has become an enabling analytical technology to study proteins in biological systems because of its molecular specificity and high-throughput capabilities [12, 13]**.** One of the more recent developments to this technology is its application to direct tissue analysis for both molecular profiling and imaging [14]. The technology allows for the analysis of molecules in tissues without the need for target specific reagents such as antibodies or the need for tissue homogenization, thereby maintaining the integrity of the tissue sample and allowing assessment of molecular spatial distribution.

The principles of MALDI MS have been described [15-19]. In brief, the analyte of interest is mixed with an energy absorbing compound (matrix) on a MALDI target plate. As the solvent evaporates, the analyte co-crystallizes with the matrix. Inside the mass spectrometer, molecules are desorbed from the sample by irradiation with a UV laser. In this process, analytes become protonated and primarily give rise to $[M+H]^+$ ions that are subsequently measured according to their mass-to-charge (*m/z*). Typically, the time-of-flight analyzers are employed to measure m/z of ions **(Figure 2).**

MALDI MS can be used to profile molecules in a tissue section. This refers to the process of analyzing a small number of discrete spots deposited throughout the sample. Additionally it can be used to image a sample, or systematically raster across a tissue section to produce an ordered array of spots. In the latter, the laser performs a raster over the tissue surface in a pre-defined two-dimensional array or grid, generating a

full mass spectrum at each grid coordinate. Mass spectra acquired in this manner typically display ions in the m/z range of 500 to over 100,000, corresponding to many hundreds of different molecules present in the tissue. The coordinates of the irradiated spots are used to generate two-dimensional ion density maps, or images, that represent individual m/z values with their corresponding intensities **(Figure 3).** Likewise, drug analysis in tissue can be accomplished by monitoring the protonated drug or its metabolites and their corresponding fragments, at each discrete coordinate of such an array.

Direct tissue analysis by MALDI MS has been used to detect drugs and their metabolites [20-24] intact proteins and peptides [25-27] and recently phospholipids [28] directly from tissue. Profiling/imaging MS has been used to study molecular aspects of cancer, providing tumor-specific markers as well as diagnostic and prognostic-specific markers [29, 30]. With regards to the kidney, our laboratory has applied profiling/imaging methodologies to glomerulosclerosis [31], clear cell renal cell carcinoma [32] and drug-induced renal toxicity [33].

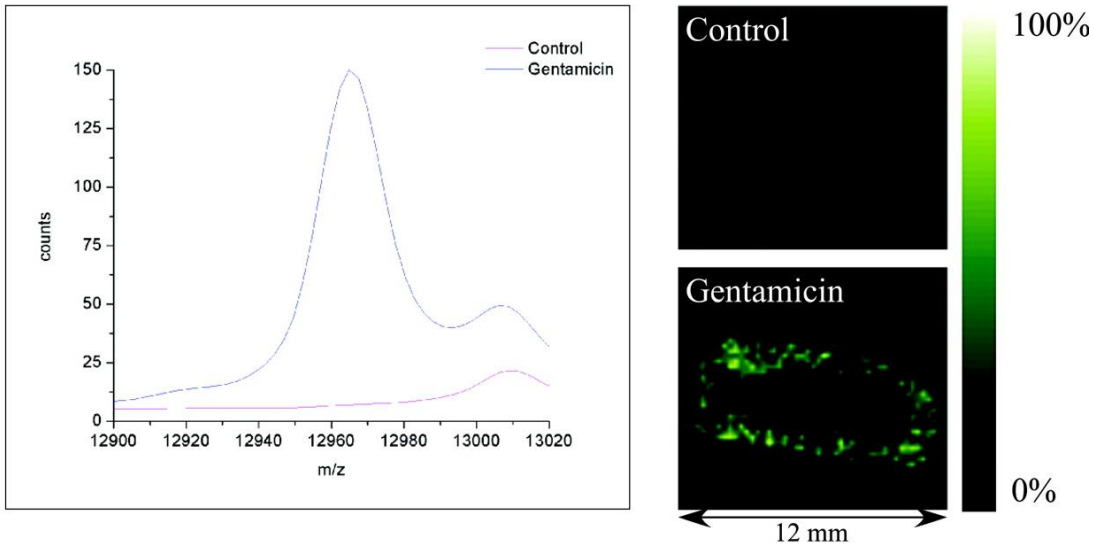

Figure 1. Transthyretin as a marker of gentamicin nephrotoxicity. Rats were dosed with gentamicin once daily for seven days, sacrificed and their kidneys excised. Differential protein expression was compared between control and dosed kidneys using IMS. This figure shows the image analysis of m/z 12959 differentially expressed in the cortex of dosed tissue with corresponding average peaks in the spectrum. Figure adapted from [33] with permission.

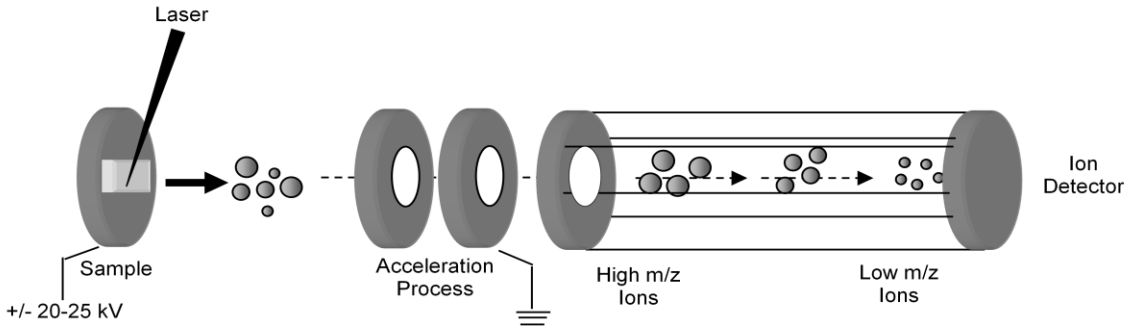

Figure 2. MALDI-TOF Schematic. A sample is irradiated with a brief laser pulse and molecules are desorbed from the surface. Energy is absorbed by the matrix and transferred to the analyte, which becomes protonated and is then accelerated down a field free drift tube. Ions collide with a detector at the end of this tube and their time-of-flight is measured and converted to a mass-to-charge ratio (m/z). Figure adapted from [32]

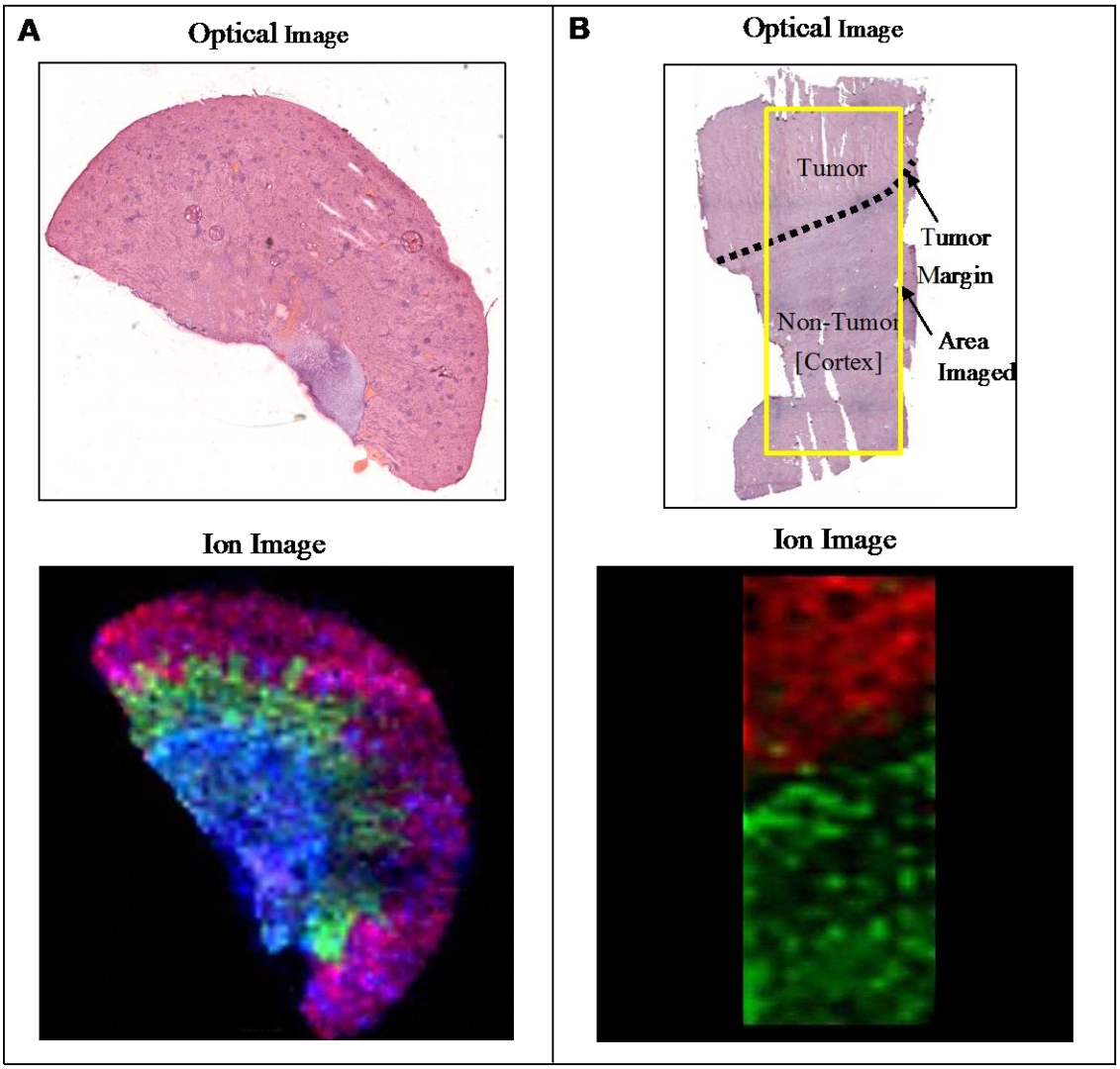

Figure 3. Images generated by Imaging MALDI MS. **A)** Optical hematoxylin and eosin stained (top) and overlaid ion images (bottom) of a normal rat kidney section. Shown are three ions given false color to show localization (pink: m/z 8451 in the cortex, green: m/z 8565 in the outer medulla, blue: m/z 4965 localized primarily in the inner medulla). **B)** Optical hematoxylin and eosin stained (top) and ion images (bottom) of a human clear cell renal cell carcinoma tissue section with tumor and adjacent non-tumor tissue. Shown are two overlaid ions represented by false color (red: m/z 4965 localized to tumor, green: m/z 6592 in non-tumor cortex). Figure reprinted with permission from [32]

S*ample Preparation for Profiling and Imaging Tissues by MS*

Direct MS analysis is usually performed on tissues that have been excised and immediately frozen in liquid nitrogen in order to maintain tissue morphology and minimize molecular degradation. Maintaining the integrity of the tissue throughout this process maximizes the information obtained in the analyses by ensuring that the original three-dimensional structure is not compromised and the molecular species monitored have not been altered as a result of the sample procurement and preparation process.

Typically, analysis is performed on frozen tissue although workflow has been developed for formalin fixed paraffin embedded samples [34, 35] and ethanol preserved specimens [36]. Tissues are sectioned in a cryostat, if necessary, using a small amount of optimum cutting temperature (OCT) media on the cutting block and for anchoring support. Preferably, tissue should not be embedded in the polymer media as surface contamination with polymer caused by the cutting process tends to reduce ionization efficiency. A cryostat temperature of between -15 ^{o}C to -25 ^{o}C is generally optimal for sectioning kidney tissue. Sections are generally cut at 12 µm thickness but may range between 10-20 µm depending on the application [13, 21]. After cutting, sections are thaw-mounted onto a MALDI target plate and/or washed or allowed to dry in a vacuum desiccator.

It is advantageous to wash tissue sections that are rich in salts and other contaminants as well as hemoglobin prior to matrix deposition because these species can contribute to a high spectral baseline and generalized signal suppression. Because of the kidney's role in filtration of blood, washing kidney sections removes excess hemoglobin and salts and enhances signal quality. The conventional tissue washing method involves

two separate 70% ethanol submersions for 20-30s followed by 10-15s in 95% 200-proof ethanol (or 100% reagent grade ethanol). Ethanol is a known tissue fixative in histology [37] and delocalization of proteins appears not to be significant; however it is noted that proteins soluble in these aqueous solutions may be removed during the washing step. Previous studies have indicated minimal protein loss during this process, but the washing procedure should be confirmed for each tissue type [38, 39].

Selection of the matrix/solvent combination for direct tissue analysis depends on the molecular weight, hydrophobicity, and salt content of the analyte. Typically, 3,5-dimethoxy-4-hydroxycinnamic acid (sinapinic acid, SA) is favorable for proteins (MW > 2 kDa), and α-cyano-4-hydroxycinnamic acid (CHCA) is optimal for peptides (500-2000 Da). Small molecule analysis, including drugs and lipids, is usually performed with 2,5-dihydroxybenzoic acid (DHB). The optimal matrix concentration range is 10-30mg/ml SA for protein analysis and 10-20 mg/ml CHCA for peptide analysis. The usual matrix solvent is 50% acetonitrile (ACN) with 0.1% trifluoroacetic acid (TFA). More nonpolar solvents such as methanol or isopropanol can be used for more hydrophobic matrices. The optimal matrix/solvent combination may vary between tissue types and analytes and must be assessed for each study.

Various methods of matrix deposition on thin tissue sections have been successfully employed. For tissue profiling, matrix can be manually deposited either with a pipette or pulled glass capillary. Syringe pumps provide an alternative, more automated approach with higher reproducibility and smaller matrix spot diameters. Robotic deposition offers superior reproducibility, smaller matrix spot diameters and a higher throughput platform, and also allows for the ability to perform histology-directed

analyses [40] and imaging. Two types of robotic devices, an acoustic spotter [38] and a chemical inkjet printer [41], have been successfully utilized for tissue profiling and imaging. General matrix deposition guidelines for both robotic types have been described [38, 41] but for each tissue type, method optimization is recommended to determine the number of matrix drops and passes required to obtain high quality spectra. In some cases matrix seeding may be desired to aid in the crystallization process [38]. The current minimum spot-to-spot spacing achievable with commercial robotic spotters is in the range of 100-200 μm. For applications that require a resolution higher than 150 μm, spray coating may be used. A spray coating device may be as simple as a glass thin layer chromatography (TLC) spray nebulizer that generates and sprays fine droplets of matrix under slight positive pressure, or automated spray devices. The matrix solution must wet the tissue surface to ensure co-crystal formation between matrix and analyte. For manual spraying methods, a one minute delay between passes provides sufficient drying time. Multiple passes are necessary to coat the entire tissue, but over-coating can suppress analyte signal. The matrix coverage can be monitored as necessary under a microscope. Specific matrix conditions used in this research will be outlined in the corresponding experimental methods section.

Histology Directed MS Analysis

Region specificity is important for analysis of heterogeneous tissue types such as kidney. One MALDI compatible method to accomplish this is to stain tissues using cresyl violet stain or other suitable stains (H&E stains give poor MS results), allowing histology and MS analysis to be performed on the same tissue section with minimal

interference in signal quality [42]. This method usually requires that tissue sections be applied to a conductive glass slide to obtain histo-pathological detail. A new method, histology-directed MS analysis, utilizes digital imaging to merge traditional histopathology, or hematoxylin and eosin tissue staining, with tissue profiling **(Figure 4).** Details of this methodology have been reported [40]. In brief, areas of interest on a stained tissue section are selected for MS analysis. The coordinates of these areas are transferred to a robotic matrix spotter and then to the mass spectrometer. This allows the profiles and other data processing algorithms such as statistical analysis, to be directly linked to the histological image and subsequently links the molecular profiles and histopathology.

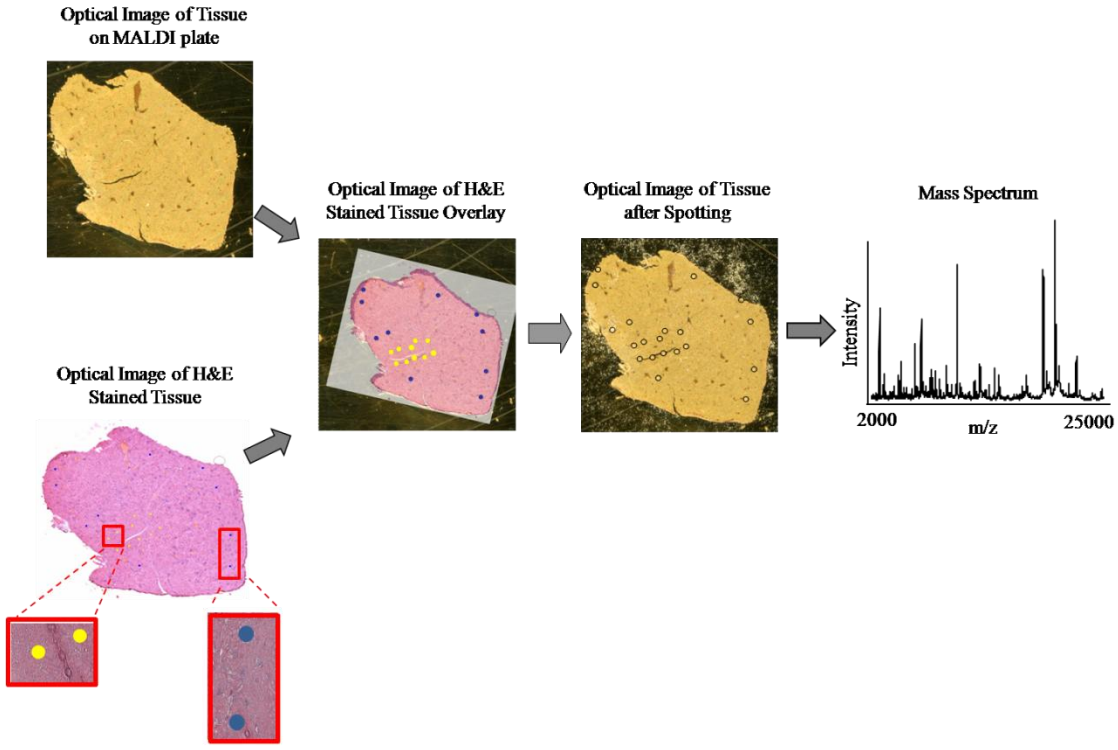

Figure 4. Histology-directed MS sample preparation for tissue analysis. A pathologist or researcher systematically selects discrete cellular areas (spots) of interest on a stained tissue section. The coordinates of the spots are transferred to the robotic spotter for matrix deposition on a co-registered serial section with subsequent laser irradiation of these spots (outlined in black for visualization) to give mass spectra. Figure reprinted with permission from [32].

MS Analysis

The mass spectral acquisition methods used in direct tissue analysis are performed in an automated fashion. When profiling or imaging discrete matrix spots, mass spectra are obtained by performing a raster over the area of interest on the tissue. The number of spectra obtained and averaged from a single spot on tissue depends on how many shots are needed to produce a spectrum having a high signal-to-noise. Most experiments sum between 250 and 500 spectra on a single spot about 150 um in diameter whereas data acquired from spray coated samples will acquire fewer spectra at a single position.

Spectral pre-processing is carried out on the acquired data to reduce inter- and intra-experimental variance. Such variations may be produced from the ionization process, background noise, and calibration offsets that result from biological or sample preparation differences. Mass spectra are processed by removing background noise, normalizing intensities, and performing a final mass realignment utilizing common peaks found in the spectra. The latter is primarily used for profiling experiments in which multiple sample groups are being compared, enhancing the efficacy of statistical analyses for determining biological patterns and changes in these patterns. Generally, imaging applications utilize background subtraction and normalization to significantly enhance the image quality. Illustrations of these processes have been presented [43].

Data Analysis

The large, complex datasets produced by these experiments require robust bioinformatics tools to assess spectral patterns and decipher molecular species that differentiate one group of samples from another. MS data from each group are

compared, to determine spectral features (peaks) that are significantly different between the two subject groups. The experimental design and biostatistical methods utilized are critical to the success of such analyses. Many of the algorithms used to decipher the vast amount of proteomic information were initially employed for genomic microarray experiments and have been adapted for proteomic dataset analyses [44-47]. The work presented herein utilized the Significance Analysis of Microarrays (SAM). The SAM statistic utilizes feature specific t-tests to determine the relationship between that feature's expression and the experimental conditions, expressed as a response variable. Multiple permutations are performed to assay the relationship between the two. This type of analysis is beneficial in that it does not make parametric assumptions about the data (Tuscher 2001). The algorithm estimates the rate of the median number of features falsely assigned as significant as a false discovery rate.

Protein Identification

Identification of statistically relevant mass spectral peaks is necessary to gain insight into biological processes. There are two approaches to protein identification. The top-down approach involves ionization and gas phase fragmentation of intact purified proteins of interest in the mass spectrometer. The bottom-up approach utilizes MS to identify peptides obtained from protease digestion of that protein, often in a mixture of other proteolytic fragments. The resulting mass spectra are searched against theoretical protein/peptide databases for corresponding sequence patterns. Searches are performed using conventional algorithms such as MASCOT and Sequest, [48, 49]. When possible, manual validation of reported identifications is recommended to reduce false positives.

Commonly, the bottom-up strategy is used due to its robustness. Many proteins are not amenable to intact fragmentation due to their size. The bottom-up strategy involves homogenization of the tissue followed by reversed-phase liquid chromatography (RP-LC) separation, where the eluate is continuously collected into fractions. Fractions are vacuumed to dryness, dissolved in 40% acetonitrile with 0.1% TFA, spotted onto a MALDI plate and analyzed for the fractions containing the peptides of interest. Based on the complexity of the fraction, one can enzymatically digest the entire fraction or further separate the mixture by one dimensional gel electrophoresis followed by excision and enzymatic digestion of the band of interest. Peptides are then subjected to further separation and fragmentation by RP-LC-tandem MS analysis and subsequent database searches.

Research Objectives

The use of antibiotics to treat gram negative bacterial infections is greatly hampered due to their propensity to exert damage on the kidney. Currently, this damage is detected by techniques that lack the sensitivity and specificity needed to be useful in clinical settings. Therefore, there is a need for a wider range of markers as well as those that will serve as early indicators of damage. Recently, direct tissue MALDI MS was used to identify transthyretin as a marker of gentamicin induced nephrotoxicity [33]. Direct tissue MALDI MS analysis is a valuable tool to differentiate various disease states. Its use to detect early protein markers of drug toxicity is explored in chapter II of this thesis.

Upon analysis of the various protein markers identified as indicators of damage, we discovered a modified form of ubiquitin. A truncated, desGG form of ubiquitin was found to be decreased as a result of drug treatment. Further exploration of this protein led us to discover that this modification was originally thought to be an experimental aritifact [50]. The history of the discovery of ubiquitin and this product is discussed further in chapter III. To further characterize and explore the nature of this modified ubiquitin we performed analyses to determine the enzyme responsible for the truncation, to examine the effect of our sample handling on presence of this protein, and to determine if this truncation occurred *in vivo*. We concluded that cathepsin B, a lysosomal protease, removed the C-terminal glycines of ubiquitin *in vivo*. The realization that desGG ubiquitin, or ubiquitin-t, is formed in vivo by cathepsin B was a unexpected and lead us to examine the localization of this protein across various tissues as well as explore its utility in differentiating another disease system with altered cathepsin B activity, cancer. This work as well as preliminary work towards understanding the origin and function of ubiquitin-t is presented in chapter IV of this thesis. Chapter V provides conclusions as well as insights into where this research is headed.

CHAPTER II

PROTEIN MARKERS OF ANTIBIOTIC INDUCED NEPHROTOXICITY

Introduction

Aminoglycoside antibiotics are commonly used to treat gram negative bacterial infections. Their use has been severely limited due to their propensity to damage the kidney. The kidney consists of two major areas: cortex and medulla. It is through these areas that millions of nephrons, the functional unit of the kidney, traverse. The cortex consists of the glomerulus, which has a 70KDa filter, as well as the proximal and distal tubules which function to concentrate and reabsorb the glomerular filtrate. The medulla is comprised of the descending and ascending loop of Henley which functions to reabsorb water and Na+ respectively, as well as the collecting duct which is the last component of the nephron and functions to collect urine. Because of the kidney's role in filtering the blood, it is particularly susceptible to damage by antibiotics as well as other drugs. Though the drugs are known to accumulate in and damage proximal tubules, the specific mechanism responsible for this toxicity has remained elusive.

Though several mechanisms of toxicity have been postulated, a commonly accepted mechanism of toxicity by antibiotics is lysosomal injury [51]. Olbricht and colleagues microdissected out segments of the proximal tubule and analyzed lysosomal protease activity following gentamicin treatment. They found that drug treatment actually led to a decrease in cathepsin B and L activity in the S1 and S2 segments [52]. In fact, current biochemical methods to detect antibiotic induced nephrotoxicity exploit

this premise of lysosomal injury being the mechanism of toxicity by measuring the levels of N-acetyl glucosaminidase (NAG), a lysosomal enzyme [53-55]. Levels of γ-glutamyl transferase (GGT), a brush border enzyme, are also used to assess damage because both of these enzymes are excreted into the lumen of the tubules when damage occurs [56]. These analyses are optimal for clinical settings since they involve non-invasive, urine analysis. The problem with these assays is that there can be other causes for the change in enzyme activity [57]. There is also great intra- and inter-individual variation in urine volume and excretion of these enzymes [58].

Nephrotoxicity is also assessed histopathologically. Once damage has occurred, the tissue morphology changes and is evident by swelling of the proximal tubules as well as large lysosomes [59]. Serum creatinine and Blood Urea Nitrogen (BUN) levels are used as indicators as well. Creatinine is a protein produced by muscle therefore it is relatively stable so the clearance of this protein per minute can be used to assess kidney function. BUN measures the amount of nitrogen that comes from urea, a waste product from the breaking down of proteins. These assays are limited in that they are not very sensitive. One will only see morphological, serum creatinine, and BUN changes after ~2/3 of the nephron is damaged [2]. Ideally, one would want an early indicator of nephroxicity or at the very least a wider range of protein markers.

Recently, research efforts have been focused on this goal. Though genes have been identified that are not only related to toxicity but could potentially be predictive of damage [60, 61], proteomics offers a unique opportunity to identify protein markers of nephrotoxocity and to indicate molecular processes involved in tissue damage. Charlwood et al. identified twenty proteins as markers of gentamicin nephroticity with

the use of 1D and 2D gels. These proteins were either involved in the citric acid cycle, gluconeogenesis, fatty acid synthesis, or stress response [62]. A protein thought to be involved in the activation of complement was identified as a potential early marker of gentamicin nephrotoxicity [63]. Numerous other studies have started to use proteomics to obtain biomarkers of toxicity. This topic is more thoroughly reviewed in [64]. More specifically, Meisterman et al. demonstrated the utility of direct tissue analysis by MALDI mass spectrometry for the identification of protein markers of gentamicin nephrotoxicity. They identified transthyretin as a marker of damage and were also able to generate an image of this protein showing that it localized to the cortex of the kidney, the major site of damage [33]. The work presented in this chapter is a continuation of this project.

MALDI mass spectrometry offers a valuable resource to not only identify protein markers of disease but to shed insight into mechanisms of drug toxicity. By examining the differential expression of proteins between treated and untreated tissues, the extensive networks to which they belong can be elucidated in what is known as expression proteomics [65]. This approach builds upon the notion that once one knows which/how proteins change between disease states, a hypothesis can be drawn and tested through functional analyses to get back to the fundamental mechanisms of the disease.

This work aimed to detect and characterize early protein markers of antibiotic induced nephrotoxicity through direct tissue profiling using MALDI MS. This would provide a robust and high throughput method to detect toxicity in early leads.

Methods

Animal studies. All animal studies were performed at Roche Center for Medical Genomics at F. Hoffman-La Roche Ltd. in Basel Switzerland. 12 week old male Wistar rats (300g), five animals per group, were dosed subcutaneously with a single dose or once daily for 7 days as noted in the Table 1 with kanamycin (80 mg/kg or 400 mg/kg) or gentamicin (6.25 mg/kg, 25 mg/kg, or 100 mg/kg) (Sigma; dissolved in saline) or vehicle. Animals were sacrificed 24 hours after the last dose by CO_2 inhalation.

Sample Preparation. Kidney samples were cut into 12 μm thick sagittal sections using a cryostat. Serial sections were cut and stained with H&E for histology directed matrix deposition [40] and subsequently photographed. On these images, ten virtual 200 μm spots were placed each in the cortex and medulla using Photoshop. After overlaying these spots onto the optical image of the MALDI target plate, their coordinates were then transferred to an Automated Reagent Multispotter (Labcyte Inc., Sunnyvale, CA). Using those coordinates, sections were spotted with sinapinic acid (20 mg/mL in 50:50 acetonitrile: water, 0.1% TFA) after an ethanol wash (70%, 90%, 100% reagent grade) and seeding with a fine powder of sinapinic acid [38].

Mass Spectrometry Analysis. Samples were analyzed in duplicate. Spectra were collected on a Bruker AutoFlex mass spectrometer in linear mode equipped with a Smartbeam laser operated at 100Hz. The spatial localization of the features was confirmed using imaging mass spectrometry at 250 μm resolution. 200 shots per spot were averaged for each spectrum in the profiling and imaging experiments. Spectra were

preprocessed using ProTS Software (Biodesix, Inc) and images visualized using BioMap (Novartis).

Statistical Analysis. Twenty spectra from each area (cortex and medulla) for each animal were averaged after visual inspection of the data to ensure that all zero data were excluded. The average spectra from each animal were generated into a feature table using ProTS Marker (Biodesix, Inc.). A Significance Analysis of Microarrays (SAM) (Tuscher 2001) was performed comparing control to low dose, low dose to high dose, and control to high dose for kanamycin and the same for gentamicin treated samples with the addition of a mid dose comparison at 24 hours and 8 days. For this study features that were found significant with a fewer than 10% false discovery rate were recorded.

Protein Identification. Tissue samples were homogenized by manual mincing with Tissue Protein Extraction Reagent (T-PER) extraction buffer (Pierce) according to manufacturers recommendation while on ice. Extracts were briefly sonicated with an electronic emulsifier (Branson Sonifier). Samples were then centrifuged for 5 min at 10,000xg and the supernatant collected and used for all further analysis.

Proteins were then identified by one of three ways as described in the chart **(Figure 5).** The tissue homogenate was separated on a Vydac C4 column by HPLC using a linear acetonitrile gradient from 2-95%. Fractions (0.5ml) were collected in a 96-well plate and then vacuumed to dryness in a Speedvac. Samples were resuspended in 20 µl 40% ACN/0.1% TFA and spotted on a MALDI target to identify the fraction of interest. Once that fraction was determined, the sample was **1)** subjected to an in solution digest

with trypsin (Promega) or LysC (Fisher), dried down and then resuspended in 2% ACN/0.1% FA followed by MS/MS analysis on a Bruker UltraFlex or LCQ or **2)** subjected further separated on a 10-20% Tricine Gel (Novex). The corresponding band was cut and digested with the aforementioned enzymes. Peptides were extracted with 60% ACN/0.1% formic acid (FA), dried down and resuspended in 2% ACN/0.1% FA, and then subjected to MS/MS analysis on the Bruker UltraFlex or LCQ. **3)** The tissue homogenate was run on a Tricine gel and the band of interest excised and digested with an enzyme followed by the previously described workflow.

ESI generated spectra were submitted to the TransProteomic Pipeline where they were searched against a SwissProt rat International Protein database. TOF-TOF spectra were processed with Flex Analysis (Bruker) and submitted to MASCOT where they were searched against the Swiss Prot database.

Identification of truncated ubiquitin. Rat kidney cortex homogenates were subjected to GluC digestion. First, homogenates were separated on a C_4 RP column by HPLC into a 96 well plate and vacuumed to dryness using a SpeedVac. Samples were reconstituted in 20 µl 40%ACN:water 0.1% TFA and manually spotted onto a MALDI target where they were mixed 1:1 with SA. The fraction containing m/z 8451 was determined by MALDI-TOF, dried down and resuspended in 25 µl of 100mM ammonium bicarbonate. The sample was reduced with 50mM DTT and alkylated with iotaacetamide. GluC (2 ul of 1 µg/µl) and digest at 37^{o}C for 16 hrs. The reaction was stopped with 0.1% formic acid (FA). The sample was vacuumed to dryness again and resuspended in 25 µl 0.1%FA. MS/MS analysis was performed on a Thermo LTQ linear ion trap, and the

resulting MS and MS/MS data searched against an International Protein Index (IPI) rat database using SEQUEST.

Kanamycin Study

Dose (mg/kg/day)	Time point
control	24 hrs
80	24 hrs
400	24 hrs
Control	8 days
80	8 days
400	8 days

N=5 each group

Gentamicin Study

Dose (mg/kg/day)	Time Point
Control	24 hrs
6.25	24 hrs
25	24 hrs
100	24 hrs
control	8 days
6.25	8 days
25	8 days
100	8 days

N=5 each group

Table 1. Outline of drug dosing.

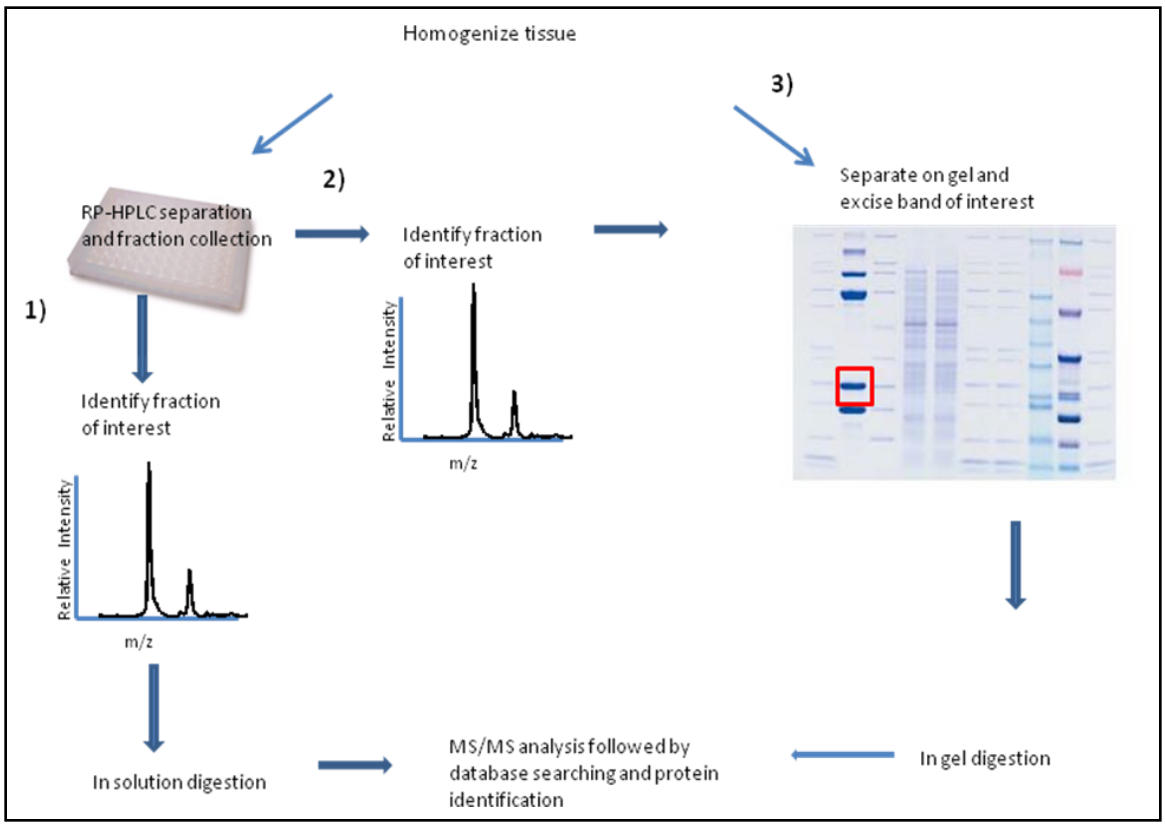

Figure 5. Protein ID Schematic. Tissue is mechanically homogenized and separated using reverse phase HPLC. Fraction of interest is determined by MALDI MS and either **1)** subjected to an in-solution digest or **2)** further separated on a 1D gel where an in-gel digest is performed. Alternatively, the tissue homogenate is **3)** separated on a 1D gel, band of interest excised and digested. All peptides were sequenced using MS/MS analysis and searched against a database.

Results and Discussion

The use of aminoglycosides such as gentamicin and kanamycin in treatment against gram negative bacterial infections has been greatly limited due to their propensity for damage to the kidney. To provide additional markers for this damage, animals were given a low or non-toxic dose of the drugs as well as a high toxic dose to evaluate the proteomic differences between the doses. As reported, treatment with these drugs results in damage to the proximal tubules [66] as is evident in the H&E stained slide (**Figure 6).**

Direct tissue profiling revealed vast changes in the proteome in response to gentamicin and kanamycin treatment with the most drastic changes occurring in the cortex of the chronic dosed animals **(Figures 7 and 8).** Since these drugs are cortical toxicants, these data are in agreement with the known localization of damage for these xenobiotics. The finding that there are proteomic changes in the medulla, as evident by the differences in intensity of several features as a result of drug treatment **(Figures 7 and 8)** is surprising since the drugs are thought to primarily damage the cortex. These data suggest a more comprehensive interplay between the drugs and the kidney. The data illustrates the effect of duration and concentration of the drugs on the kidney proteome. The longer and higher the dose of both drugs, the greater the observed effect on features observed in the MALDI spectra.

The first objective of the study was to identify early markers of toxicity. For this purpose, an early marker was defined as a feature that exhibited significant changes as early as 24hrs after a low dose of either kanamycin or gentamicin. Using these guidelines, one protein, lysozyme, was identified as an early marker of kanamycin toxicity **(Figure 9).** This protein is a lysosomal protease that was originally used as a

urinary marker of proximal tubule damage but it was found to lack the sensitivity needed to reliably diagnosis damage making it unsuitable for analysis [67-69]. Lysozyme was not determined as an early marker of gentamicin toxicity, though it was identified as showing differential expression as a result of chronic gentamicin treatment. These results suggest that lysozyme could be a viable marker for kanamycin toxicity *in situ*. Using the aforementioned constraints, analysis of gentamicin treated samples did not lead to the discovery of any early markers.

Though the initial aim of the study was to determine early markers of toxicity, proteins that exhibited differential expression as a result of maximum dosage or chronic drug treatment were investigated. These features were termed "general markers" of toxicity and the results from are illustrated in **Tables 2-7.** An important observation to note is the abundance of features that are decreased in the cortex of chronic dosed animals. This underscores the biological and morphological changes in the tissue. Interestingly, we did detect significant changes in features in the medulla as a result of drug treatment. One feature m/z 4508 was decreased as a result of a single mid-dose of gentamicin whereas 17 features were decreased as a result of an eight day regiment of gentamicin treatment **(Table 4).** These features included m/z 8039, 9977, 3477, 15202, 15411, 16155, 5484, 7576, 3432, 7598, 9937, 7700, 8253, 9717, 12436, 7931, and 8364. Three features, m/z 7616, 15197, and 15153 were significantly increased after a single high dose of kanamycin when compared to a lower mid-dose **(Table 7)**. Two features m/z 6104 and 8450 were significantly decreased after a chronic high dose of kanamycin compared to control animals **(Table 7).** This finding suggests that although these drugs

exert their primary damage on the cortex, there are some secondary effects in the medulla.

There were several features that were differentially expressed 24 hr post a high dose of both gentamicin and kanamycin that corresponded to changes observed after a chronic 8 day dosing. Eight features from the gentamicin study were identified that fit this criterion. They were m/z 17583, 8450, 6030, 4988, 8040, 9978, 15826, and 8927 (**Tables 2 and 3)**. Six features from the kanamycin study were identified that fit this criterion. They were m/z 14853, 8791, 17389, 12563, 8040, and 7842 **(Tables 5 and 6)**.

Only one feature, m/z 17583, displayed a consistent significant decrease with a lower dose of gentamicin as compared to the high dose at 24hr **(Table 2).** In a comparison of 8 day dosed samples 22 features displayed a consistent significant decrease across all doses of gentamicin **(Table 3)**. They were m/z 12344, 5485, 5903, 6030, 8040, 9665, 8365, 12132, 9978, 14005, 6663, 8123, 6178, 8450, 10260, 15828, 10812, 15202, 9326, 4923, 7576 and 7598.

Performing a corresponding analysis with the kanamycin treated samples demonstrated two features in common between the comparison of control to low dose and control to high dose samples at 24 hrs post dose: m/z 14853 and 7444 **(Table 5).** But a comparison between low dose to high dose and control to high dose samples yielded seven features in common (m/z 12563, 7922, 7929, 15855, 5904, 8040, and 10280) **(Table 5)**. Comparing features identified as significant in the 8 day chronic dosed gave similar results. Though no features were common between all of the doses, 47 features were in common between a comparison between low dose to high dose and control to high dose. These were m/z 12957, 14853, 17323, 3832, 17263, 17388, 8659, 8791,

17582, 8848, 10201, 6030, 5406, 10183, 6867, 12294, 4989, 6049, 4463, 8040, 12131, 8927, 4182, 10143, 10495, 4225, 7106, 8365, 8450, 6104, 10365, 14212, 8123, 5485, 7883, 6178, 13468, 5466, 6648, 7043, 9717, 9665, 4924, 14085, 10260, 12345, and 9938 **(Table 6).** These results suggest that the features in common could potentially be useful diagnosis tools due to their appearance at lower doses.

From this study twelve proteins were identified from the list of statistically significant features indicative of nephrotoxicity by methods previously described **(Table 8).** Eight of these proteins were found significant in both the gentamicin and kanamycin studies. Two of these proteins were increased in the cortex of drug treated samples, transthyretin and lysozyme **(Figure 10).** Lysozyme was discussed earlier in this chapter. Transthyretin, or prealbumin has been used as a marker of nutritional stress [70-72] and breast cancer [73]. It was recently identified as a marker of gentamicin nephrotoxicity [33]. This work extends this identification to kanamycin nephrotoxicity as well. Interestingly, lysozyme and transthyretin (TTR) are both ligands of the megalin receptor [74, 75]. Megalin is also the receptor for the aminoglycosides gentamicin and kanamycin [76, 77]. These data suggest that these drugs preferentially bind to megalin, thereby preventing uptake and release of lysozyme and TTR into the bloodstream [33]. Additionally, three of the other proteins identified as markers of nephrotoxicity, cytochrome C, and hemoglobin α and β are also ligands of the megalin receptor [74, 78]. This work supports the hypothesis that treatment with a megalin antagonist would alleviate antibiotic induced nephrotoxicity. Recently, cytochrome C was demonstrated to inhibit gentamicin accumulation in the kidney cortex consequently preventing damage [79]. A more detailed description of megalin can be found in the fourth chapter.

Eight proteins were identified as having a statically significant decrease in the cortex of drug treated samples **(Figure 11).** Two of these are involved in energy production- ATP synthase coupling factor 6 and ATP synthase subunit epsilon. ATP synthase is a mitochondrial enzyme that is composed of two units [80]. The first unit, F_1, is the catalytic unit and is comprised of five other subunits, one of which is subunit epsilon. ATP synthase coupling factor 6 is associated with the second unit F_0, the energy transduction unit. The identification of ATP synthase subunit epsilon and coupling factor 6 as being decreased in response to drug treatment points towards the role of mitochondrial injury in nephrotoxicity. Investigators have shown that gentamicin impairs cellular energy production and inhibits mitochondrial phosphorylation [81, 82].

Two other proteins, cytochrome C and cytochrome C oxidase polypeptide Va are integral in apoptosis. Cytochrome C is released from mitochondria in response to pro-apoptotic stimuli. A decrease in these proteins points not only points to an impaired apoptotic mechanism which could potentially protect the kidney from damage, but this too suggests a role of mitochondrial injury in nephrotoxicity.

Macrophage inhibitory factor (MIF), a protein involved in regulating immunity was also decreased. Though MIF is constituitively expressed, it has been shown that MIF is increased in kidney diseases such as experimental and human glomerulonephritis and kidney transplant rejection [83-85]. We would expect that MIF would be increased with damage to the kidney. It was surprising to discover a decrease in this protein as a result of drug treatment. It is possible that aminoglycosides inhibit the release of MIF.

Hemoglobin α 1/2 and β were decreased as well. These proteins are involved in oxygen transport and lend credence to the role of oxidation in nephrotoxicity [86, 87].

Hemoglobin was recently identified as a urinary marker of nephrotoxicity [88]. It would follow that a decrease of hemoglobin in tissue is indicative of an increase in urine.

Our analysis resulted in the discovery of a C-terminal desGG ubiquitin. The formation of this protein is tryptic in nature, therefore trypsin was not used to digest the protein for identification. An alternate enzyme, Glu-C, was used to verify the sequence of Ub-t. The analysis yielded the confident ID of the C-terminal des-GG peptide of ubiquitin with an Xcorr=4.24 and 30/88 ions matched **(Figure 12)**. Despite this strong SEQUEST score, the algorithm did not identify the base peak of the spectrum, m/z 872.04 nor the next most intense peak m/z 992.43. However, this provided further confidence in the identification after manual inspection revealed these ions would account for the y_{22}^{+3} and y_{16}^{+2} fragment ions, respectively, which represent expected predominant cleavages due to the presence of aspartic acid and the sequestration of the mobile protons by basic arginine residues . To be more specific, the SEQUEST algorithm does not account for enhanced cleavage at specific amino acid residues such as aspartic acid, as observed in the **Fig. 12**. These cleavages are in agreement with the predicted cleavage sites as determined by the mobile proton model which states that peptide fragmentation requires a proton at the cleavage site. If that proton is sequestered, or bound by a basic amino acid side-chain, then energy will be required to mobilize that proton to the peptide backbone to induce fragmentation [89]. In the peptide of interest, cleavage at the aspartic acid residues is preferred because the mobile proton(s) are being sequestered by the arginine residues, thereby allowing the acidic side chain of aspartic acid to initiate cleavage. It has been established in the literature that this enhanced cleavage occurs only if the number of protons added to the peptide is less than or equal to

the number of arginines present [90]**.** This correlates well with the presence of two arginines in the y_{16}^{+2} peptide and three arginines in the y_{22}^{+3} peptide **(Figure 12)**.

Interestingly we found that desGG ubiquitin (Ub-t) was decreased in the cortex of drug treated samples **(Figure 13).** This was intriguing since it has been demonstrated that the C-terminal glycines are necessary for activation of ubiquitin and subsequent protein degradation [50]. Oxidatively modified proteins are degraded by the ubiquitin proteosome system. The observation that Ub-t, or inactive ubiquitin is decreased with drug treatment suggests the cells' role in combating oxidative damage due to the drugs [86, 87]. The finding that there was a modified form of ubiquitin was quite intriguing and one in which we decided to further explore. This work will be discussed in subsequent chapters.

In summary, we have used direct tissue MALDI MS to detect protein markers of antibiotic induced nephrotoxicity. One protein, lysozyme, was identified as an early marker of damage using the guidelines that a significant change was observed as early as 24 hours following a non-toxic dose. Adjusting the definition of an early marker to a feature that exhibits statistically significant changes as early as 24 hours post a toxic dose yielded eight features from the gentamicin treated samples and six from the kanamycin treated samples. Twenty two features were identified as general markers of gentamicin damage due to their statistical changes after 8 days of a toxic dose of the drug. Twenty-three features were identified as general markers of kanamycin damage due to their stastical changes after 8 days of a toxic dose of the drug. Ten proteins were identified as markers for both gentamicin and kanamycin damage. Among those identified were proteins that suggest the role of megalin, mitochondrial and lysosomal injury, as well as

oxidation in mediating toxicity. Interestingly a truncated form of ubiquitin was identified as a cortical marker of damage. This novel finding will be further explored in the next chapter. Taken together this work demonstrates the utility of direct tissue MALDI MS in detecting early markers of antibiotic induced nephrotoxicity. This data not only potentially supplements the known protein markers but can possibly shed insight into the mechanism of toxicity.

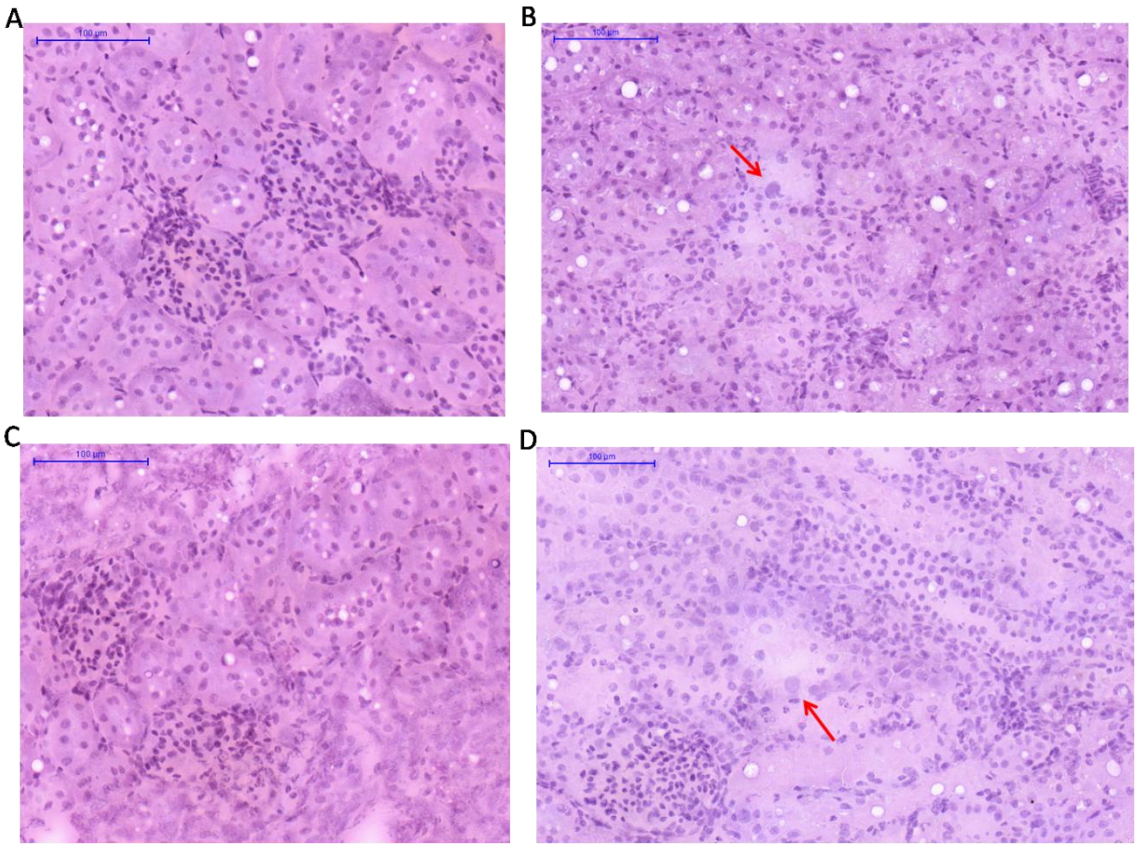

Figure 6. Histopathological analysis of gentamicin and kanamycin treated kidneys. Samples from control (A and C), 8 day 400 mg/kg kanamycin (B) and 100 mg/kg gentamicin treated samples. Proximal tubules are disrupted and cells are enlarged as indicated by arrows in drug treated samples. Scale bar=100µm

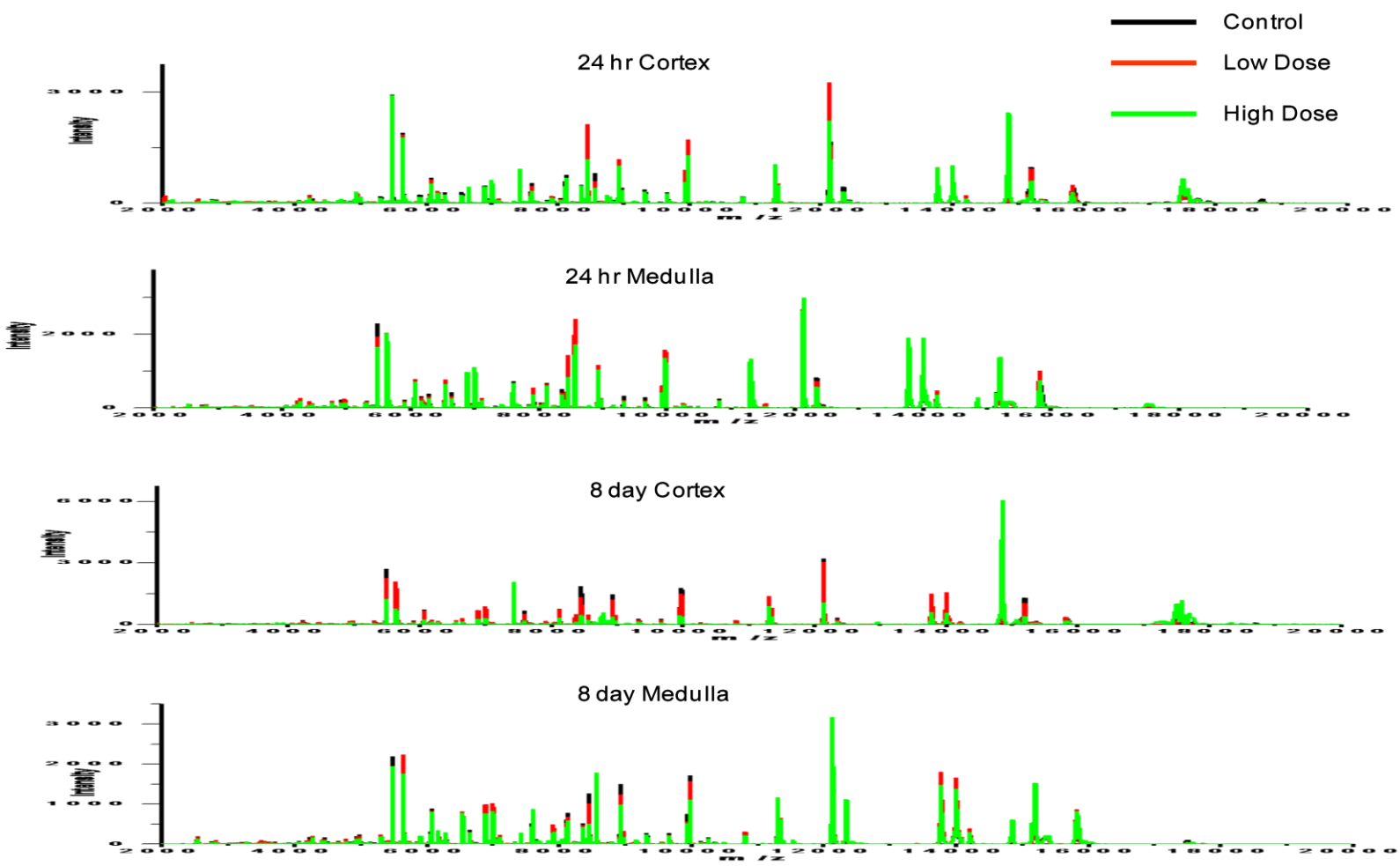

Figure 7. Protein profiles from kanamycin study. Average spectra (100) from each group were plotted from m/z 2000 to m/z 20000. A decrease in intensity of features is evident in the cortex of high dose treated animals as seen with a green line with the most dramatic decrease occurring after 8 days of treatment.

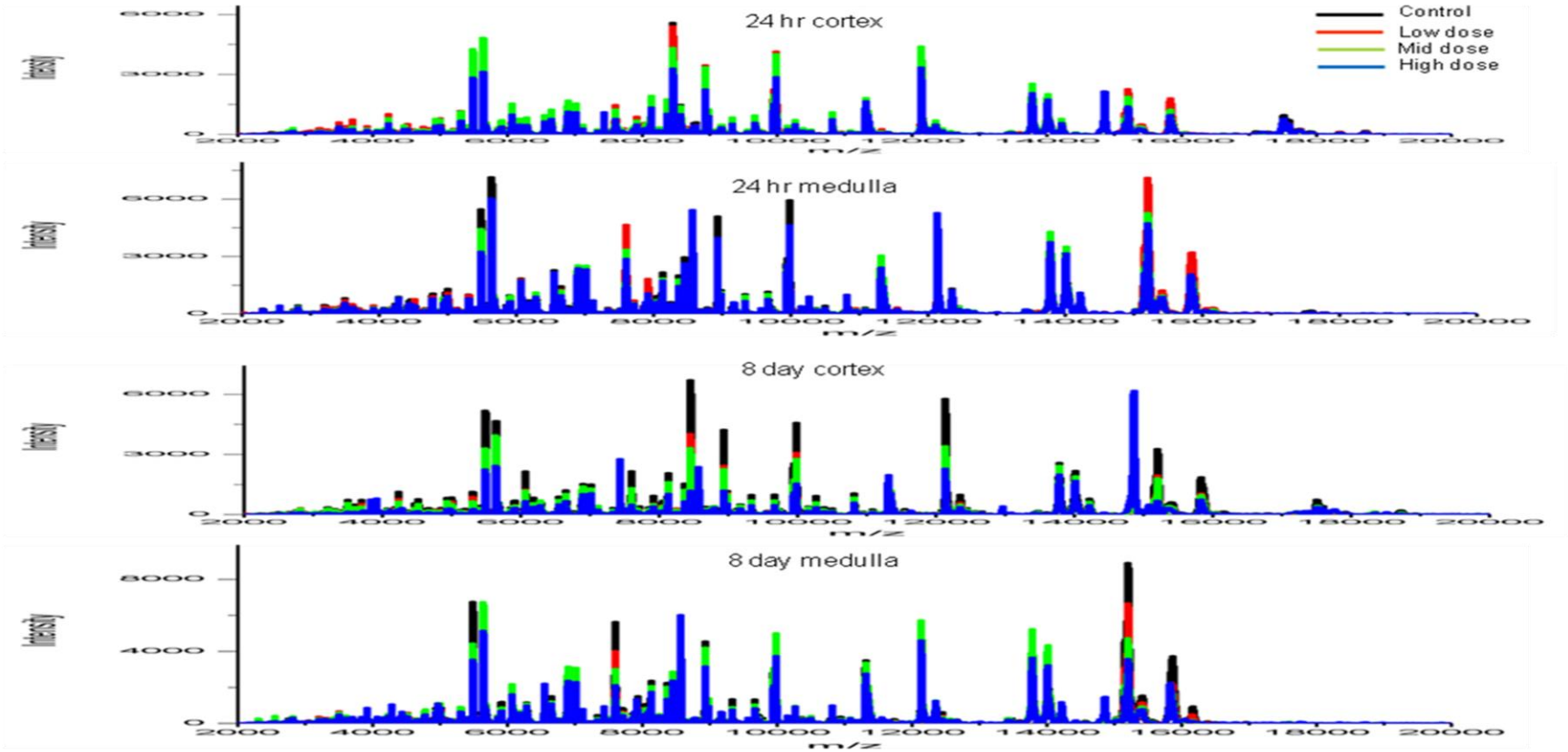

Figure 8. Protein profiles from gentamicin study. Average spectra (100) from each group were plotted from m/z 2000 to 20000. A decrease in intensity of features is evident in the cortex of high dose treated samples as indicated by a blue line. The most dramatic decrease is seen after 8 days of treatment.

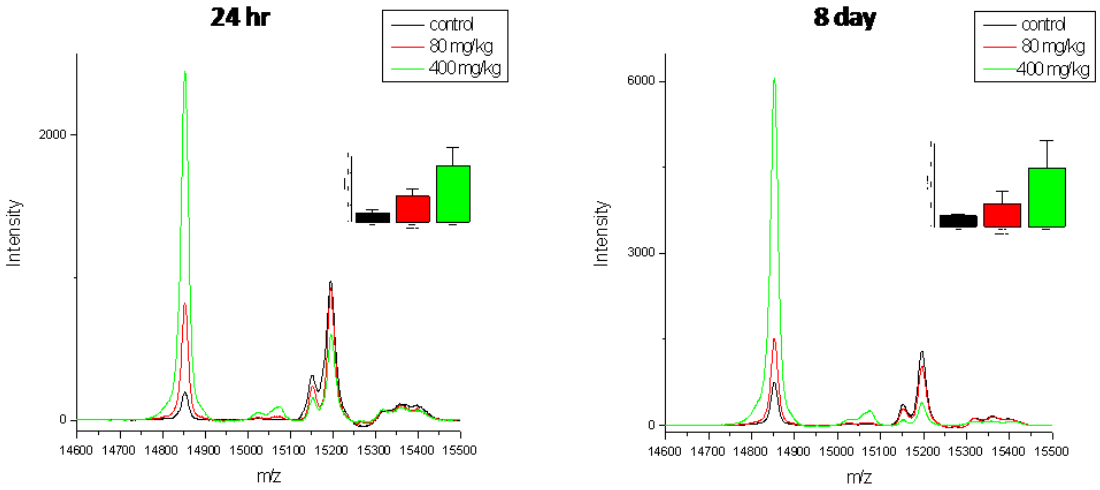

Figure 9. Lysozyme as an early marker of kanamycin toxicity. Average spectra from control, low and high dose animals after 24hrs and 8 days of kanamycin treatment. Intensity of peak at m/z 14860 shows a steady increase even after 24hrs with standard error in inset.

Table 2. Top differentially expressed features as determined by SAM comparing cortex of 24hr gentamicin treated tissue. Data is presented with respect to higher dosed tissue: black-up, red-down (ex. Control vs. low dose- Up in low dose/down in low dose). FDR <10%. N/A indicates there were no features identified that met the indicated criteria. LD-low dose; MD-mid dose; HD-high dose. Values listed in order of decreasing SAM score.

Control vs. LD	Control vs. MD		Control vs. HD	
n/a	6066	17583		17583
	12565			8661
	12132			8450
	8365			16038
	9169			6030
	15202			4988
	6887			9561
	4181			8040
	6275			5199
	5635			9978
	10143			17098
	10812			18723
	5405			5302
	6544			15826
	7598			5841
	12437			6065
	12655			11540
	10368			8927
	5302			9685
	15368			8564
	15409			17910
	9665			2415
	4923			9132
	6648			7930
	8323			
	8122			

Control vs. LD			
	13470		10812
	11306		4462
	6292		8040
	5903		8754
	17754		9665
	18721		9938
	8123		9168
	8254		11080
	8927		6178
	5200		10496
	5485		8365
	17504		9977
	7542		5635
	12343		5841
	3967		15828
	14005		7576
	17586		6663
	7330		5405
	10260		15202
	8564		10282
	13778		12437
	10369		8450
	4859		4923
	12132		6275
	5313		4181
	9326		7598
	12565		6030
	6065		14854
	13422		

Control vs. MD			
6048	8927		15828
	12344		15411
	5485		10812
	5903		15202
	6030		7930
	3292		9326
	8040		14214
	9665		10496
	8365		5841
	12132		4923
	5301		17504
	9978		9938
	4462		7576
	14005		3477
	6663		7598
	8564		6648
	4988		5635
	8123		4224
	6178		7513
	8450		7911
	10260		13778
	5405		

Control vs. HD			
3832	8365		7106
14854	4923		7576
17197	8123		10260
12958	6292		11080
	4988		12132
	8927		6648
	5485		6178
	5903		14214
	10812		8450
	9665		4224
	10369		15202
	6030		15411
	6663		7598
	12344		6544
	6275		9938
	8040		14005
	8970		17586
	7003		4748
	9978		15828
	9326		13778
	5635		9168
	5313		4331

Table 3. Top differentially expressed features as determined by SAM comparing cortex of 8 day gentamicin treated tissue. Data is presented with respect to higher dosed tissue: black-up, red-down (ex. Control vs. low dose- Up in low dose/down in low dose). FDR <10%. LD-low dose; MD-mid dose; HD-high dose. Values listed in order of decreasing SAM score.

Table 4. Top differentially expressed features as determined by SAM comparing medulla of A) 24hr and B) 8 day gentamicin treated tissue. Data is presented with respect to higher dosed tissue: black-up, red-down (ex. Control vs. low dose- Up in low dose/down in low dose). FDR <10%. N/A indicates there were no features identified that met the indicated criteria. LD-low dose; MD-mid dose; HD-high dose. Values listed in order of decreasing SAM score.

A)

Control vs. LD	Control vs. MD		Control vs. HD
n/a		4508	n/a

B)

Control vs. LD	Control vs. MD	Control vs. HD	
n/a	n/a	14854	8039
			9977
			3477
			15202
			15411
			16155
			5484
			7576
			3432
			7598
			9937
			7700
			8253
			9717
			12436
			7931
			8364

Control vs. LD	
14853	
7444	

LD vs. HD	
8735	9938
8756	12563
17582	5904
8791	8564
8781	7842
14853	12294
17501	7929
	10280
	8040
	15855
	14212
	7922
	15820
	12132
	10183
	7910
	13468
	11534
	10202
	6914
	6276
	6066
	8238
	11633

	7689
	8451
	10143
	10365
	10260
	15359
	14085
	9685
	9717
	6867
	15152
	10785
	6084
	15401
	15316
	11388
	9978
	15196
	7576
	4968
	8122
	7023

Control vs. HD	
14853	7922
7445	7929
7086	15855
8791	12563
8756	11539
17582	5904
4950	8040
17389	11552
	7842
	12087
	10281

Table 5. Top differentially expressed features as determined by SAM comparing cortex of 24hr kanamycin treated tissue. Data is presented with respect to higher dosed tissue: black-up, red-down (ex. Control vs. low dose- Up in low dose/down in low dose). FDR <10%. LD-low dose; HD-high dose. Values listed in order of decreasing SAM score.

Control vs. LD	
3612	
6084	
9540	

LD vs. HD			
12957	10201		5485
8736	6030		3492
17389	8238		7883
17263	5406		6178
17582	10183		13468
3832	6867		5466
8849	12294		4061
17323	4989		5636
8791	6049		5693
17692	6065		5302
17198	12169		6648
17501	9978		7043
15076	4463		9717
8756	8040		9665
8659	10311		14005
14853	5904		7015
	7842		4924
	12131		7023
	6293		14085
	8927		10260
	6084		12344
	4182		5313
	10143		2817
	10495		9938
	4225		6545
	7106		4282
	8365		6887
	8450		9168
	6104		13774
	10365		5674
	14212		6276
	8123		

Control vs. HD			
12957	6030		10143
17198	4635		4463
14853	9358		9717
17323	6867		10785
3832	10201		8927
17263	5485		5313
17388	5903		6048
7538	13468		4611
8659	12294		12343
8791	5466		7106
18340	9998		6178
17582	5406		7043
8848	8365		5302
	12131		4061
	8450		6327
	8040		10260
	9976		14212
	10183		3491
	6293		7598
	10811		12435
	7842		6914
	4663		5636
	10495		7701
	4182		7340
	4924		7910
	6104		10755
	5099		15196
	4832		7679
	9326		14085
	12563		3324
	4989		9938
	6648		7002
	4225		7883
	9665		4510
	5693		6895
	8123		4485
	10365		7576

Table 6. Top differentially expressed features as determined by SAM comparing cortex of 8 day kanamycin treated tissue. Data is presented with respect to higher dosed tissue: black-up, red-down (ex. Control vs. low dose- Up in low dose/down in low dose). FDR <10%. LD-low dose; HD-high dose. Values listed in order of decreasing SAM score.

Table 7. Top differentially expressed features as determined by SAM comparing medulla of A) 24 hr and B) 8 day kanamycin treated tissue. Data is presented with respect to higher dosed tissue: black-up, red-down (ex. Control vs. low dose- Up in low dose/down in low dose). FDR <10%. N/A indicates there were no features identified that met the indicated criteria. LD-low dose; HD-high dose. Values listed in order of decreasing SAM score.

A)

Control vs. LD	LD vs. HD		Control vs. HD
n/a	7616		n/a
	15197		
	15153		

B)

Control vs. LD	LD vs. HD	Control vs. HD
n/a	n/a	6104
		8450

m/z	Protein Name	TPP Score	# Peptides Seen	% Coverage	Gent.	Kana.
12960	transthyretin	1	4	59.1	+	+
14860	Lysozyme C type 1 precursor	1	5	42.6	+	+
11542	thioredoxin	1	2	21.2	+#	+#
15197	hemoglobin α 1/2	1	13	75.9	+	+
5636	ATP synthase subunit epsilon, mitochondrial	1	4	61.4	+	+
12346	Macrophage Inhibitory factor	1	2	28.1	+	+
12132	Cytochrome C somatic	*			+	+
12436	Cytochrome C oxidase polypeptide 5a	1	4	16.4		+
15851	hemoglobin β2	1	8	93.2		+#
8451	ubiquitin-t	^			+	+
8565	ubiquitin	1	1	11.6	+#	
8927	ATP synthase coupling factor 6	1	1	17.6	+	

Table 8. Markers identified from gentamicin and kanamycin studies. Proteins were found to be significantly increased (1st two listed) or decreased (others listed) after 8 days of gentamicin and kanamycin treatment except where noted. TPP- Transproteomic Pipeline; Gent.-protein found in gentamicin study; Kana.-protein found in kanamycin study; #- marker after 24hrs; *-protein identified previously in lab; ^-protein identified as described in text

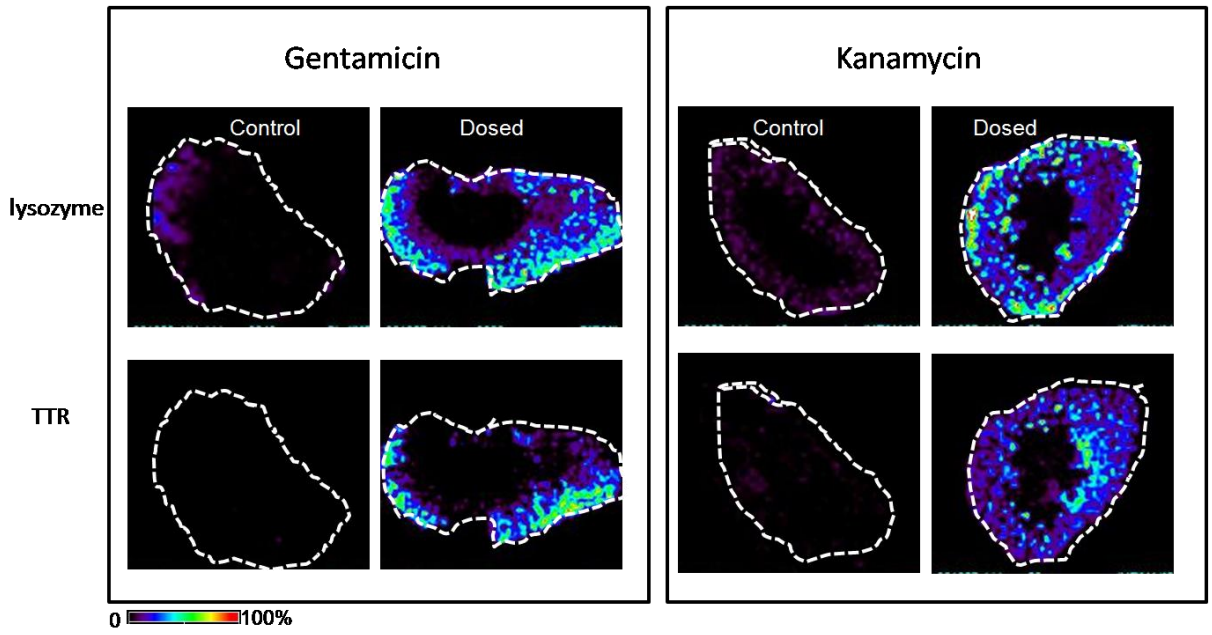

Figure 10. Images of proteins increased in the cortex with drug treatment. Images shown are kidneys from 8 day control and high dosed gentamicin and kanamycin treated animals. The localization of the indicated proteins is visualized as a heat map. Images acquired at 250 µm resolution.

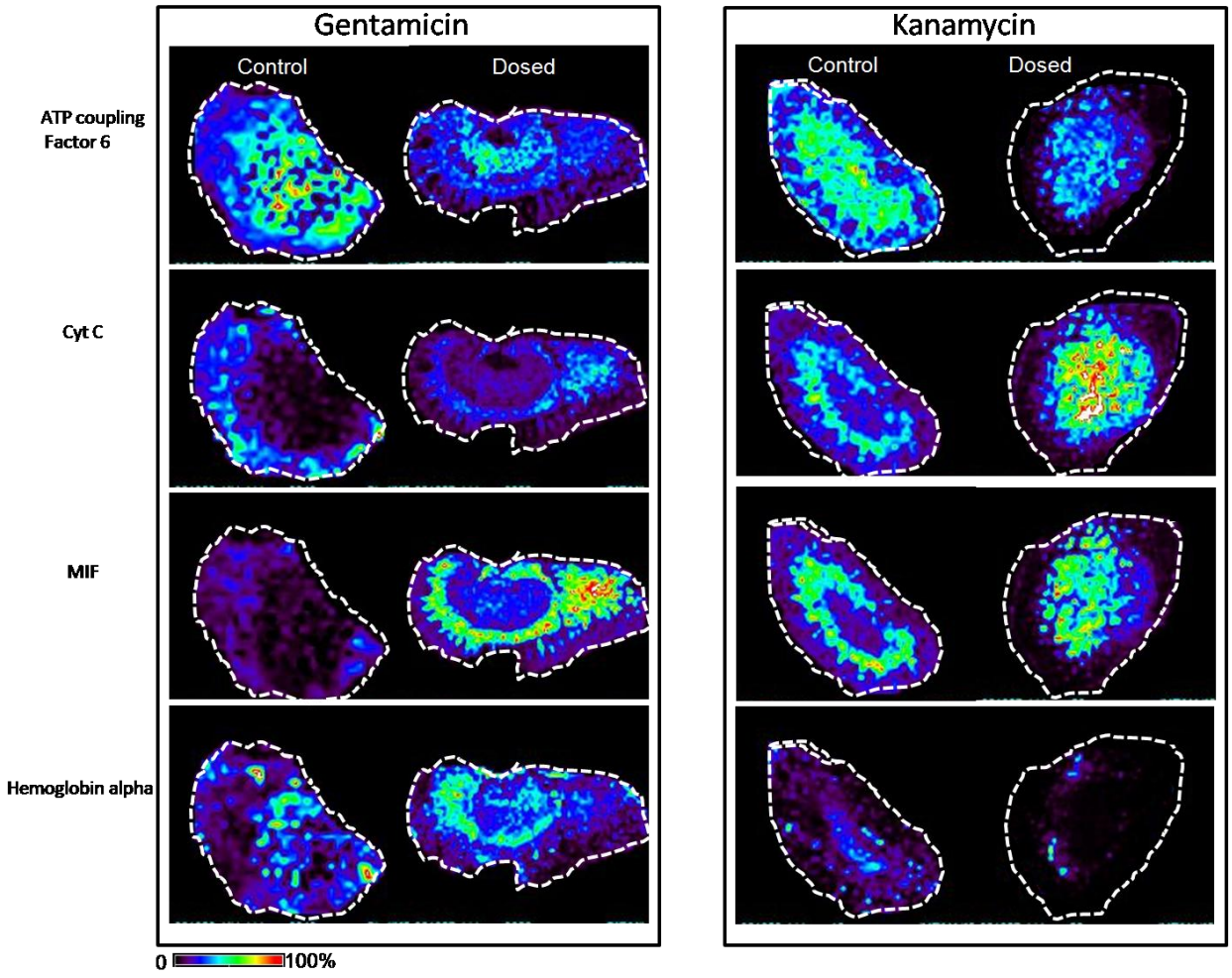

Figure 11. Images of proteins decreased in cortex with drug treatment. Images shown are kidneys from 8 day control and high dosed gentamicin and kanamycin treated animals. The localization of the indicated proteins is visualized as a heat map. Images acquired at 250 µm resolution.

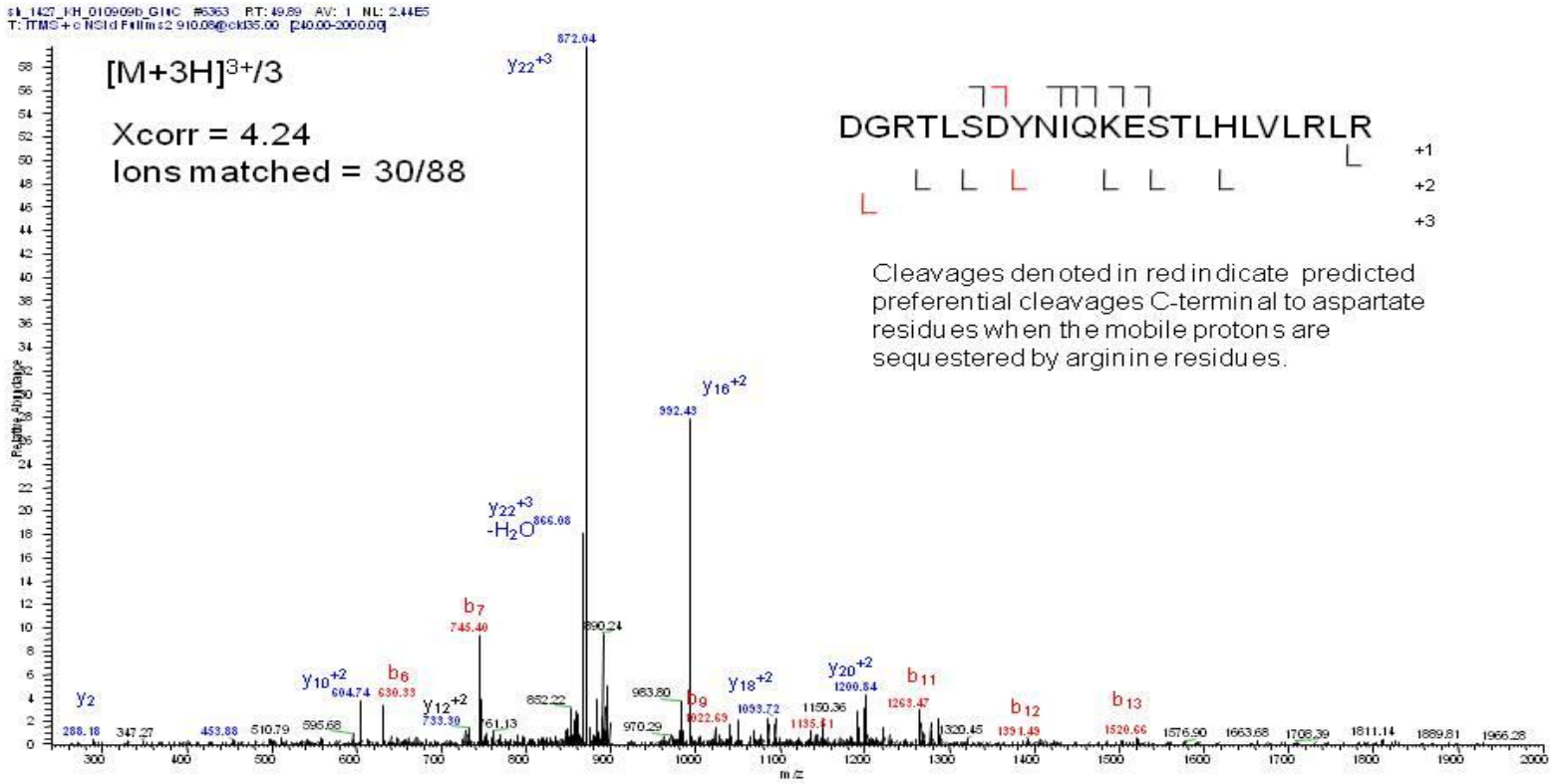

Figure 12. Identification of Ub-t. Samples were prepared as described in the text. Resulting MS/MS spectrum obtained from the triply charged peptide is displayed and annotated above.

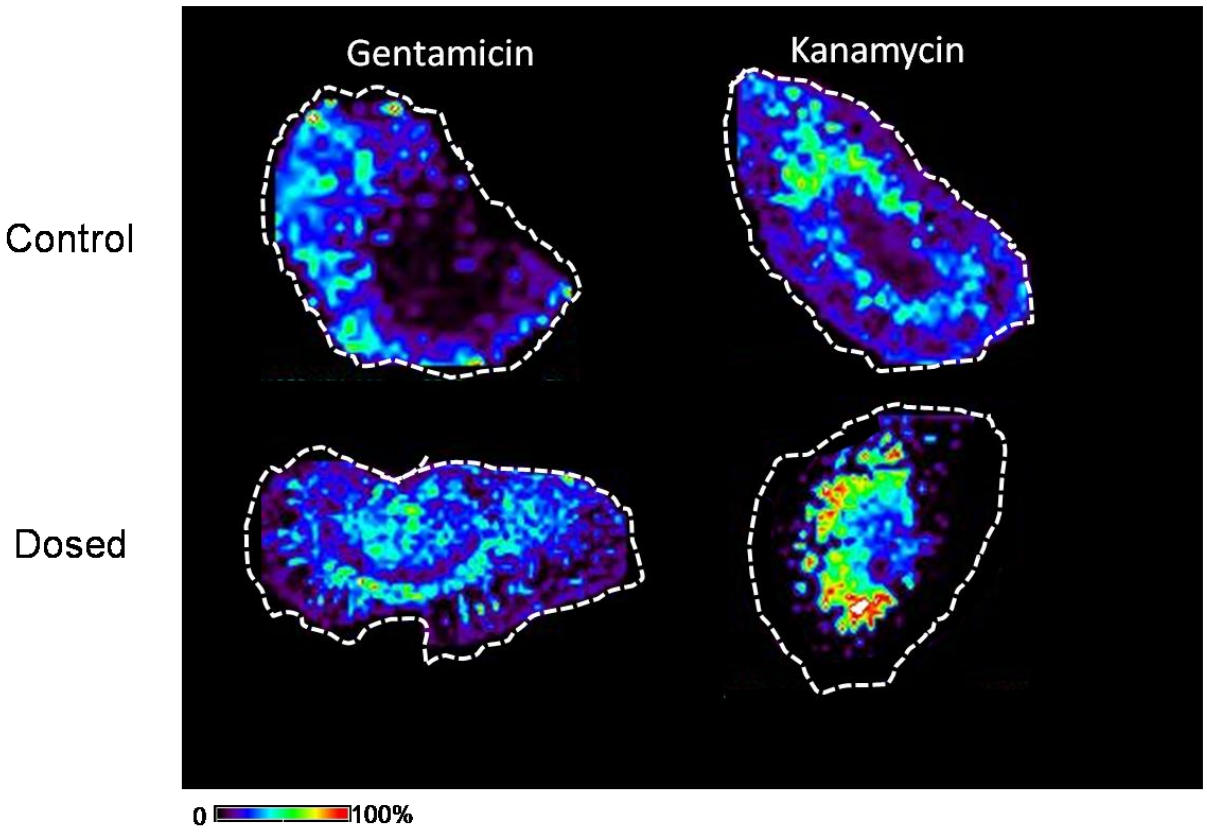

Figure 13. Localization of truncated ubiquitin as a result of antibiotic treatment. Images shown are kidneys from 8 day control and high dosed gentamicin and kanamycin treated animals. Localization of protein is visualized as a heat map. Images acquired at 250 µm resolution.

CHAPTER III

UBIQUITIN DISCOVERY AND FUNCTION

Overview

This chapter will chronicle the original discovery of ubiquitin from bovine thymus as a 74 amino acid protein and then its subsequent acceptance as a 76 amino acid protein involved in protein degradation. This chapter will provide the backdrop for the inquiry into the validation of in vivo expression of ubiquitin-t.

Ubiquitin Discovery

In 2004, the nobel prize for chemistry was awarded to Aaron Ciechanover, Avram Hershko, and Irwin Rose for the discovery of ubiquitin and the ubiquitin proteasome system. This discovery revolutionized the view the scientific community held with regards to intracellular proteolysis. It was originally proposed that protein degradation was mostly lysosomal, but several pieces of data started to suggest otherwise. Researchers could not explain the ATP requirement, varying half-lives of several proteins, nor insensitivity to several lysosomal inhibitors [91] involved in protein degradation. Then in 1977, the first cell-free proteolytic prep was obtained from rabbit reticulocytes [92]. This was pivotal because this extract was free of lysosomes yet still was able to degrade hemoglobin with the addition of ATP. Soon thereafter, Ciechanover and colleagues fractionated the reticulocyte crude extract into two fractions. It was in the

first fraction that the active component was purified and identified to be an 8.5kDa protein then termed ATP-dependent Proteolysis Factor 1, or APF-1 [93].

Concomitantly, a 74 amino acid protein of unknown function was purified during the isolation of thymopoeitin that had protein degradation activity [94]. It was found to be expressed in all cells and appeared to be involved in the immune response [95, 96]. Though this was later found to be incorrect [97], it was named ubiquitous immunopoietic polypeptide (UBIP) [95].

Soon thereafter, investigators began to suspect that APF-1 and ubiquitin were the same protein. Ciechanover et al. characterized APF-1 from reticulocytes and found that it had the same molecular weight as well as amino acid composition as ubiquitin[98]. In 1980 Wilkinson et al. demonstrated that ubiquitin was APF-1 [99].

At this point ubiquitin, a heat stable protein with an energy requirement for protein degradation, was accepted to be a 74 amino acid protein ending in arginine [96]. Then conflicting reports on the both the structure and activity of ubiquitin started to arise. Researchers were finding that some preparations of ubiquitin were unable to trigger proteolysis [99]. Sequencing of these samples led to the discovery that in some cases a short glyclglycine tag was attached to the end of ubiquitin [100]. This led to confusion as to the actual structure of the protein in question. It was known that the C-terminal glycines were necessary for protein degradation [100] but it was not clear as to the origin of the dipeptide. To complicate matters, Wilkinson found that not only did the samples with inactive ubiquitin have a completely different species in them as determined by HPLC but, that active ubiquitin could be converted to an inactive form with trypsin**.** Then in 1985, Arthur Haas and his colleagues made the discovery that ubiquitin actually

has 76 amino acids, including a C-terminal diglycine tail, that can be cleaved by an unnamed lysosomal protease [50]. This protease with trypsin-like specificity, but presumably a cathepsin-like enzyme because of its molecular weight and specificity, can become activated at acidic pH and released during homogenization, thereby cleaving the C-terminal glycine residues and effectively inactivating the protein**.** It was Haas' recommendation, and the accepted view in the field that this cleavage was an artifact of sample handling and that only the full 76 AA protein should be referred to as ubiquitin. The 74 amino acid cleavage product should be referred to as ubiquitin-t for truncated.

Ubiquitin Activity

The ubiquitination process is one that has been heavily studied and characterized. We now know that an E1 activating enzyme covalently attaches to Gly^{76} of ubiquitin, then ubiquitin is transferred to an E2 conjugating enzyme through a thioester bond, and finally an E3 ligase covalently attaches it to lysine residues in the target protein for degradation [101, 102]. Four or more ubiquitin moieties attached to Lys^{48} of ubiquitin signal for a target protein to be degraded by the proteosome [103]. The proteosome is a large protease consisting of a 20S catalytic core of four stacked rings where polyubiquitinated proteins are digested into peptides in a caspase, trypsin, and chymotrypsin-like manner [104]. The proteosome also has a 19S regulatory subunit that functions to recognize and allow polyubiquitinated proteins into the catalytic subunit [105, 106]. Important to note is that the proteasome releases free ubiquitin with the aid of deubiquitinases that recognize and cleave the isopeptide bond between Gly^{76} of ubiquitin

and the ε-NH_2 group of lysine on the target protein. In this sense, ubiquitination is a reversible post-translational modification, allowing for the recycling of free ubiquitin.

But, ubiquitination does not only signal proteosomal protein degradation. There are several alternative processes triggered by ubiquitin attachment. The various functions of ubiquitin modification are outlined in **Figure 14.** There is evidence that polyubiquitin chains constructed through Lys^{63} of ubiquitin are involved in activation of transcription factors [107] and could play a key role in regulating transcription as reviewed in Conaway et al [108]. It is now known that mono- and diubiquitination are involved in protein trafficking through receptor mediated endocytosis [109]. In this process, ubiquitinated membrane proteins are internalized, taken into early endosomes, and transported to multivesicular bodies which are then fused to lysosomes for degradation.

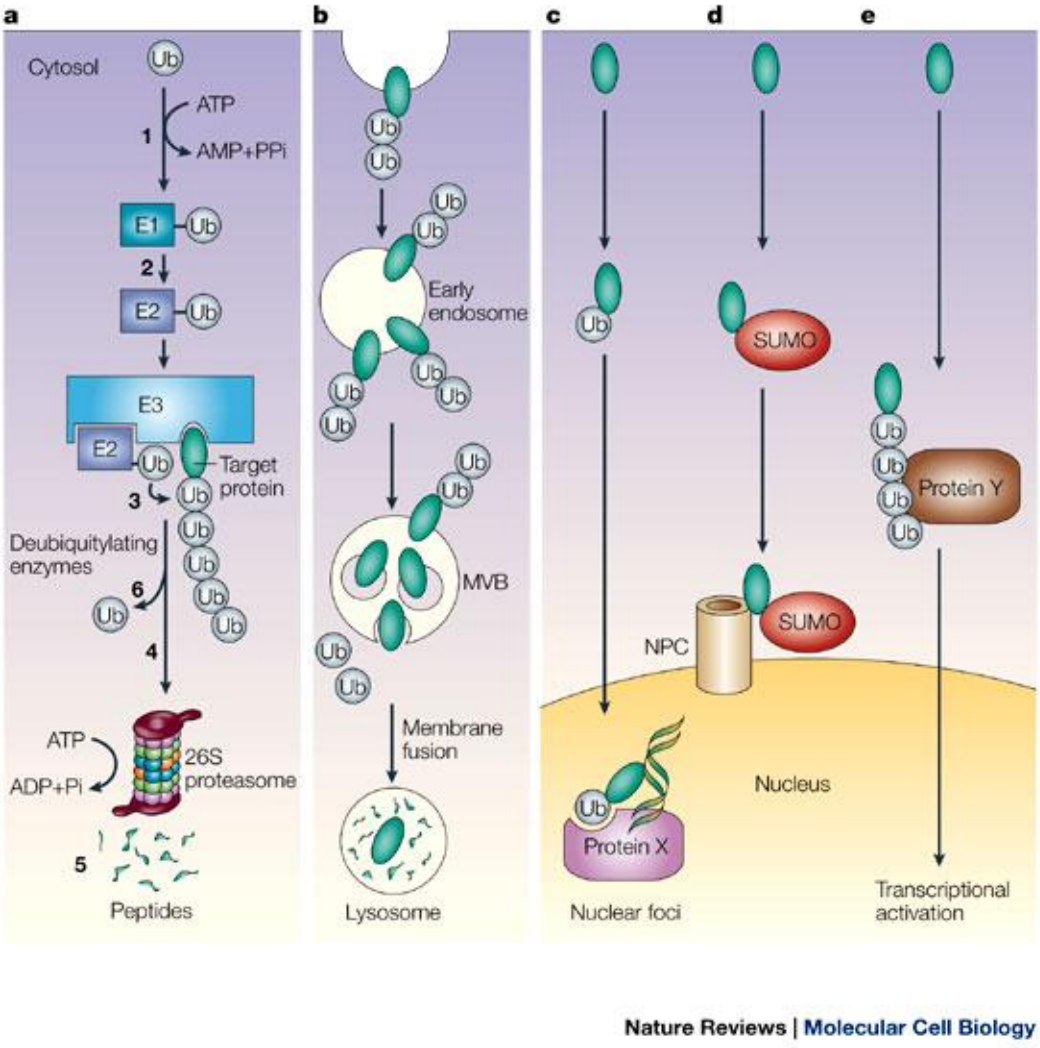

Figure 14. Schematic of the various functions of ubiquitin. A) Ub activation, conjugation and ligation to a target protein for degradation in the proteasome. **B)** Ubiquitin mediated endocytosis and trafficking of membrane proteins to the lysosome. **C)** Monoubiquitination targeting proteins to nuclear foci leading to signaling. **D)** Ubiquitin like proteins such as SUMO target proteins to the nuclear pore complex. **E)** Polyubiquitin through Lys63 leading to activation of transcription. Reprinted with permission from Macmillan Publishers Ltd: [91]

Lysosomal Proteolysis

The lysosome is an intracellular membranous organelle that contains various proteases that function optimally at an acidic pH. Proteins are targeted to the lysosome through receptor mediated endocytosis, pinocytosis, phagocytosis, and autophagy as described in **Figure 15** where they are cleaved by lysosomal cathepsins. Cathepsins can be divided into three groups: cysteine, the largest and best known, aspartic and serine hydrolases. There are 11 human cysteine cathepsins B, C, F, H, L, K, O, S, V, W, and X. Cathepsin D and E are aspartic hydrolase and cathepsins A and G are serine hydrolases. Most of these enzymes behave as endoproteinases with the exception of cathepsin B which can act as both an endo and exoproteinase [110]. A more detailed description of cathepsin B can be found in chapter IV. Though cathepsins exert most of their activity primarily in the lysosome, they can be secreted and act to digest extracellular proteins and membranes, something that has proved key in cancer progression [111-113].

Ubiquitin has a key role in two of the lysosomal trafficking mechanisms: receptor mediated endocytosis, discussed previously and autophagy. Autophagy is the process by which a cell degrades its own organelles. In this process a membrane termed an autophagic vacuole, surrounds ubiquitinated proteins and shuttles them to the late endosome and subsequently, the lysosome [114].

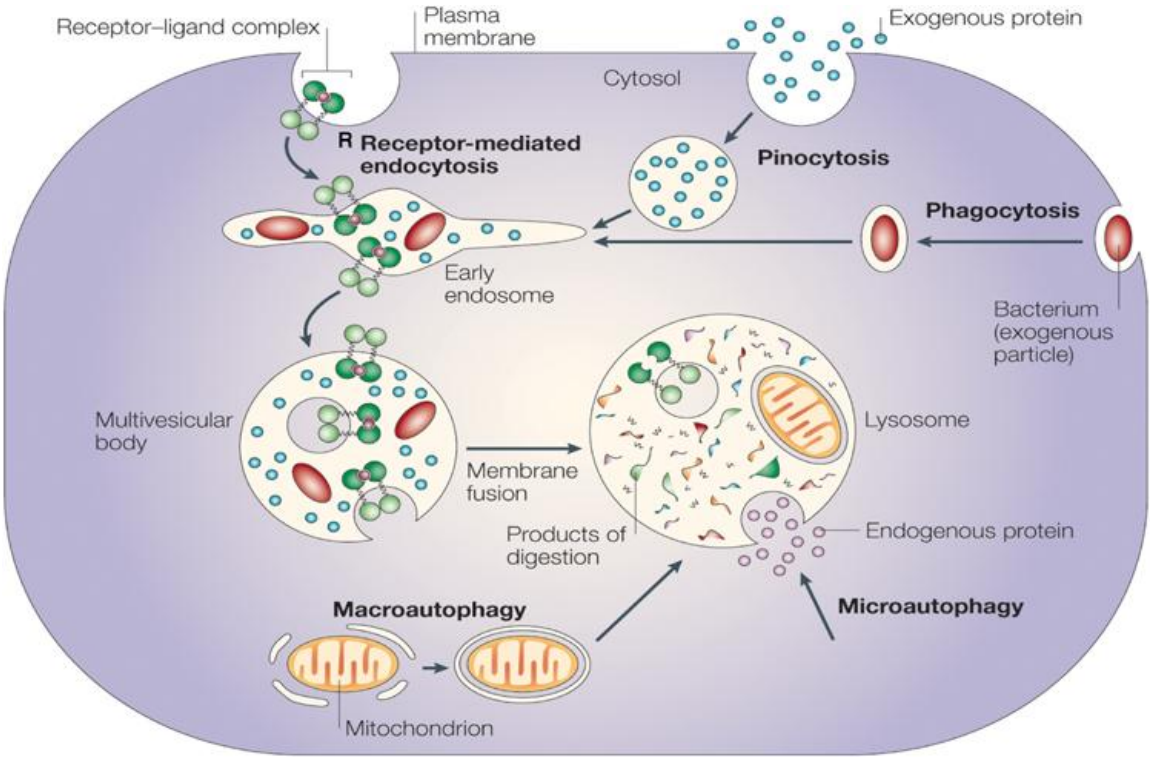

Figure 15. Schematic of the four proteolytic processes mediated by the lysosome. 1) Specific receptor-mediated endocytosis. **2)** Pinocytosis (nonspecific engulfment of proteins in extracellular fluid **3)** Phagocytosis (engulfment of extracellular particles) and **4)** Autophagy (micro- and macro-; of intracellular proteins and organelles). Reprinted with permission from Macmillan Publishers Ltd: [91]

CHAPTER IV

CHARACTERIZATION OF UBIQUITIN-T

Overview

Using MALDI imaging mass spectrometry, this chapter presents the finding that ubiquitin-t naturally occurs in kidney and that this cleavage is not a sample handling artifact but is created by cathepsin B *in vivo.* Additional work examining the presence of this protein in other diseased and normal tissue populations will be presented as well as preliminary results aimed at determining the origin and function of this protein.

Ubiquitin-t

In our analysis of early markers of drug induced kidney toxicity, we discovered that a C-terminal truncated form of ubiquitin (ub-t) was reduced with drug treatment. Recently, several researchers have reported the presence of this cleaved ubiquitin *in silico* [115] and *in situ* [33]. These investigators found the ub-t form of ubiquitin as a kidney cortex marker by direct tissue experiments using MALDI mass spectrometry. Similarly, Goncalves et al. identified this cleavage product as a potential biomarker for breast cancer in human breast cancer cells by surface enhanced laser desorption ionization MS. Neither study focused on investigating the origin of the truncated ubiquitin although the latter suggested that the truncation was a result of trypsin cleavage due to increased ubiquitination [115]. The authors also suggested that the truncation was not an artifact of their analysis due to their use of protease inhibitors in their homogenization procedure

[115]. Nonetheless, it needs to be conclusively shown that this form of the protein is not an artifact of the experimental protocol.

Methods

Localization of cleaved ubiquitin in kidney. Frozen rat kidney was sectioned at 12 μm thickness on a cryostat and thaw mounted onto a gold-coated MALDI target. Samples were allowed to dry in a vacuum dessicator and washed with a series of reagent grade ethanol washes (70%, 90%, 100%). Sinapinic acid (SA) matrix was applied (20 mg/ml 50:50 ACN:water 0.1% TFA) using a TLC nebulizer (25 mg/ml 50:50 ACN:water 0.1% TFA). Samples were analyzed on a Bruker AutoFlex II mass spectrometer using a smartbeam laser in linear mode. Images were reconstructed using FlexImaging Software (Bruker Daltonics).

Ubiquitin In Situ Cleavage. Mammalian ubiquitin (Ub) (1 mg) (Boston BioChem) was dissolved in 1 ml 0.1M ammonium acetate buffer with 1mM EDTA and DTT pH 5.4 [116]. Fresh frozen rat kidneys were sectioned in a cryostat at 12 μm thickness and thaw mounted onto gold coated MALDI targets. Samples were allowed to dry in a vacuum dessicator for atleast 30 minutes and were spotted with or without cathepsin B& L inhibitor (10 μl and 5 μl respectively) (Biovision, Inc.) in a 250 μm array using the Portrait 630 (Labcyte) followed by application of 20 mg/ml sinapinic acid matrix (SA).

Ubiquitin In Vitro Cleavage. Cathepsin B, D, and L (Sigma) and carboxypeptidase Y (Sigma) were added to 250 μl of 1 mg/ml ubiquitin in ammonium acetate buffer (100mM

with 1mM EDTA and DTT pH 5.4) according to manufacturer's guidelines. In brief 12.5 µl cathepsin B, 25 µl cathepsin D, 5 µl cathepsin L, and 100 µl carboxypeptidase Y were added. The solution was incubated at 37^{o}C with aliquots taken out after 5, 10, 20, 30, and 60 minutes and overnight. The reaction was stopped by adding acetonitrile (ACN) 1:1 (v/v). The reaction solution (250 nl) was deposited manually on a gold coated MALDI target followed by manual deposition of 250 nl 20 mg/ml SA.

In Situ inhibition Studies. *Cold inhibition experiment.* Frozen rat tissue sectioned as above and placed on a gold-coated MALDI target. Cathepsin B inhibitor (1 µl) (Biovision,Inc.) was spotted onto the tissue in the kidney cortex at -15^{o}C after having the vial on ice for ~30minutes. The tissue section was then thaw-mounted and placed in a vacuum desiccator for at least ~30minutes. SA (250 nl of 20 mg/ml) was manually deposited directly on top of the inhibitor spots. Once dried another manual deposit of matrix was applied and spots analyzed using a Bruker Autoflex.

Inhibition tissue overlay studies. Multiple spots of ubiquitin (500nl 1mg/ml in acetate buffer prepared as previously described) with or without cathepsin B inhibitor (premixed 10 µl ubiquitin and 1 µl inhibitor) were manually deposited onto a MALDI target plate and allowed to dry. Rat kidney tissue sectioned as described was placed on top of the dried spots and thaw mounted. Samples were placed in a vacuum dessicator and allowed to dry. SA was applied as described above and spots analyzed using a Bruker Autoflex.

Desiccation time course study. Rat kidney tissue was sectioned and thaw mounted as described before and placed in a vacuum desiccator. Samples were taken out and given an ethanol rinse as described after 5, 10, 15, 20, 30, 60 and 120 min in the desiccator as well as overnight. Two sections were cut for each time point. Five spots of SA were manually deposited in the kidney cortex as described on each tissue. Spectra acquired as above and averaged for each animal.

In vivo Cathepsin B inhibition. Male Fischer 344 rats from Charles River Laboratories (Wilmington, MA) were dosed i.p. with 5 mg (5X1mg/ml in saline and dimethylsulfate every 6 hrs) L-3-*trans*-(Propylcarbamyl) oxirane-2-carbonyl)-L-isoleucyl-L-proline methyl ester (CA074ME) or empty vector (saline and DMSO) in accordance to animal protocol M/08/059. Animals were sacrificed 6 hrs post dose and their kidneys excised and immediately frozen and stored at -80^{o}C until analysis. Tissue was then sectioned, thaw mounted, and analyzed as described above.

Cathepsin B (CATB) and L (CATL) Activity Assay. Kidney homogenates from control and CA074Me treated animals as well as gentamicin and kanamycin treated animals were assayed for cathepsin B and L activity following manufacturer's protocol (Biovision) using the substrates' Ac-RR-AFC and Ac-FR-AFC respectively. In brief 200 µg of the tissue homogenate were incubated with 50 µl of the respective reaction buffer and 2 µl of the appropriate substrate for 2 hours at 37^{o}C.

Spectral Processing. All spectra were externally calibrated and then baselined, normalized and aligned using ProTS Data (BioDesix, Inc) software. Images were visualized and normalized using Flex Analysis (Bruker Daltonics).

Diglycine Addition Experiment. ^{13}C labeled diglycine was synthesized by Junhai Yang. A 1.2 mg/ml solution of ^{13}C labeled diglycine was added to 1 mg/ml ubiquitin in activating acetate buffer and cathepsin B (Sigma) in the presence of a cell free rabbit reticulocyte extract (Boston BioChem) with excess ATP. The mixture was incubated at $37^{o}C$ overnight. The solution of ^{13}C labeled diglycine was also manually deposited onto rat kidney tissue with 1 mg/ml ubiquitin and excess ATP. SA was manually deposited on the tissue to analyze by MALDI.

Ubiquitin Endocytosis Experiments. *Cell culture.* L2-RYC rat yolk sac embryonic carcinoma cells (American Type Culture Collection, Manassas, VA) were cultured as described in Dulbecco's Modified Medium containing 10% fetal calf serum [117].

Cellular uptake of ubiquitin. Cells were grown for 3 days on 6 cover slips in serum free media. Alexa488-conjugated ubiquitin was synthesized by Junhai Yang according to manufacturers protocol (Molecular Probes) and filtered using a G-25 PD-10 column to remove low molecular weight contaminating free probe. Fluorescent ubiquitin (30µl of 1mg/ml) was added to the media with and without a megalin blocking antibody previously described [118] (gift from Pierre Verrhoust), receptor associated protein (30µl of 2.5 mg/ml) (Molecular Innovations, Novi, MI), and gentamicin (100µl of 50 mg/ml)

(CellGro). After 5 hr incubation, cells were washed twice with 1X PBS and then fixed for 15 minutes in 4% formaldehyde/1X PBS. Uptake was visualized using a Leica confocal microscope.

Results and Discussion

Several researchers have reported the presence of desGG ubiquitin (Ub-t) in kidney [33] and breast tumor cell lines and tissue [115]. The source of this cleavage was not addressed. The observation that Ub-t was a marker of antibiotic-induced nephrotoxicity led us to investigate if this cleavage occurs in vivo.

Localization of ubiquitin-t in kidney.

The localization of ubiquitin-t in kidney was determined with imaging mass spectrometry. A two dimensional ion map was constructed using m/z 8451 **(Figure 16).** Ub-t can be seen in the kidney cortex whereas full length ubiquitin is found primarily in the medulla.

In situ and in vitro ubiquitin cleavage

The regionalized localization of Ub-t in these samples suggested that this protein is a natural metabolite and is not an artifact. The first objective was to recapitulate the cleavage directly on tissue. Ubiquitin standard (in an acidic buffer) was spotted onto unwashed kidney tissue to facilitate cleavage by a lysosomal protease. Mass spectrometry analysis revealed a peak at m/z 8451 corresponding to the removal of the C-terminal glycines from ubiquitin in the kidney cortex, the outermost layer of the kidney (data not shown). Using this information, a 250 μm array containing ubiquitin in the activating buffer was printed on the tissue spanning across the cortex and medulla. **Figure 17a** (top panel) shows the resulting image indicating presence of the cleaved ubiquitin in the cortex. In vitro experiments using various proteases and ubiquitin

standard revealed complete conversion of full length to cleaved ubiquitin as early as 5 minutes with cathepsin B as seen by presence of a peak at m/z 8451 (**Fig 18**). Though all the proteases tested cleaved the Gly-gly from Ub, cathepsin B was found to be the most effective protease using the conditions outlined in the experiment. As a result, a cathepsin B inhibitor was chosen to use for on-tissue inhibition studies. **Figure 17b** (bottom panel) shows that addition of the inhibitor did in fact prevent cleavage of ubiquitin as evident by lack of a signal at m/z 8451.

From this work it was determined that the in situ cleavage of exogenous ubiquitin does not occur after the tissue is washed, presumably because of inactivation of the enzyme responsible. If this were an artifact it would have to occur before this step. The tissue is sectioned at below zero temperatures which significantly retard enzyme activity. If this was an artifact of the sample preparation then it would have to occur upon thaw mounting and/or in the vacuum desiccator.

Effect of experimental protocol on Ub-t

To evaluate if cleavage of ubiquitin occurs upon thaw mounting the tissue on the MALDI plate, a cathepsin B inhibitor was spotted onto the tissue cold, before thawing the tissue on the plate. The tissue was placed on the plate and the inhibitor deposited manually while in the cryostat. Upon deposition the inhibitor spread and essentially thawed the tissue onto the plate. The tissue was then thaw mounted and analyzed using MALDI mass spectrometry for presence of m/z 8451. **Figure 19a** shows that addition of "cold" inhibitor did not prevent the appearance of m/z 8451.

Since the deposition of the inhibitor in the cryostat appeared to anneal the tissue to the plate it was thought that this action could have provided enough heat to cleave ubiquitin ex vivo or that the inhibitor is not effective at this temperature. To address this issue, ubiquitin mixed with the inhibitor was deposited onto a MALDI target and allowed to dry. Rat kidney tissue was then overlaid on top of the spots and analyzed using mass spectrometry. Comparison of the spectra from tissue with ubiquitin and the inhibitor underneath versus just the ubiquitin underneath revealed the presence of the mass corresponding to the ubiquitin-t **(Figure 19b).** Our previous work demonstrated that the cleavage of exogenous ubiquitin was inhibited by the addition of the same cathepsin B inhibitor at room temperature. Taken together it can be concluded that cleavage of ubiquitin did not occur upon thaw mounting of the tissue.

The next step in the sample handling process where this cleavage could occur is during vacuum desiccation of the tissue. Tissue is usually kept in the desiccator for ~2 hrs for optimal drying and matrix crystal formation. If cleavage of ubiquitin was occurring or was enhanced in the desiccator, it is expected that an increase in intensity of this ion over time would be observed. To test this hypothesis, the kidney tissue was washed after 5, 10, 20, 30, 60, and 120 minutes in the desiccator and analyzed on the mass spectrometer. After averaging the spectra from five spots on each tissue and plotting the intensity of m/z 8451 with the standard error from each tissue, no clear trend can be seen although the highest intensity for the ion was observed after 120 minutes **(Figure 20).** These results led to the conclusion that the cleavage of ubiquitin is not an artifact of the sample handling.

Ubiquitin cleavage in vivo

To investigate the possibility that this cleavage occurs in vivo, a rat was dosed with a cathepsin B inhibitor and then assayed for presence of m/z 8451. One rat was dosed with 1 ml of 1mg/ml CA074Me, a cell permeable cathepsin B inhibitor, five times every six hours for a final dose of 5mg due to the enzyme kinetics [119]. The structure of the nonderivatized inhibitor is found in **Figure 21**. MALDI images comparing a kidney from a control (saline dosed) and dosed rat show a noticeable difference in the appearance of cleaved ubiquitin **(Figure 22).** The images show that the animal dosed with CA074Me showed a marked inhibition in the cleavage of ubiquitin, demonstrating that ubiquitin is cleaved by cathepsin B in vivo. These data correspond to a decrease in cathepsin B activity as determined by a fluorometric assay **(Figure 23).** Though CA074Me is reported to inhibit CATB specifically, Cathepsin L activity was assayed as well since our in vitro cleavage studies indicated this protease could cleave ubiquitin as well. The results do show a decrease in CATL activity but not to the extent of CATB **(Figure 24).**

It has been shown that gentamicin treatment inhibits the activity of cathepsin B [52]. These data are consistent with the hypothesis that gentamicin inhibits CATB activity, thereby decreasing the production of ubiquitin-t in drug treated samples. To support this hypothesis, we performed a CATB activity assay. Since I previously demonstrated that CATL can produce ubiquitin-t in vitro, we subsequently performed a CATL activity assay. The results indicate a significant decrease in CATB activity as a result of drug treatment suggesting the corresponding decrease in ubiquitin-t was as a result of decreased CATB activity **(Figure 24).**

Cathepsin B

Cathepsin B is a dipeptidyl carboxypeptidase that functions optimally at acidic pH. It is translated as a 37kDa propeptide in rat and then cleaved to become an active 28kDa protein. This enzyme is unique in that it has an occluding loop that partially blocks key residues in the active site **(Figure 26).** This structural moiety limits access and essentially allows two residues to enter into the enzyme's active site, effectively allowing CATB to remove C-terminal dipeptides [120]. Its specificity is such that it prefers a basic and hydrophobic amino acid at the P1 and P2 site respectively [121]. This information correlates well with the structure of ubiquitin and its subsequent cleavage fragments as determined by our in vitro experiments **(Figure 27).** Immunohistochemistry experiments have revealed an increased expression of CATB in the kidney cortex [122] a finding that correlates well with our imaging data.

In summary, it has been demonstrated that the removal of the C-terminal glycines from ubiquitin, and subsequent inactivation, is facilitated by cathepsin B in vivo. This cleavage can be recapitulated directly on tissue and by utilizing imaging mass spectrometry, the localization of this cleavage product can be determined. The data suggests that the decrease in ubiquitin-t seen as a result of drug treatment is due to a decrease in cathepsin B activity. This work not only further suggests the role of lysosomal injury in cortical toxicant nephropathy, but it opens the door for further investigation into ubiquitin storage and function.

Ubiquitin-t in the context of other work in the laboratory

The discovery of ubiquitin-t as a marker of drug toxicity was surprising and this led us to examine other diseases that were characterized as having altered cathepsin B activity-cancer. Cathepsin B is known to be increased in several forms of cancer and is thought to serve multiple roles in progression [123]. Defects in ubiquitination itself have been linked to cancer pathogenesis [124-126]. In a comparison of normal breast stroma to desmoplastic tumor stroma from 17 human breast tumors, ubiquitin-t was identified as having a >5 fold increase in tumor stroma as determined by a student's T-test [127]. Additionally, when the ratio of ubiquitin-t to ubiquitin is compared in 52 invasive breast cancer tissue samples, the patients with a higher grade cancer also had a higher percentage of ubiquitin-t in their MALDI profiles **(Figure 28)** [128]. In an analysis of lymph nodes from 52 patients with stage III melanoma and a median survival time of 19.9 months, ubiquitin-t was identified as an indicator of poor survival **(Figure 30)** [129]. In work done to analyze the tumor margin in clear cell renal cell carcinoma (CCRCC), ubiquitin-t was not only able to classify high grade vs. low grade with a 71% accuracy, but it was also one of the features that changed well after the histological tumor margin **(Figure 31)** [130]. These findings not only underscore the role of CATB in cancer progression but now also suggest a link to ubiquitin. In fact, disregulation of the ubiquitin-system has been documented in cancer and is reviewed in [131]. This work adds another layer of complexity to the ubiquitin/cancer relationship that could potentially lead to discovery of a new drug target.

Though the focus of the work in this thesis was on the kidney, the discovery of ubiquitin-t in various cancer tissues was a rather curious one that led us to examine its

spatial localization in other tissues. Compiling data from our lab, I found ubiquitin-t was localized in the area surrounding the embryo in a mouse implantation site [132], in the granular layer of the brain, and in the initial segment of the epididymus [133] **(Figure 32).**

Ubiquitin-t Origin

The observation that ubiquitin can interact and subsequently become truncated by cathepsin B is a surprising one. Traditionally, it was not thought that ubiquitin entered the lysosome. Deubiquitinases (DUB) have extensively been shown to remove ubiquitin before entering that particular organelle so as to facilitate recycling [134]. But, recently ubiquitinated proteins have been found in exosomes [135] and free ubiquitin in lysosomes of CATB and CATL null brains [136]. These data suggest a faulty DUB or possibly entry into the lysosome by another method, either autophagy or receptor-mediated endocytosis, both of which were discussed in Chapter III, indicating extracellular ubiquitin.

The concept of extracellular ubiquitin is a relatively new and not yet understood phenomenon. Ubiquitin is secreted from human and mouse embryos [137], cultured leptomeningeal cells [138], as well as neuroblastoma cells [139] and the proteasome found in human alveolar space [140]. Ubiquitin has been detected in human seminal plasma [141], serum and plasma as a result of infection or disease [142-147], bovine epididymal fluid [148], and a 1-72 amino acid form of ubiquitin detected by MALDI in cerebral spinal fluid [149]. This information led to the hypothesis that the origin of ubiquitin-t could be a result of extracellular uptake and subsequent cleavage.

Recently Majetschak and colleagues demonstrated uptake of extracellular ubiquitin by human acute monocytic leukemia cells [150]. They proposed that this uptake was regulated by receptor mediated endocytosis. The receptor remained undetermined. Using the localization of ubiquitin-t as determined from our imaging studies, as well as the finding that half of the proteins indentified from our drug toxicity study were ligands of the megalin receptor, we hypothesized that megalin was the endocytic receptor responsible for uptake and subsequent cleavage of ubiquitin. Megalin is a 600kDa, single transmembrane receptor that binds low molecular weight proteins and transports them to lysosomes. It has been heavily studied and reviewed [151]. Importantly, megalin is expressed in the initial segment of the epididymus [152], the endometrium and oviduct [153-155], kidney proximal tubule cells [156], and brain capillaries and choroid plexus [157] which correlates quite nicely with our imaging data. Interestingly, cathepsin B was recently identified as a ligand of the megalin receptor [158].

To test the hypothesis that ubiquitin-t was a result of extracellular ubiquitin being endocytosed through the megalin receptor and targeted to the lysosome where it is cleaved by CATB, fluorescence studies were performed with a cell line known to express high amounts of megalin [159, 160]. I was able to demonstrate uptake of ubiquitin in rat yolk sac epithelial cells as evident by green fluorescence **(Figure 33a).** Upon addition of a megalin blocking antibody **(Figure 33b)** and receptor associated protein (RAP), a chaperone that inhibits interaction with the receptor, **(Figure 33c)**, no fluorescence is detected indicating an inhibition of uptake of ubiquitin. These data suggest that ubiquitin is a ligand of the megalin receptor. Further binding assays using purified megalin and

ubiquitin are necessary to demonstrate direct binding. Though cleavage as a result of uptake has not been directly proven, at the very least these data suggest ubiquitin-t is a marker for megalin localization.

Addition of gentamicin, another known ligand of megalin also prevented uptake of ubiquitin **(Figure 33d).** This suggests that the decrease we observed in ubiquitin-t as a result of drug treatment could not only be due to inhibition of CATB activity as discussed in the last chapter, but possibly because of gentamicin inhibiting uptake of ubiquitin. Further work is necessary to determine which mechanism is responsible.

Ubiquitin-t function

Due to the nature of the truncation indicative of ubiquitin-t, its function is not likely associated with the canonical proteasomal degradation pathway. This suggests a novel function. It was proposed that ubiquitin-t was a storage form of ubiquitin to prevent unnecessary ubiquitination. In brief, cathepsin B would cleave ubiquitin in the lysosome when ubiquitination isn't needed. The product would then be recycled back out to the cytosol, where it would remain inactivated pending a signal for ubiquitination and subsequent ligation of the C-terminal glycines back onto ubiquitin. To test this hypothesis we added ^{13}C labeled diglycine to cathepsin B cleaved ubiquitin with excess ATP in solution (cell free extract) and directly on tissue. A peak corresponding to full length ubiquitin was not found (data not shown). This indicated that under the conditions used in our experiment, the glycine residues could not be added back onto ubiquitin-t, suggesting that this does not occur *in vivo*.

Additionally, Goncalves et al. suggested that the cleaved and native ubiquitins have different binding partners, suggesting a role in cell signaling [115]. Further work will need to be done to elucidate this protein's intracellular function.

Alternatively, ubiquitin-t could be transcytosed out of the cell. It was recently shown that megalin mediates transcytosis of thyroglobulin, a novel function for this receptor [161]. Though in this case, uptake of thyroglobulin by megalin was used to bypass the lysosomal degradative pathway, it is possible that megalin not only facilitates cleavage of ubiquitin but also mediates its export from the cell. Transcytosis experiments like those performed for thyroglobulin should be done to test this hypothesis.

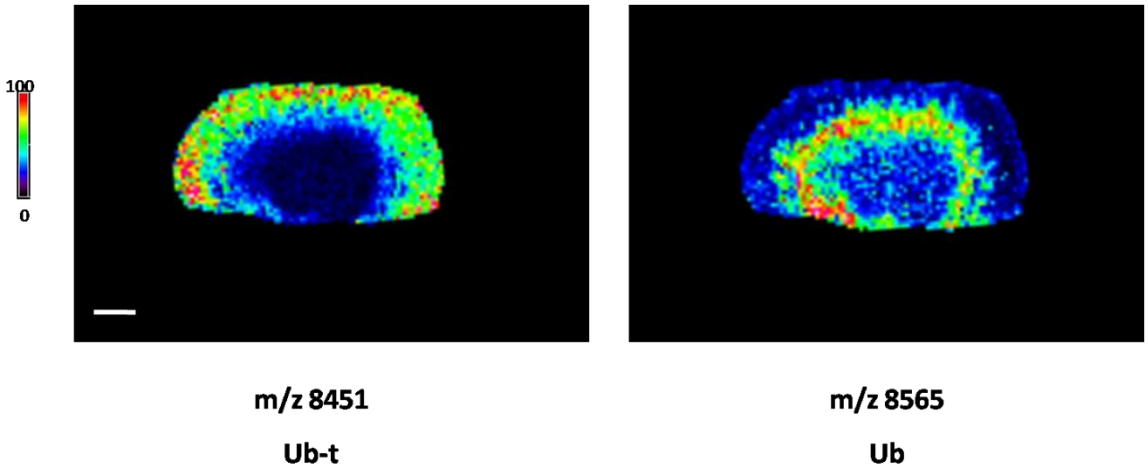

Figure 16. Localization of cleaved ubiquitin in rat kidney. MALDI images were obtained from rat kidney as described in the text at 250 µm spatial resolution. Cleaved ubiquitin is along the outer edge of the kidney (cortex) whereas full length ubiquitin is found further inside the kidney (medulla). Scale bar=2mm.

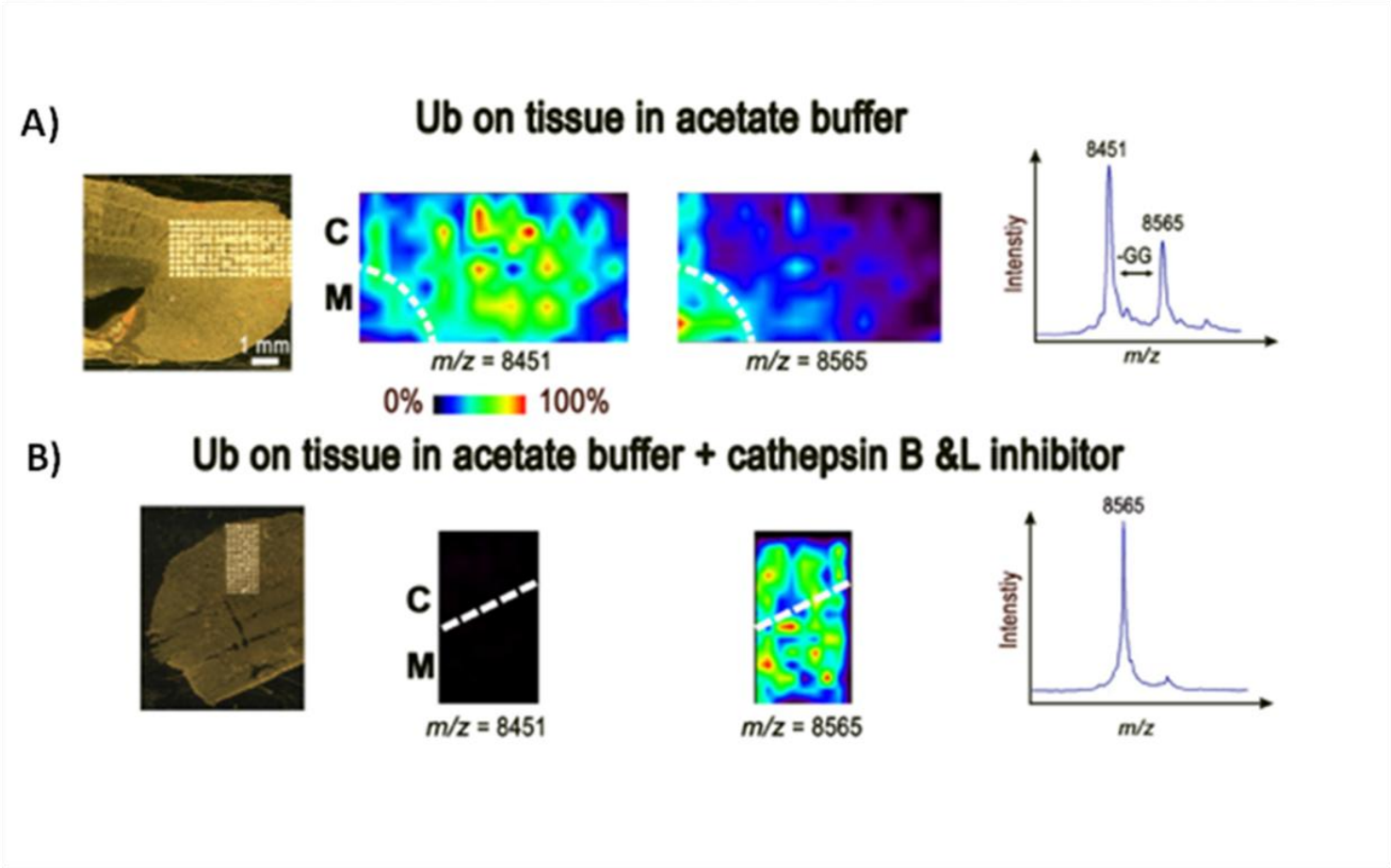

Figure 17. In situ ubiquitin cleavage. MALDI images of the cleavage of exogenous ubiquitin directly on the tissue. A) Image of the distribution of full length (8565) and desGG (8451) ubiquitin in activating buffer across the cortex and medulla of the kidney. B) Image of the distribution of full length (8565) and desGG (8451) ubiquitin in activating buffer across the cortex and medulla of the kidney with the addition of a cathepsin B inhibitor. C-cortex, M-medulla

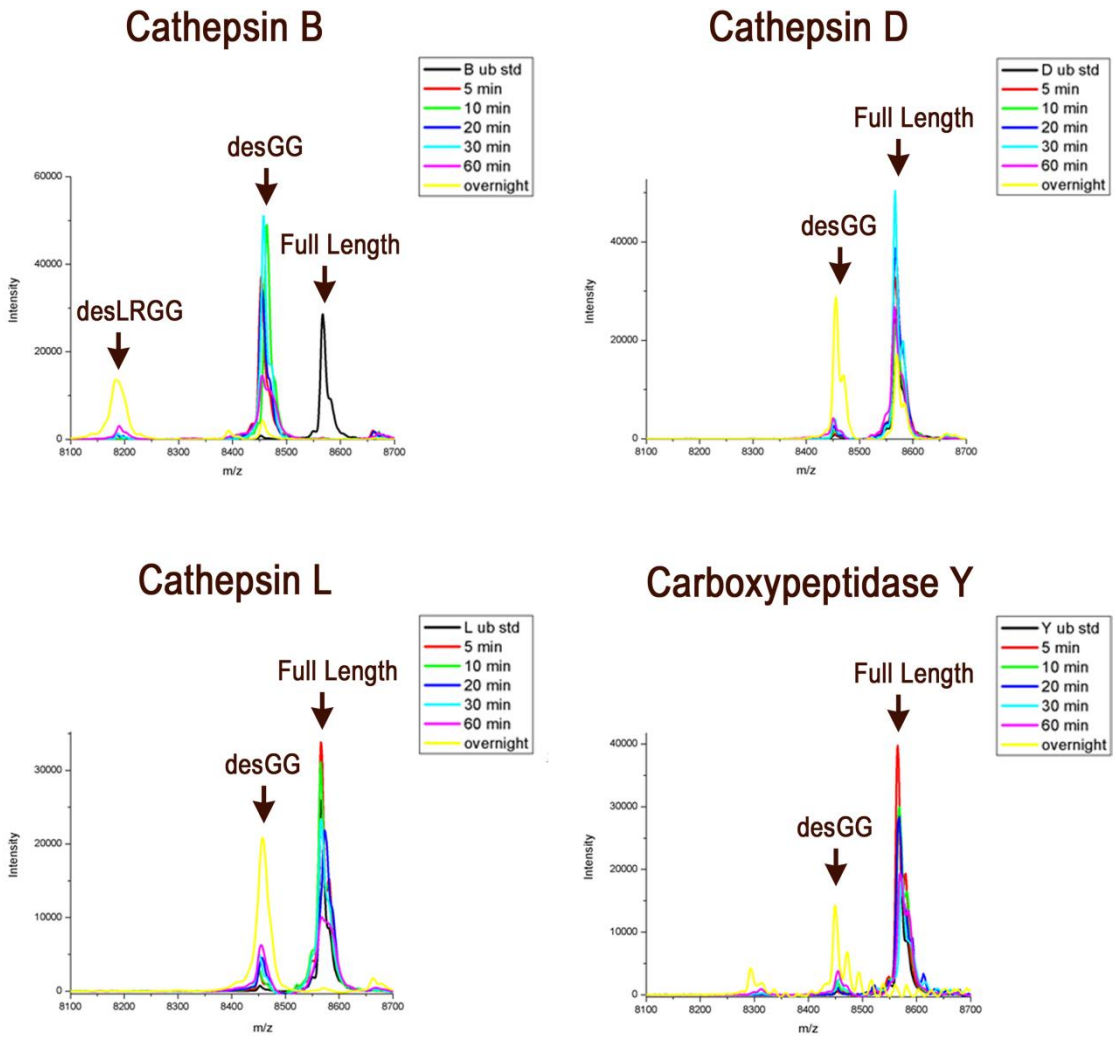

Figure 18. In vitro cleavage of ubiquitin. MALDI spectra from a time course study with various carboxypeptidases. Samples were prepared as described in the text. The resulting spectra from each time point was overlayed and displayed for each enzyme as labeled. Though all enzymes tested produced desGG ubiquitin as indicated on each spectrum, cathepsin B effectively cleaved the residues completely and as quickly as 5 minutes after incubation. Cathepsin B was the only enzyme tested that removed the preceeding dipeptide LR as well as indicated on the spectrum.

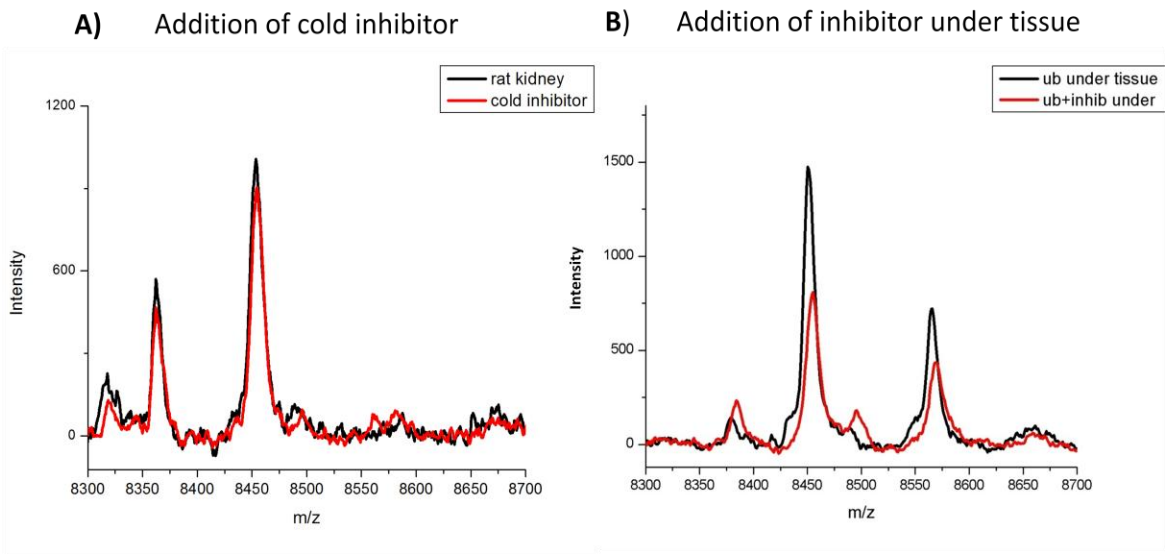

Figure 19. Effect of addition of cathepsin B inhibitor on endogenous ubiquitin cleavage. Representative MALDI spectra from analysis of rat kidney with the addition of a CATB inhibitor applied a) at ~-20^{o}C, prior to thaw mounting and b) on the MALDI plate and allowed to dry at room temperature prior to thaw mounting of the tissue.

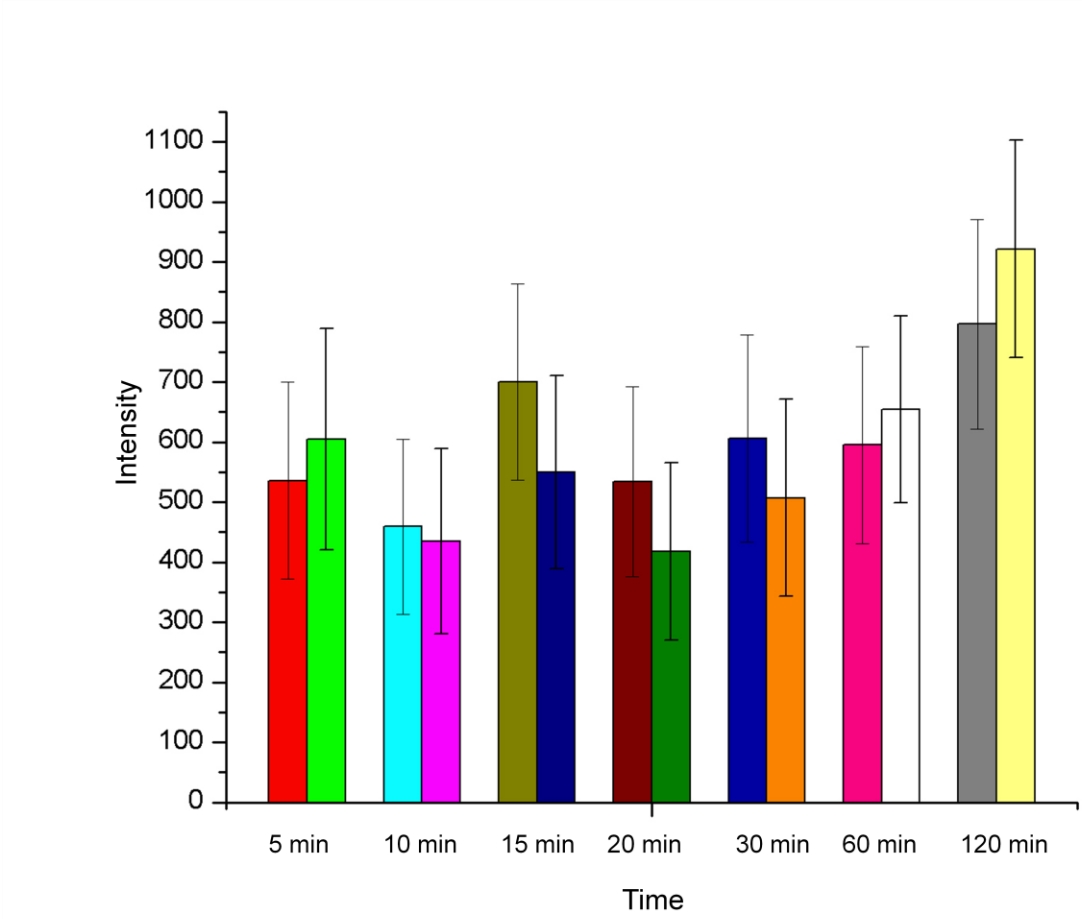

Figure 20. Time course study on the effect of dessication on cleavage of ubiquitin. Rat kidney sections were thaw mounted and placed in a vacuum dessicator for the indicated times before ethanol washing and downstream analysis. Five matrix spots per section were averaged and the average intensity of ubiquitin-t plotted as a bar graph with the associated error. The analysis was performed in duplicate with the resulting data displayed as pairs of bars at each time point.

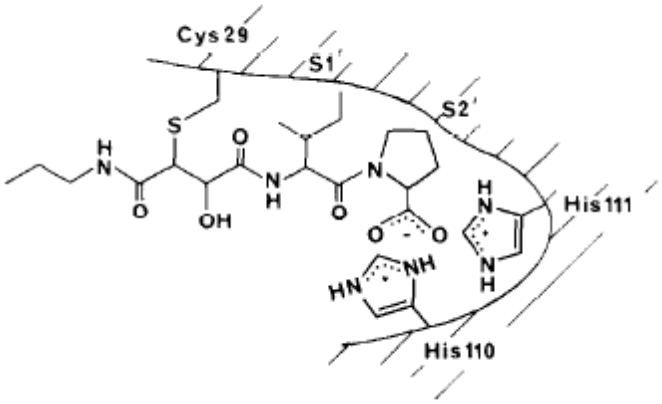

Figure 21. Structure of CA074. Inhibitor is shown in its proposed binding orientation to CATB. Reprinted with permission from [162]

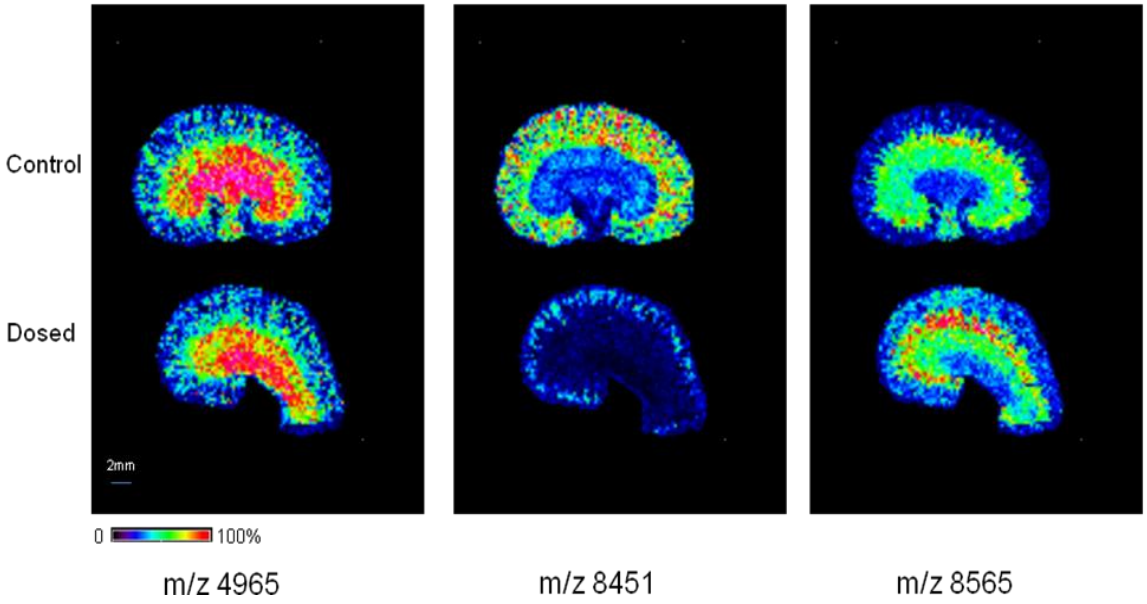

Figure 22. Inhibition of cleavage of ubiquitin in vivo. MALDI kidney image of a control and CA074ME dosed animal. Animals were dosed i.p. with empty vector (saline and DMSO) or CA074ME, a cathepsin B inhibitor. Samples were prepared and analyzed as described in the text. Resulting images were acquired at 250 µm spatial resolution. Localization of m/z 4965 is shown as a control. A decrease in the intensity of m/z 8451 is demonstrated in the dosed animal.

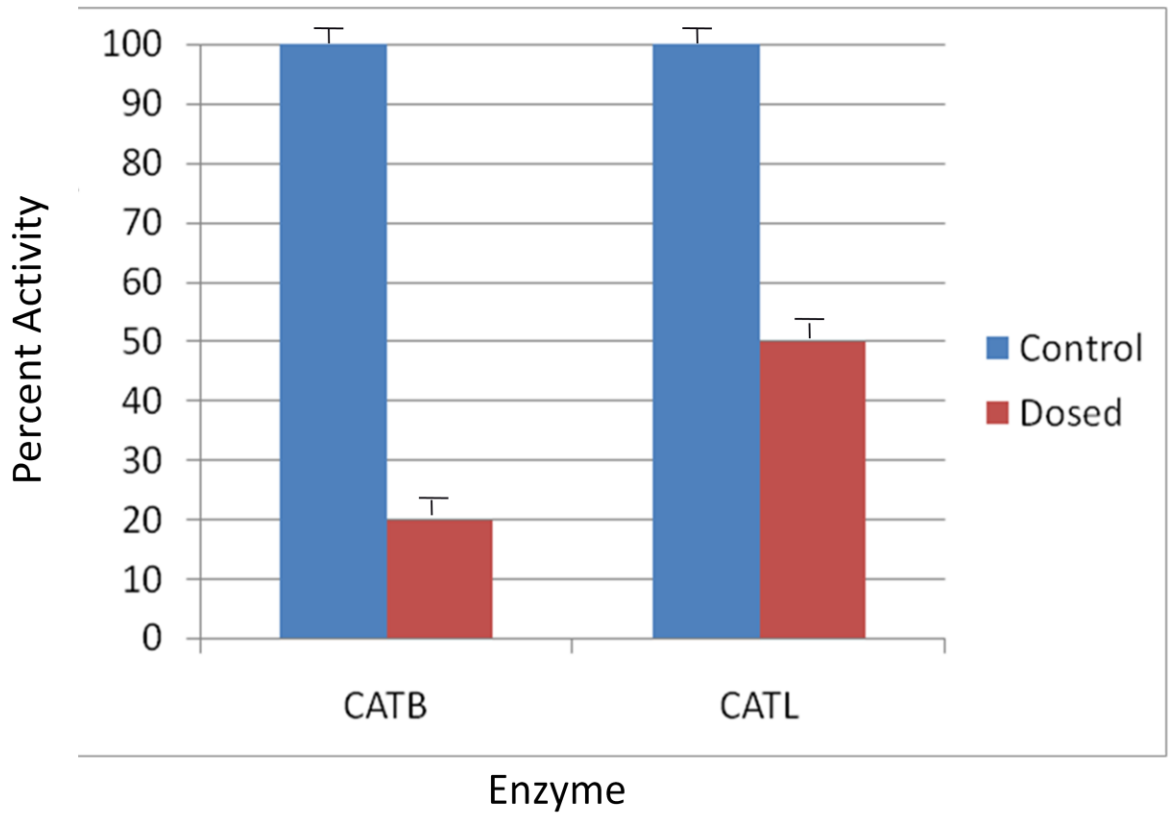

Figure 23. Cathepsin B and L Fluorometric Activity Assay from CA074Me treated sample. Kidneys from control and CA074Me treated rats were assayed for CATB and CATL activity as described in the text. Analysis was done in triplicate and the average result plotted as a bar graph with the corresponding error. A significant decrease in CATB activity is observed in the CA074Me treated sample. CATL activity was decreased as well but not to the extent of CATB.

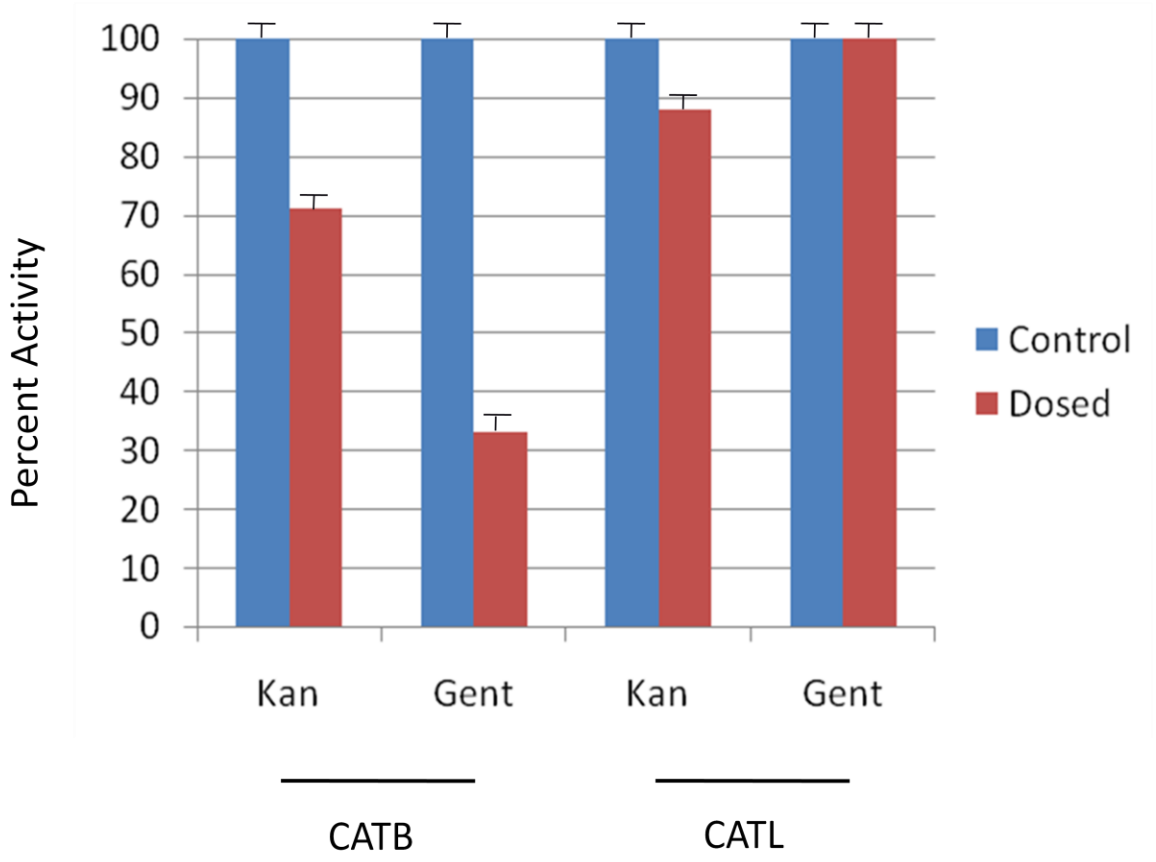

Figure 24. CATB and CATL activity assay from antibiotic treated samples. Kidneys from control and drug (kan-kanamycin; gent-gentamicin) treated rats were assayed for CATB and CATL activity as described in the text. Analysis was done in triplicate and the average result plotted as a bar graph with the corresponding error. A significant decrease in CATB activity is observed in the drug treated samples. CATL activity was decreased in the kanamycin sample as well but not to the extent of CATB.

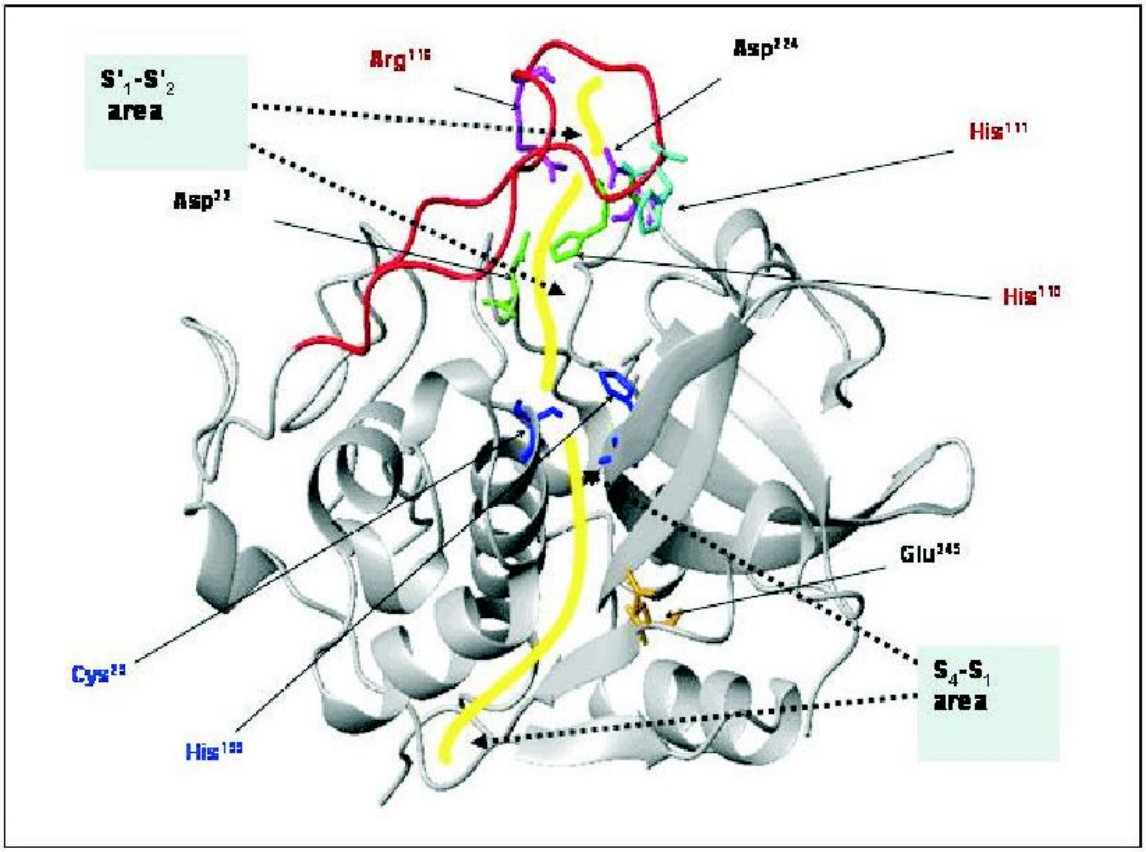

Figure 25. Crystal structure of cathepsin B (EC 3.4.22.1; 1HUC from PDB). Red-Occluding loop (Ile105–Pro126) and symbols of its crucial residues. Green-Side chains forming salt bridges (Asp22↔ His110) and pink (Arg116↔ Asp224); Yellow-catalytic cleft; Blue-catalytic center. Reprinted with permission from [163].

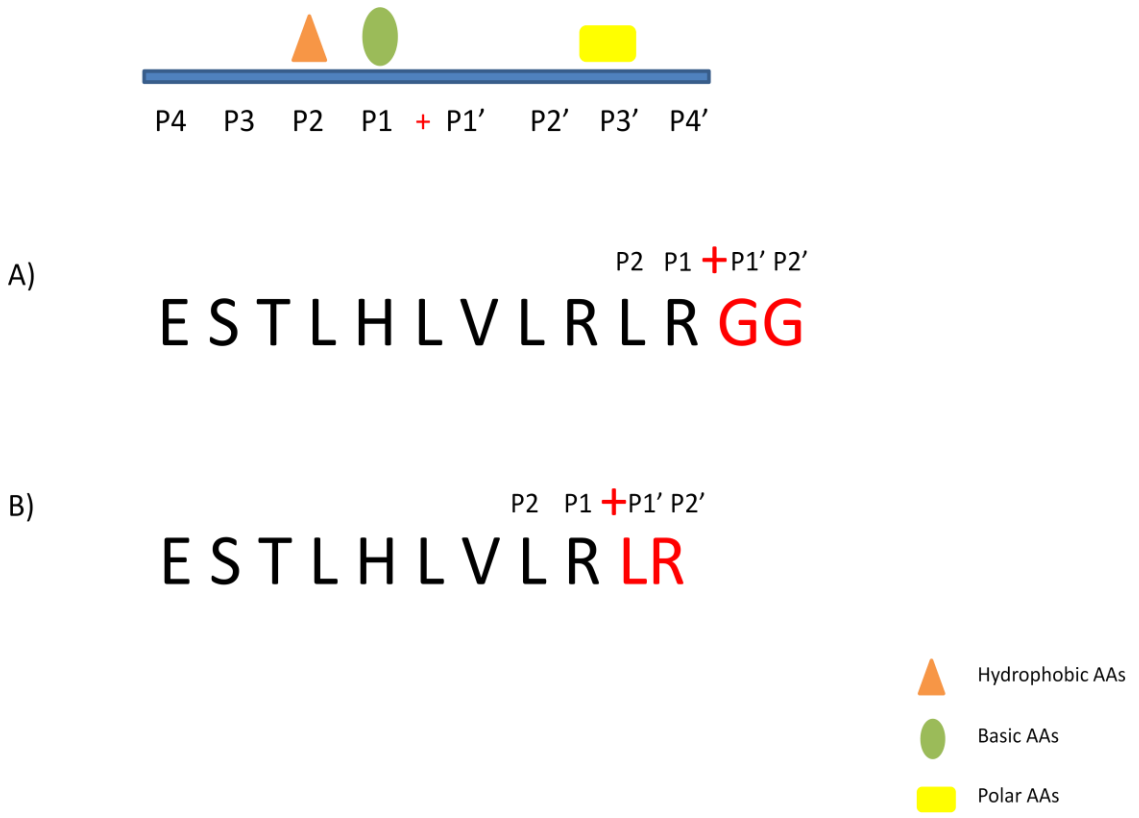

Figure 26. Diagram of cathepsin B specificity with respect to ubiquitin cleavage. C-terminal peptide of ubiquitin shown with cleaved residues in red after a a) five minute and b) overnight incubation with cathepsin B. Top schematic outlines the preferred amino acids and their positions in the substrate. **+:** scissile bond

Sample	intensity of 8451	intensity of 8565	% of total 8451
G1 -A	374.70288	33346.346	1.111183941
G1 -B	3055.8466	62149.997	4.686461261
G1 -C	4566.5954	73673.124	5.836671495
G3 -A	580.96119	8245.0596	6.582368248
G3 -B	5147.0513	71883.53	6.681828455
G1 -D	6794.2889	89134.745	7.082619957
G1 -E	3280.8837	39711.72	7.631274726
G1 -F	5816.9365	66528.722	8.040477647
G1 -G	3776.4503	40559.786	8.517751201
G1 -H	5387.1433	56901.616	8.648660465
G3 -C	5291.1764	48056.315	9.918322795
G1 -I	13851.607	99613.121	12.20785282
G1 -J	6305.5116	44004.228	12.53338151
G3 -D	16794.456	116293.85	12.61903206
G1 -K	7058.2408	44092.548	13.79888945
G1 -L	2246.9956	13504.974	14.26485485
G3 -E	34468.207	181951.86	15.92653005
G3 -F	3288.7066	15161.863	17.82441774
G1 -M	6464.9616	26877.677	19.38947207
G3 -G	4726.1247	19002.203	19.91764763
G3 -H	15644.977	62816.531	19.93968431
G3 -I	20203.075	68771.379	22.70660183
G3 -J	10670.693	34012.318	23.88087275
G3 -K	8459.756	26927.852	23.90598426
G1 -N	9765.3358	30553.69	24.22016804
G1 -O	4297.4857	13297.731	24.42417035
G3 -L	11672.537	32271.391	26.56234327
G3 -M	3774.1332	9158.1077	29.18390733
G3 -N	36304.16	80935.427	30.96578633
G3 -O	14360.809	29282.136	32.90522443
G3 -P	3396.9385	5959.6302	36.30538725
G3 -Q	18526.325	26805.339	40.8683983
G3 -R	17258.118	20674.143	45.49720355
G3 -S	11062.474	11149.71	49.8036303
G3 -T	21100.597	21259.943	49.81191694
G3 -U	7190.817	7020.7431	50.59836464
G3 -V	5225.6679	5092.8088	50.64379222
G3 -W	5398.5341	4918.7982	52.32490282
G3 -X	9747.1181	7199.3879	57.51697784
G3 -Y	32444.915	23846.004	57.63792025
G3 -Z	28211.979	14952.014	65.35998419
G3 -AA	40286.666	20003.161	66.82166462
G1 -P	53075.405	21523.79	71.14742324
G3 -BB	30155.056	12011.006	71.51499232
G3 -CC	33911.251	12038.206	73.80120074
G3 -DD	28234.644	9865.1195	74.10713717
G3 -EE	28969.27	6570.3772	81.51254242
G3 -FF	10601.37	2344.3745	81.89077113
G3 -GG	27401.698	5583.9553	83.07156372
G3 -HH	55794.668	9280.269	85.73910413
G3 -II	30031.02	4637.3538	86.62367659

Figure 27. Comparative analysis of the ratio of ubiquitin-t to ubiquitin in invasive mammary carcinoma. 52 samples from patients with invasive mammary carcinoma were analyzed by direct tissue MALDI MS. The ratio of the intensity of the ion corresponding to ubiquitin-t (m/z 8451) to ubiquitin (m/z 8565) was determined and expressed as a percentage. Overall, higher grade samples clustered together and have a higher percentage ubiquitin-t. G1-grade 1; G3-grade 3; yellow-low grade; white-high grade. Figure courtesy of Erin Seeley [128].

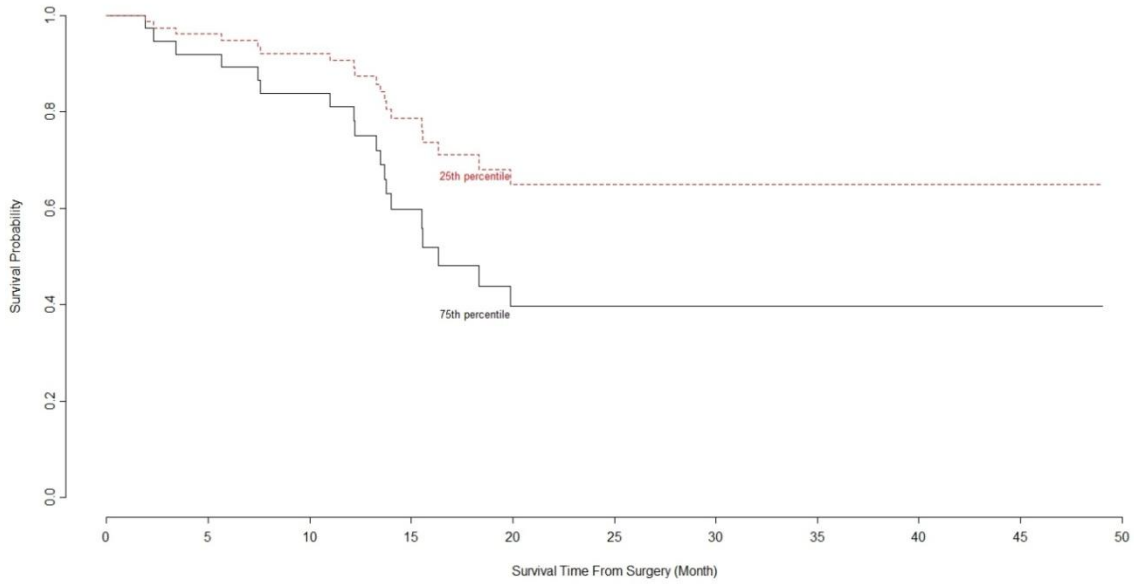

Figure 28. Survival analysis of metastatic melanoma patients expressing m/z 8451 (ubiquitin-t). Lymph nodes from 52 patients with stage III melanoma were analyzed by direct tissue MALDI MS. Patients with a higher intensity of m/z 8451 had a lower survival probability than those exhibiting a lower intensity of m/z 8451. Red line-lowest intenstity quartile; Black line-highest intensity quartile. Figure courtesy of William Hardesty [129].

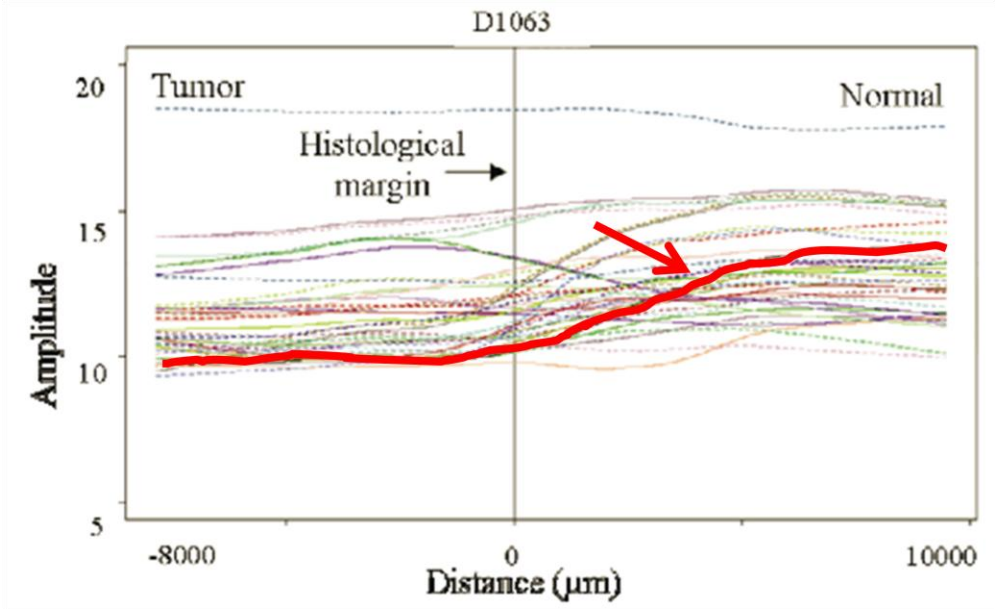

Figure 29. Ubiquitin-t surpasses histological tumor margin. LOWESS plot of m/z 8451 from clear cell renal cell carcinoma highlighted in red. This feature changes well beyond the histologically defined tumor margin. Figure adapted from [130].

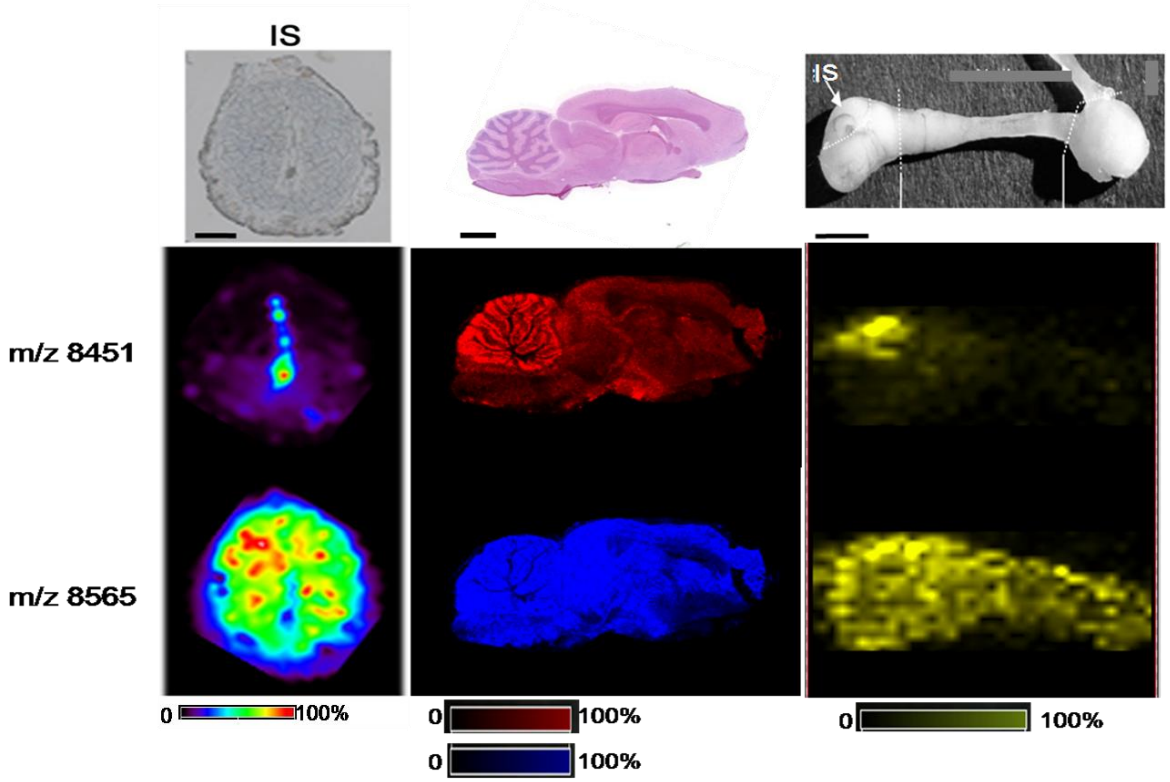

Figure 30. Localization of cleaved ubiquitin across various tissues. MALDI images were obtained from each tissue specimen as described in the text. Tissues from left to right: mouse embryo implantation site (IS) (scale bar=700μm), rat brain (scale bar=2mm), and mouse epididymus (IS-initial segment) (scale bar=1mm).

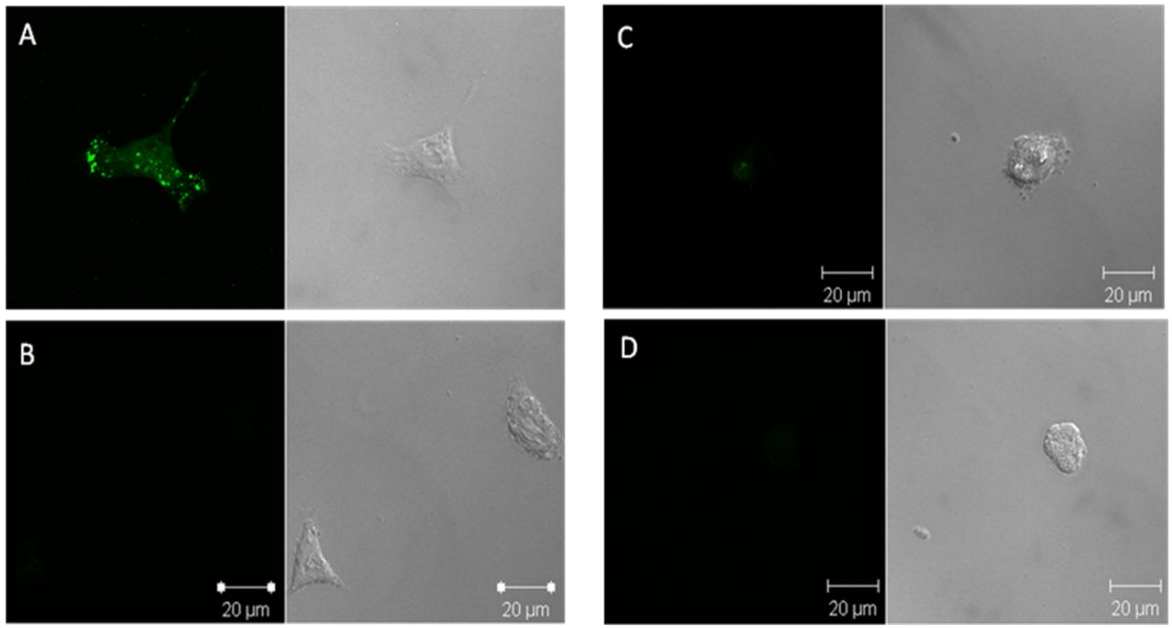

Figure 31. Ubiquitin uptake experiments. A) Alexa488-ubiquitin was added to L2-RYC cells in the presence of B) megalin blocking antibody, C) receptor associated protein (RAP), and D) gentamicin

CHAPTER V

DISCUSSION AND CONCLUSION

Overview

This chapter will discuss the implications of the work as well as provide a summary of the work accomplished. Additionally, thoughts as to where the work is headed will be presented.

Protein Markers of Nephrotoxicity

This study utilized MALDI MS to profile and image kidneys from antibiotic treated rats for indicators of damage. Twelve proteins were identified as being differentially expressed as a result of gentamicin and kanamycin treatment. There are three points to consider when examining this data. First, though these changes were detected in the cortex, a comparison of data obtained from the medulla revealed statistically significant changes, suggesting that though the cortex is the primary site of damage, there are secondary effects in the medulla. This opens the door for further analysis of the interplay between damage in the cortex and the medulla.

Second, out of the twelve proteins identified, only three were unique to either gentamicin or kanamycin treatment. The overlap in the protein markers was expected since the drugs are in the same class, but the discovery that some proteins exhibited changes only in response to a single drug's treatment was intriguing. This suggests that

there could be unique mechanisms of damage for each nephrotoxicant adding credence to the need for further research.

Third, all of the proteins identified can be linked to proposed mechanisms of toxicity. This not only speaks to the utility of the technology to detect changes that are relevant to disease, but to the promise of expression proteomics. The idea that one can assess the protein changes associated with a disease and subsequently develop a hypothesis to gain mechanistic insight is an emerging one with data mounting daily [REF]. This study was a true example of utilizing expression proteomics to shed mechanistic insight. Ub-t was discovered as a cortical marker of antibiotic induced nephrotoxicity. Through a series of experiments it was determined that this protein was not an experimental artifact as previously reported [50] but was produced in vivo by CATB. It has previously been demonstrated that gentamicin decreases CATB and CATL activity [52]. It was therefore hypothesized that the decrease in Ub-t observed in the kidney cortex of drug treated animals, was due to inhibition of CATB by gentamicin. Preliminary data to this end was presented.

Adding proteins to the current caudre of markers will serve to enhance as well as potentially expedite the diagnosis of damage. Traditional protein markers do not exhibit changes until the onset of damage [2]. Interest is mounting in the potential to detect damage earlier to not only save money in the drug discovery process, but to enhance quality of life as well. The promise of this technology identifying an early marker of disease was demonstrated with the finding that lysozyme, a lysosomal protease, was increased in the kidney cortex of antibiotic treated rats at a dose and time point where traditional biochemical indicators of toxicity were lacking.

Future Work

More extensive identification as well as further validation and quantitation of the proteins identified as markers of gentamicin and kanamycin induced nephrotoxicity is necessary for their use in clinical diagnostics. Part of the difficulty in identifying many of the markers in this study is that many of them could possibly be post-translationally modified as demonstrated with the discovery of Ub-t and transthyretin discussed elsewhere [33]. Efforts to identify the remaining markers will need to focus in this area. Validation could be achieved with a number of antibody based techniques including immunohistochemistry and immunoprecipitation or in situ hybridization. Once the markers are validated their presence in urine should be monitored to provide a noninvasive diagnosis tool. Urine analysis has been demonstrated for this application before [164].

Additionally, a more refined analysis with a smaller laser size would be advantageous due to the fine structure of the nephron. This would provide deeper levels of understanding of not only what changes are occurring in the kidney, but where, thereby adding specificity and perhaps gaining new insight into mechanism of toxicity.

The integration of these protein markers into other known proteomic, genomic, and metabonomic [165] markers should be explored. A query of lipidomic features could also provide beneficial information. In particular, the analysis of differential phospholipid expression should be examined. One of the proposed mechanisms of antibiotic induced nephrotoxicity is phospholipidosis [166-168]. Aminoglycosides such as gentamicin, are hydrophilic, polycationic drugs which bind to negatively charged phospholipid bilayers and subsequently inhibit enzymes responsible for phospholipid

metabolism [166]. This accumulation of phospholipids is referred to as phospholipidosis. An analysis of the types and locations of phospholipids differentially expressed as a result of drug treatment would be worthwhile. Though several methods exist to image phospholipids directly from tissue by MALDI MS [169], a recent technique demonstrated the power of a dry coating method [28]. This method was used to examine the spatial and temporal location of phospholipids involved in embryo implantation [132].

In situ Assessment of Endogenous Enzyme Activity

As discussed previously, cathepsins are lysosomal enzymes that play an instrumental role in protein degradation. They can act as endo- or exoproteinases, and are mostly active in acidic environments [170, 171]. Cathepsin B, one of the 11 cysteine cathepsins, is a lysosomal dipeptidyl carboxypeptidase [110]. It is constitutively expressed by all cells and though originally thought to have broad substrate specificity, it was recently shown to play a significant role in Alzheimer's [172] and cancer [123, 173]. Therefore considerable interest in assessing this and other cathepsins' activities has grown.

Current methods to assess this enzyme and other members of this enzyme family's activity rely on homogenization of tissue and use of a fluorescently tagged substrate [174]. In brief, the homogenate is pre-incubated with the tagged substrate at 37^{o}C for ~ 1 hour where hydrolysis of the tag occurs upon interaction with the enzyme. The free tag's fluorescence can be detected and quantified using a fluorescence plate reader. Presumably, the fluorescent tag only becomes activated upon cleavage by a cathepsin. The specificity of these methods relies on specialized substrates to assess

activity for each cathepsin by an indirect measurement which could become costly in a large scale analysis. This technique also does not lend itself to visualization of enzyme activity across a tissue section, something that could become important when assessing tumor margins.

MALDI IMS has been used to assess protein, peptide, and lipid localization [14, 25, 175-178], detect biomarkers of drug toxicity [66], assess drug localization [21, 179, 180], and to identify proteins directly from tissue [41]. The latter application uses exogenous enzyme to identify proteins in a tissue section. The utilization of IMS to assess endogenous enzyme activity directly from tissue sections allows for a quick, high-throughput, label-free analysis while maintaining the spatial localization of the enzymatic products. This dissertation represents the first application of IMS for *in situ* analysis of cathepsin B activity. This methodology can be applied to various other substrates as demonstrated in **Figure 32** with the Hep B peptide. By spotting the peptide with the CATB activating buffer onto the kidney cortex, the cleavage products were observed. An image can be reconstructed much the same as the Ub data was. The methodology can also potentially be expanded to assess the activity of other enzymes with the corresponding activating buffer and substrate. This tool will allow pathologists to register tissue morphology or type directly to endogenous enzyme activity, further aiding in diagnosis of disease.

Conclusion

In this study, MALDI MS was used to assess differential protein expression as a result of antibiotic treatment in rat kidneys. Through profiling and imaging mass

spectrometry protein markers of drug-induced nephrotoxicity were identified. This analysis led to the first reported discovery of an in vivo C-terminal truncation of ubiquitin. The promise of not only further exploring the data generated from this study but also the impact of this technology onto the field of drug discovery is exciting and its implications will be seen in years to come.

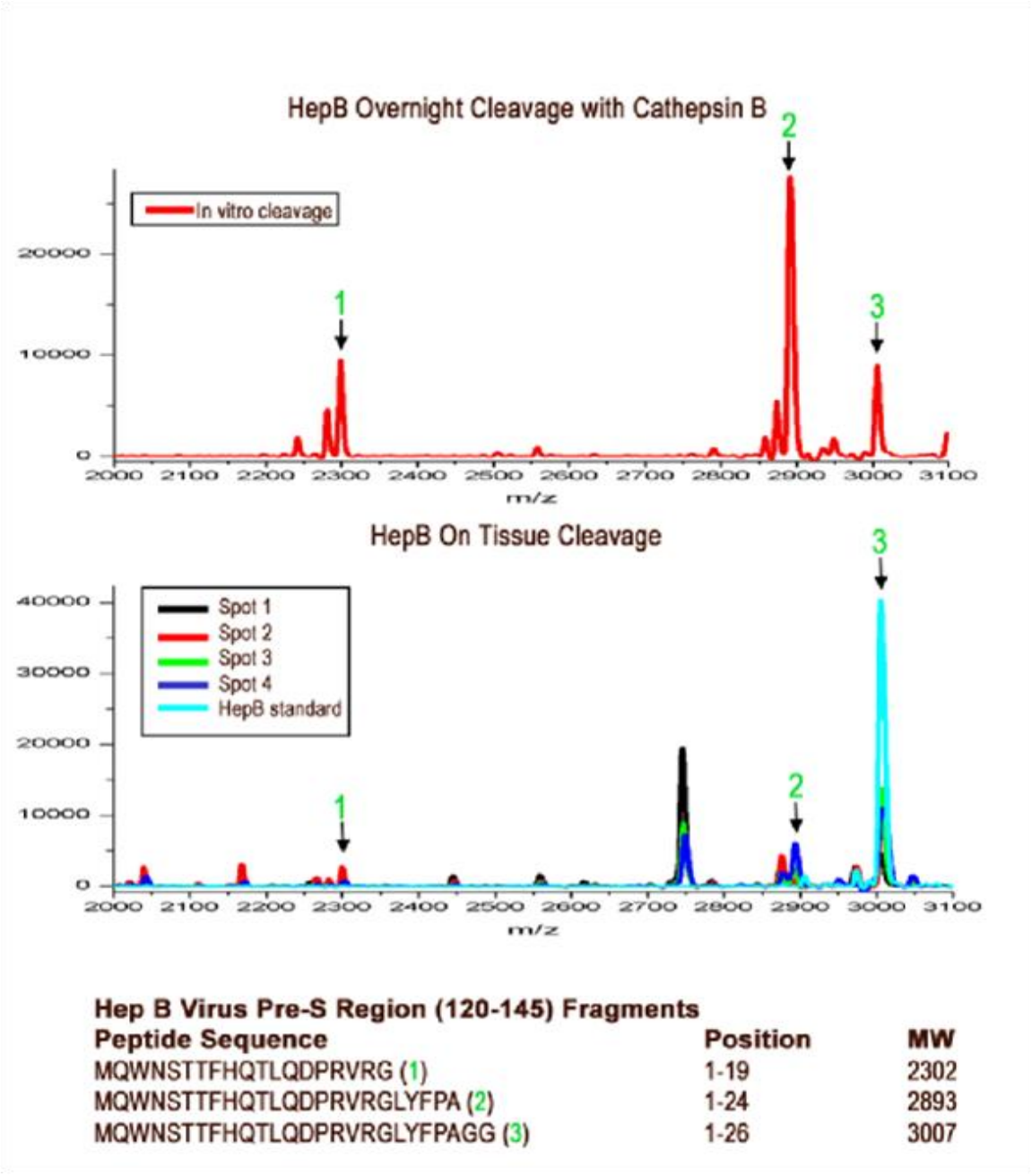

Hep B Virus Pre-S Region (120-145) Fragments

Peptide Sequence	Position	MW
MQWNSTTFHQTLQDPRVRG (1)	1-19	2302
MQWNSTTFHQTLQDPRVRGLYFPA (2)	1-24	2893
MQWNSTTFHQTLQDPRVRGLYFPAGG (3)	1-26	3007

Figure 32. Hep B Pre-S Region Fragment in vitro and in situ cleavage by cathepsin B. Hep B Pre-S Region Fragment was digested with cathepsin B in activating buffer in an overnight in vitro assay (top). The assay resulted in three peaks labeled 1) 1-22 fragment 2) 1-25 fragment and 3) full length fragment. After manual deposition of this peptide in four spots of the kidney cortex, the same fragments from the in vitro cleavage assay can be seen in the resulting spectra as well as one additional peak that could be the result of cleavage by another enzyme (bottom).

References

1. Bieck, P., and Potter, WZ, *Molecular biomarkers in drug development.* Drug Discovery Today, 2004. **9**: p. 976-983.

2. Loeb, W., *The measurement of renal injury.* Toxicol Pathol, 1998. **26**: p. 26-28.

3. Marrer E, D.F., *Promises of biomarkers in drug development--a reality check.* Chem Biol Drug Des., 2007. **69**(6): p. 381-94.

4. Unlü M, M.M., Minden JS., *Difference gel electrophoresis: a single gel method for detecting changes in protein extracts.* Electrophoresis, 1997. **18**(11): p. 2071-7.

5. Marouga R, D.S., Hawkins E., *The development of the DIGE system: 2D fluorescence difference gel analysis technology.* Anal Bioanal Chem. , 2005. **382**(3): p. 669-78.

6. Van den Bergh G, C.S., Cnops L, Vandesande F, Arckens L., *Fluorescent two-dimensional difference gel electrophoresis and mass spectrometry identify age-related protein expression differences for the primary visual cortex of kitten and adult cat.* J Neurochem., 2003. **85**(1): p. 193-205.

7. Link AJ, E.J., Schieltz DM, Carmack E, Mize GJ, Morris DR, Garvik BM, Yates JR 3rd., *Direct analysis of protein complexes using mass spectrometry.* Nat Biotechnol., 1999. **17**(7): p. 676-82.

8. Gygi SP, R.B., Gerber SA, Turecek F, Gelb MH, Aebersold R., *Quantitative analysis of complex protein mixtures using isotope-coded affinity tags.* Nat Biotechnol. , 1999. **17**(10): p. 994-9.

9. Gevaert K, I.F., Ghesquière B, Van Damme P, Lambrechts A, Vandekerckhove J., *Stable isotopic labeling in proteomics.* Proteomics. , 2008. **8**(23-24): p. 4873-85.

10. Hillenkamp, F., et al., *Matrix-assisted laser desorption/ionization mass spectrometry of biopolymers.* Anal Chem, 1991. **63**(24): p. 1193A-1203A.

11. Karas, M. and F. Hillenkamp, *Laser desorption ionization of proteins with molecular masses exceeding 10,000 daltons.* Anal Chem, 1988. **60**(20): p. 2299-301.

12. Chaurand, P. and R.M. Caprioli, *Direct profiling and imaging of peptides and proteins from mammalian cells and tissue sections by mass spectrometry.* Electrophoresis, 2002. **23**(18): p. 3125-35.

13. Schwartz, S.A., M.L. Reyzer, and R.M. Caprioli, *Direct tissue analysis using matrix-assisted laser desorption/ionization mass spectrometry: practical aspects of sample preparation.* J Mass Spectrom, 2003. **38**(7): p. 699-708.

14. Caprioli RM, F.T., and Gile J, *Molecular imaging of biological samples: localization of peptides and proteins using MALDI-TOF MS.* Analytical Chemistry, 1997. **69**(23): p. 4751-60.

15. Hillenkamp F, K.M., Beavis RC, Chait BT., *Matrix-assisted laser desorption/ionization mass spectrometry of biopolymers.* Anal Chem., 1991. **63**(24): p. 1193A-1203A.

16. Zenobi, R. and R. Knochenmuss, *Ion Formation in MALDI Mass Spectrometry.* Mass Spectrometry Reviews, 1998. **17**: p. 337-336.

17. Karas, M., M. Gluckmann, and J. Schafer, *Ionization in matrix-assisted laser desorption/ionization: singly charged molecular ions are the lucky survivors.* Journal of Mass Spectrometry, 2000. **35**(1): p. 1-12.

18. Wiley, W.C. and I.H. McLaren, *Time-of-Flight Mass Spectrometer with Improved Resolution.* The Review of Scientific Instruments, 1955. **26**(12): p. 1150-1157.

19. Cotter, R.J., *The new time-of-flight mass spectrometry.* Analytical Chemistry, 1999. **71**(13): p. 445A-451A.

20. Reyzer ML, a.C.R., *MALDI-MS-based imaging of small molecules and proteins in tissues.* Current Opinions in Chemical Biology, 2007. **11**(1): p. 29-35.

21. Khatib-Shahidi, S., et al., *Direct molecular analysis of whole-body animal tissue sections by imaging MALDI mass spectrometry.* Anal Chem, 2006. **78**(18): p. 6448-56.

22. Reyzer ML, H.Y., Ng K, Korfmacher WA, and Caprioli RM, *Direct analysis of drug candidates in tissue by matrix-assisted laser desorption/ionization mass spectrometry.* Journal of Mass Spectrometry. **38**(10): p. 1081-92.

23. Troendle FJ, R.C., and Yost RA, *Detection of pharmaceutical compounds in tissue by matrix-assisted laser desorption/ionization and laser desorption/chemical ionization tandem mass spectrometry with a quadrapole ion trap.* Journal of the American Society of Mass Spectrometry, 1999. **10**: p. 1315-1321.

24. Cornett, D., Frappier, SR, and Caprioli RM, *MALDI-FTICR imaging mass spectrometry of drugs and metabolites in tissue.* Anal Chem, 2008. **80**: p. 5648-53.

25. Stoekli M, C.P., Hallahan DE, and Caprioli RM, *Imaging mass spectrometry: a new technology for the analysis of protein expression in mammalian tissues.* Nature Medicine, 2001. **7**(4): p. 493-6.

26. Chaurand P, C.D., and Caprioli RM, *Molecular imaging of thin mammalian tissue sections by mass spectrometry.* Current Opinions in Chemical Biotechnology. **17**(4): p. 431-6.

27. Burnum KE, T.S., Mi D, Daikoku T, Dey SK, Caprioli RM., *Imaging mass spectrometry reveals unique protein profiles during embryo implantation.* Endocrinology, 2008. **149**: p. 3274-8.

28. Puolitaival SM, B.K., Cornett DS, Caprioli RM., *Solvent-free matrix dry-coating for MALDI imaging of phospholipids.* JMS, 2008. **19**: p. 882-6.

29. Schwartz, S.A., et al., *Protein profiling in brain tumors using mass spectrometry: feasibility of a new technique for the analysis of protein expression.* Clin Cancer Res, 2004. **10**(3): p. 981-7.

30. Schwartz, S.A., et al., *Proteomic-based prognosis of brain tumor patients using direct-tissue matrix-assisted laser desorption ionization mass spectrometry.* Cancer Res, 2005. **65**(17): p. 7674-81.

31. Xu, B.J., et al., *Proteomic patterns and prediction of glomerulosclerosis and its mechanisms.* J Am Soc Nephrol, 2005. **16**(10): p. 2967-75.

32. Herring, K., Oppenheimer, SR, and Caprioli RM, *Direct tissue analysis by matrix-assisted laser desorption ionization mass spectrometry: application to kidney biology.* Seminars in Nephrology, 2008. **27**: p. 597-608.

33. Meistermann H, N.J., Aerni HR, Cornett DS, Friedlein A, Erskine AR, Augustin A, De Vera Mudry MC, Ruepp S, Suter L, Langen H, Caprioli RM, Ducret A., *Biomarker discovery by imaging mass spectrometry: transthyretin is a biomarker for gentamicin-induced nephrotoxicity in rat.* Mol Cell Proteomics, 2006. **5**: p. 1876-86.

34. Lemaire R, D.A., Tabet JC, Day R, Salzet M, Fournier I., *Direct analysis and MALDI imaging of formalin-fixed, paraffin-embedded tissue sections.* J Proteome Research, 2007. **6**: p. 1295-305.

35. Groseclose MR, M.P., Chaurand P, Caprioli RM., *High-throughput proteomic analysis of formalin-fixed paraffin-embedded tissue microarrays using MALDI imaging mass spectrometry.* Proteomics, 2008. **8**: p. 3715-24.

36. Chaurand P, L.J., Lane KB, Mobley JA, Polosukhin VV, Wirth PS, Nanney LB, Caprioli RM., *Imaging mass spectrometry of intact proteins from alcohol-*

preserved tissue specimens: bypassing formalin fixation. J Proteome Research, 2008. **7**: p. 3543-55.

37. Srinivasan, M., D. Sedmak, and S. Jewell, *Effect of fixatives and tissue processing on the content and integrity of nucleic acids.* Am J Pathol, 2002. **161**(6): p. 1961-71.

38. Aerni, H.R., D.S. Cornett, and R.M. Caprioli, *Automated acoustic matrix deposition for MALDI sample preparation.* Anal Chem, 2006. **78**(3): p. 827-34.

39. Xu, B.J., et al., *Direct analysis of laser capture microdissected cells by MALDI mass spectrometry.* J Am Soc Mass Spectrom, 2002. **13**(11): p. 1292-7.

40. Cornett, D.S., et al., *A novel histology-directed strategy for MALDI-MS tissue profiling that improves throughput and cellular specificity in human breast cancer.* Mol Cell Proteomics, 2006. **5**(10): p. 1975-83.

41. Groseclose, M.R., et al., *Identification of proteins directly from tissue: in situ tryptic digestions coupled with imaging mass spectrometry.* J Mass Spectrom, 2007. **42**(2): p. 254-62.

42. Chaurand, P., et al., *Integrating histology and imaging mass spectrometry.* Anal Chem, 2004. **76**(4): p. 1145-55.

43. Norris, JL, Cornett DS, Mobley JA, Andersson M, Seeley EH, Chaurand P, Caprioli RM., *Processing MALDI mass spectra to aid biomarker discovery and improve mass spectral image quality.* International Journal of Mass Spectrometry, 2006. **260**(2-3): p. 212-221

44. Tusher, V.G., R. Tibshirani, and G. Chu, *Significance analysis of microarrays applied to the ionizing radiation response (vol 98, pg 5116, 2001).* Proceedings of the National Academy of Sciences of the United States of America, 2001. **98**(18): p. 10515-10515.

45. Naiman, D.Q., *Random data set generation to support microarray analysis.* Methods Enzymol, 2006. **411**: p. 312-25.

46. Hedenfalk, I., et al., *Gene-expression profiles in hereditary breast cancer.* N Engl J Med, 2001. **344**(8): p. 539-48.

47. Storey, J.D. and R. Tibshirani, *Statistical significance for genomewide studies.* Proc Natl Acad Sci U S A, 2003. **100**(16): p. 9440-5.

48. Hirosawa, M., et al., *MASCOT: multiple alignment system for protein sequences based on three-way dynamic programming.* Comput Appl Biosci, 1993. **9**(2): p. 161-7.

49. Link, A.J., et al., *Direct analysis of protein complexes using mass spectrometry.* Nat Biotechnol, 1999. **17**(7): p. 676-82.

50. Haas AL, M.K., Bright PM., *The inactivation of ubiquitin accounts for the inability to demonstrate ATP, ubiquitin-dependent proteolysis in liver extracts.* J Biological Chemistry, 1985. **260**: p. 4694-703.

51. Ali, B., *Gentamicin Nephrotoxicity in Humans and Animals: Some Recent Research.* Gen Pharmac, 1995. **26**: p. 1477-1487.

52. Olbricht, C.F., M and Gutjhar, E, *Alterations in lysosomal enzymes of the proximal tubule in gentamicin nephrotoxicity.* Kidney Inter, 1991. **39**: p. 639-646.

53. Benner, E., *Comparison of the renal toxicity of gentamicin and tobramycin in humans during clinical therapy of infections.* Clin Chem Acta, 1976. **69**: p. 85-91.

54. Kunin, C., Chesney, RW, Craig, WA, England AC, and DeAngelis C, *Enzymuria as a marker of renal injury and disease: studies of N-acetyl-beta-glucosaminidase in the general population and in patients with renal disease.* Pediatrics, 1978. **62**: p. 751-760.

55. Schentag JJ, P.M., Cerra FB., *Comparative nephrotoxicity of gentamicin and tobramycin: pharmacokinetic and clinical studies in 201 patients.* Antimicrob Agents Chemother, 1981. **19**: p. 859-866.

56. Gibey R, D.J., Alber D, Leconte des Floris R, Henry JC, *Predictive value of urinary N-acetyl-beta-D-glucosaminidase (NAG), alanine-aminopeptidase (AAP) and beta-2-microglobulin (beta 2M) in evaluating nephrotoxicity of gentamicin.* Clin Chem Acta, 1981. **116**: p. 25-34.

57. Kramer JA, P.S., Amin RP, Bertram TA, Car B, Cunningham M, Curtiss SW, Davis JW, Kind C, Lawton M, Naciff JM, Oreffo V, Roman RJ, Sistare FD, Stevens J, Thompson K, Vickers AE, Wild S, Afshari CA., *Overview on the application of transcription profiling using selected nephrotoxicants for toxicology assessment.* Evironmental Health Perspectives, 2004. **112**: p. 460-4.

58. Naidu, S., Lee, FT Jr., *Contrast nephrotoxicity: predictive value of urinary enzyme markers in a rat model.* Acad Radiol, 1994. **1**: p. 3-9.

59. Amin RP, V.A., Sistare F, Thompson KL, Roman RJ, Lawton M, Kramer J, Hamadeh HK, Collins J, Grissom S, Bennett L, Tucker CJ, Wild S, Kind C, Oreffo V, Davis JW 2nd, Curtiss S, Naciff JM, Cunningham M, Tennant R, Stevens J, Car B, Bertram TA, Afshari CA., *Identification of putative gene based markers of renal toxicity.* Environ Health Perspect., 2004. **112**: p. 465-479.

60. Davis, J.I., Goodsaid, FM, Bral, CM, Obert, LA, Mandakas G, Garner CE II, Collins ND, Smith RJ, and Rosenblum IY, *Quantitative gene expression analysis in a nonhuman primate model of antibiotic-induced nephrotoxicity.* Toxicol Applied Pharm, 2004. **200**: p. 16-26.

61. Fielden MR, E.B., Natsoulis G, Jarnagin K, Banas D, Kolaja KL., *A gene expression signature that predicts the future onset of drug-induced renal tubular toxicity.* Toxicol Pathol, 2005. **33**: p. 675-83.

62. Charlwood J, S.J., King N, Camilleri P, Lord P, Bugelski P, Atif U, *Proteomic analysis of rat kidney cortex following treatment with gentamicin.* J Proteome Res, 2002. **1**: p. 73-82.

63. Kennedy, S., *Proteomic profiling from human samples: the body fluid alternative.* Toxicol Letters, 2001. **120**: p. 379-384.

64. Kennedy, S., *The role of proteomics in toxicology: identification of biomarkers of toxicity by protein expression analysis.* Biomarkers, 2002. **7**: p. 1-22.

65. Thongboonkerd V, M.P., *Renal and urinary proteomics: current applications and challenges.* Proteomics, 2005. **5**: p. 1033-1042

66. Meistermann, H., et al., *Biomarker discovery by imaging mass spectrometry: transthyretin is a biomarker for gentamicin-induced nephrotoxicity in rat.* Mol Cell Proteomics, 2006. **5**(10): p. 1876-86.

67. Raab, W., *Nephrotoxcity of various aminoglycoside antibiotics, evaluated by renal enzyme excretion studies*, in *Current chemotherapy. Proceedings of the 10th International Congress of Chemotherapy*, W. Siegenthaler, and Luthy, R, Editor. 1978, American Society for Microbiology: Washington, DC. p. 938-939.

68. REED, M.D.V., MARY W.; STERN, ROBERT C.; CHENG, P. W.; POWELL, STEPHEN H.; BOAT, THOMAS F. , *Are Measurements of Urine Enzymes Useful during Aminoglycoside Therapy?. .* Pediatric Research, 1981. **15**: p. 1234-1239.

69. Schentag JJ, P.M., Cerra FB, Wels PB, Walczak P, and Buckley RJ, *Aminoglycoside nephrotoxicity in critically ill surgical patients.* J Surg Res, 1979. **26**: p. 270-279.

70. Bernstein, L., and Ingenbleek, Y, *Transthyretin: its response to malnutrition and stress injury-clinical usefulness and economic implications.* Clin Chem Lab Med, 2002. **40**: p. 1344-1348.

71. Ingenbleek, Y., and Young, V, *Transthyretin (prealbumin) in health and disease: nutritional implications.* Annu Rev Nutr, 1994. **14**: p. 495-533.

72. Sreedhara, R., Avram, M., Blanco, M., Batish, R., and Mittman, N, *Prealbumin is the best nutritional predictor of survival in hemodialysis and peritoneal dialysis.* Am J Kidney Dis, 1996. **28**: p. 937-942.

73. Zhang, Z., Bast, R. C., Yu, Y., Li, J., Sokoll, L. J., Rai, A. J., Rosenzweig, J. M., Cameron, B., Wang, Y. Y., Meng, X.-Y., Berchuck, A., Haaften-Day, C. v., Hacker, N. F., de Bruijn, H. W. A., van der Zee, A. G. J., Jacobs, I. J., Fung, E. T., and Chang, D. W, *Three biomarkers identified from serum proteomic analysis for the detection of early stage ovarian cancer.* Cancer Res, 2004. **64**: p. 5882-5890.

74. Orlando RA, R.K., Authier F, Yamazaki H, Posner BI, Bergeron JJ, Farquhar MG, *Megalin is an endocytic receptor for insulin.* J Am Soc Nephrol, 1998. **9**: p. 1759-66.

75. Sousa, M.M., Nordern, A. G. W., Jacobsen, C., Willnow, T. E., Christensen, E. I., Thakker, R. V., Verroust, P. J., Moestrup, S. K., and Saraiva, M. J, *Evidence for the role of megalin in renal uptake of transthyretin.* J Biol Chem, 2000. **275**: p. 38176-38181.

76. Moestrup, S.K., Cui, S., Vorum, H., Bregengard, C., Bjorn, S. E., Norris, K., Gliemann, J., and Christensen, E. I, *Evidence that epithelial glycoprotein 330/megalin mediates uptake of polybasic drugs.* J Clin Investig, 1995. **96**: p. 1404-1413.

77. Nagai, J., Tanaka, H., Nakanishi, N., Murakami, T., and Tanako, M, *Role of megalin in renal handling of aminoglycosides.* Am J Physiol, 2001. **281**: p. F337-F344.

78. Gburek J, V.P., Willnow TE, Fyfe JC, Nowacki W, Jacobsen C, Moestrup SK, Christensen EI, *Megalin and cubilin are endocytic receptors involved in renal clearance of hemoglobin.* J Am Soc Nephrol, 2002. **13**: p. 423-430.

79. Watanabe A, N.J., Adachi Y, Katsube T, Kitahara Y, Murakami T, Takano M., *Targeted prevention of renal accumulation and toxicity of gentamicin by aminoglycoside binding receptor antagonists.* J Control Release, 2004. **95**(423-33).

80. Boyer, P., *THE ATP SYNTHASE—A SPLENDID MOLECULAR MACHINE.* Annual Review of Biochemistry, 1997. **66**: p. 717-749.

81. Klune, W.a.H., JB, *Functional nephrotoxicity of gentamicin in the rat.* Toxicol App Pharmac, 1978. **45**: p. 163-175.

82. Simmons, C., Ronald TB, Humes HD, *Inhibitory effects of gentamicin on renal mitochondrial phosphorylation.* J Pharmac Exp Therap, 1980. **214**: p. 709-719.

83. Lan HY, M.W., Yang N, Meinhardt A, Nikolic-Paterson DJ, Ng YY, Bacher M, Atkins RC, Bucala R, *De novo renal expression of macrophage migration inhibitory factor during the development of rat crescentic glomerulonephritis.* Am J Pathol 1996. **149**: p. 1119-1127.

84. Lan HY, Y.N., Nikolic-Paterson DJ, Yu XQ, Mu W, Isbel NM, Metz CN, Bucala R, Atkins RC, *Expression of macrophage migration inhibitory factor in human glomerulonephritis.* Kidney Int 2000. **57**: p. 499-509.

85. Lan HY, Y.N., Brown FG, Isbel NM, Nikolic-Paterson DJ, Mu W, Metz CN, Bacher M, Atkins RC, Bucala R, *Macrophage migration inhibitory factor expression in human renal allograft rejection.* Transplantation 1998. **66**: p. 1465-1471.

86. Walker, P.a.S.S., *Evidence suggesting a role for hydroxyl radical in gentamicin-induced acute renal failure in rat.* J Clin Investig, 1988. **81**: p. 334-341.

87. Shah, S.a.W.P., *Reactive oxygen metabolites in toxic acute renal failure.* Renal Failure, 1992. **14**: p. 363-370.

88. Guder, W., and Hoffman W, *Clinical role of urinary low molecular weight proteins: their diagnostic and prognostic implications.* Scand J Clin Lab Invest Suppl. , 2008. **241**: p. 95-8.

89. Wysocki VH, T.G., Smith LL, Breci LA., *Mobile and localized protons: a framework for understanding peptide dissociation.* J Mass Spectrom., 2000. **35**(12): p. 1399-1406.

90. Gu C, T.G., Breci L, Wysocki VH., *Selective gas-phase cleavage at the peptide bond C-terminal to aspartic acid in fixed-charge derivatives of Asp-containing peptides.* Anal Chem., 2000. **72**(23): p. 5804-13.

91. Ciechanover, A., *Intracellular protein degradation: from a vague idea thru the lyososome and the ubiquitin-proteasome system and onto human diseases and drug targeting.* Cell Death and Differentiation, 2005. **12**: p. 1178-1190.

92. Etinger, J., and Goldberg AL, *A soluble ATP-dependent proteolytic system responsible for the degradation of abnormal proteins in reticulocytes.* PNAS, 1977. **74**: p. 54-58.

93. A Ciechanover, Y.H.A.H., *A heat-stable polypeptide component of an ATP-dependent proteolytic system from reticulocytes* Biochem. Biophsics. Res Common, 1978. **81**: p. 1100-1105.

94. Goldstein, G., *Isolation of bovine thymin, a polypeptide hormone of the thymus.* Nature, 1974. **247**: p. 11-14.

95. Goldstein, G.S., M Hammerling, U Schlesinger DH and Naiall HD and Boyse EA, *Isolation of a polypeptide that has lymphocyte-differentiating properties and is probably represented universally in living cells.* PNAS, 1975. **72**: p. 11-15.

96. Schlessinger DH, G.G.a.N.H., *The complete amino acid sequence of ubiquitin, and adenylate cyclase stimulating polypeptide probably universal in living cells.* Biochemistry, 1975. **14**: p. 2214-2218.

97. Low, T.a.G.A., *The chemistry and biology of thymosin: amino acid analysis of thymosin α1 and polypeptide B1.* J Biological Chemistry, 1979. **254**: p. 987-995.

98. Ciechanover, A.E.S.H.H.F.S.a.H.A., *Characterization of the heat stable polypeptide of the ATP-dependent proteolytic system from reticulocytes* J Biological Chemistry, 1980. **255**: p. 7525-7528.

99. Wilkinson KD, U.M.a.H.A., *Ubiquitin is the ATP-dependent proteolysis factor of rabbit reiculocytes.* J Biological Chemistry, 1980. **255**: p. 7529-7532.

100. Wilikinson, K.a.A.T., *Stimulation of ATP-dependent proteolysis requires ubiquitin with the COOH-terminal sequence Arg-Gly-Gly.* J Biological Chemistry, 1981. **256**: p. 9235-41.

101. Ciechanover, A.E.S.H.H.a.H.A., *'Covalent affinity' purification of ubiquitin-activating enzyme.* J Biological Chemistry, 1982. **257**: p. 2537-2542.

102. Hershko, A.H.H.E.S.a.C.A., *Components of ubiquitin-protein ligase system: resolution, affinity purification and role in protein breakdown.* J Biological Chemistry, 1983. **258**: p. 8206-8214.

103. Pickart, C., *Ubiquitin in chains.* Trends Biochem Sci, 2000. **25**(544-8).

104. Wehenkela, M., Jin Tae Hongb and Kyung Bo Kim, *Proteasome modulators: essential chemical genetic tools for understanding human diseases* Mol. BioSyst., 2008. **4**: p. 280-286.

105. Myung, J., K. B. Kim and C. M. Crews, *The ubiquitin-proteasome pathway and proteasome inhibitors.* Med. Res. Rev, 2001. **21**: p. 245–273.

106. Hershko, A., and A Ciechanover *THE UBIQUITIN SYSTEM.* Annu. Rev. Biochem, 1998. **67**: p. 425-479.

107. Muratani, M.T.W., *How the ubiquitin-proteasome system controls transcription.* Nat Rev Mol Cell Biol., 2003. **4**: p. 192-201.

108. Conaway, R.B.C.C.J., *Emerging roles of ubiquitin in transcription regulation.* Science, 2002. **296**: p. 1254-1258.

109. Hicke, L., *Protein regulation by monoubiquitin.* Nat Rev Mol Cell Biol. , 2001. **2**: p. 195-201.

110. Musil D, Z.D., Turk D , Engh RA , Mayr I, Huber R, Popovic T, Turk V, Towatari T, Katunuma N and Bode W *The refined 2.15 A X-ray crystal structure structure of human liver cathepsin B: the structural basis for its specificity.* The EMBO Journal, 1991. **10**(9): p. 2321-2330

111. Cavallo-Medved D, D.J., Linebaugh BE, Sameni M, Rudy D, Sloane BF, *Mutant K-ras regulates cathepsin B localization on the surface of human colorectal carcinoma cells.* Neoplasia, 2003. **5**: p. 507-519.

112. Collette J, B.J., Ahn K, Chapman RL, Godbold G, Yeyeodu S, Erickson AH., *Biosynthesis and alternate targeting of the lysosomal cysteine protease cathepsin L.* Int Rev Cytol, 2004. **241**: p. 1-51.

113. Roshy S, S.B., and Moin K, *Pericellular cathepsin B and malignant progression.* Cancer Metastasis Rev, 2003. **22**: p. 271-286.

114. Purdy, G., and Russell DG, *Ubiquitin Trafficking to the Lysosome: Keeping the House Tidy and Getting Rid of Unwanted Guests.* Autophagy, 2007. **3**: p. 399-401.

115. Gonçalves A, C.-J.E., Bertucci F, Audebert S, Toiron Y, Esterni B, Monville F, Tarpin C, Jacquemier J, Houvenaeghel G, Chabannon C, Extra JM, Viens P, Borg JP, Birnbaum D, *Protein profiling of human breast tumor cells identifies novel biomarkers associated with molecular subtypes.* Mol Cell Proteomics, 2008. **7**: p. 1420-33.

116. Baumgrass R, W.M., Price PA., *Identification of peptide fragments generated by digestion of bovine and human osteocalcin with the lysosomal proteinases cathepsin B, D, L, H, and S.* J Bone Miner Res, 1997: p. 447-55.

117. Saito A, K.J., Iino N, Cho K, Sato N, Yamazaki H, Oyama Y, Takeda T, Orlando RA, Shimizu F, Tabata Y, Gejyo F., *Bioengineered implantation of megalin-expressing cells: a potential intracorporeal therapeutic model for uremic toxin protein clearance in renal failure.* J Am Soc Nephrol, 2003. **14**: p. 2025-2032.

118. Moestrup SK, B.H., Fischer PB, Petersen CM, Verroust PJ, Sim RB, Christensen EI, Nexø E., *Megalin-mediated endocytosis of transcobalamin-vitamin-B12 complexes suggests a role of the receptor in vitamin-B12 homeostasis.* PNAS, 1996. **93**: p. 8612-8617.

119. Ohshita T, N.T., Towatari T, Katunuma N., *Effects of selective inhibition of cathepsin B and general inhibition of cysteine proteinases on lysosomal proteolysis in rat liver in vivo and in vitro.* Eur J Biochem, 1992. **209**: p. 223-31.

120. Illy C, Q.O., Wang J, Purisima E, Vernet T, Mort JS., *Role of the occluding loop in cathepsin B activity.* J Biological Chemistry, 1997. **272**: p. 1197-202.

121. Rawlings ND, M.F., Kok CY, Kong J, Barrett AJ., *MEROPS: the peptidase database.* Nucleic acid res, 2008. **36**: p. D329-D325. http://merops.sanger.ac.uk/index.htm.

122. Kominami E, T.T., Bando Y, and Katunuma N, *Distribution of Cathepsins B and H in Rat Tissues and Peripheral Blood Cells.* J Biochemistry, 1985. **98**: p. 87-93.

123. Mohamed MM, a.S.B., *Cysteine cathepsins: multifunctional enzymes in cancer.* Nat Rev Cancer, 2006. **6**: p. 764-775.

124. Cardozzo, T.a.P.M., *The SCF ubiquitin ligase: insights into a molecular machine.* Nat Rev Mol Cell Biol., 2004. **5**: p. 739-751.

125. Brooks, C., and Gu W, *p53 ubiquitination: Mdm2 and beyond.* Mol Cell 2006. **21**: p. 307-315.

126. Nakayama, K., and Nakayama, K, *Ubiquitin ligases: cell-cycle control and cancer.* Nat Rev Cancer, 2006. **6**: p. 369-381.

127. Dias, E., *unpublished work.* 2008, Vanderbilt University: Nashville.

128. Seeley, E., *unpublished work.* 2008, Vanderbilt University: Nashville.

129. Hardesty, W., *unpublished work.* 2008, Vanderbilt University: Nashville.

130. Oppenheimer, S., *A Molecular Assessment of Tumor Margins by MALDI Mass Spectrometry in Renal Carcinoma*, in *Chemistry*. 2007, Vanderbilt University: Nashville.

131. Hoeller, D., Hecker CM, and Dikic I, *Ubiquitin and ubiquitin-like proteins in cancer pathogenesis.* Nat Rev Cancer, 2006. **6**: p. 776-788.

132. Burnum, K., *Temporal and Spatial Analysis of Proteins and Phospholipids in Embryo Implantation by Imaging Mass Spectrometry*, in *Biochemistry*. 2008, Vanderbilt University: Nashville.

133. Chaurand P, F.S., DaGue BB, Xu BJ, Reyzer ML, Orgebin-Crist MC, Caprioli RM., *Profiling and imaging proteins in the mouse epididymis by imaging mass spectrometry.* Proteomics, 2003. **3**(11): p. 2221-39.

134. Nicholson B, M.J., Butt TR, Mattern MR., *Deubiquitinating enzymes as novel anticancer targets.* Future Oncol, 2007. **3**: p. 191-9.

135. Bushow SI, L.J., Wubbolts R, and Stoorbogel W, *Exosomes contain ubiquitinated proteins* Blood Cells, Molecules, and Diseases, 2005. **35**: p. 398-403.

136. Stahl S, R.Y., Asan E, Mothes W, Conzelmann E, Sickmann A, Felbor U, *Proteomic analysis of cathepsin B and L-deficient mouse brain lysosomes.* Biochimica et Biophysica Acta, 2007. **1774**: p. 1237-1246.

137. Katz-Jeffe MG, S.W., Gardner DK, *Analysis of protein expression (secretome) by human and mouse preimplantation embryos.* Ferility and Sterility, 2006. **86**: p. 678-685.

138. Ohe Y, I.K., Itoh Z, Tatemoto K., *Cultured leptomeningeal cells secrete cerebrospinal fluid proteins.* J Neurochem, 1996. **67**: p. 964-71.

139. Sandoval JA, H.D., Woodruff HA, Powell RL, Jay CL, Grosfeld JL, HickeyD RJ, Malkas LH, *Novel peptides secreted from human neuroblastoma: useful clinical tools?* J Pediatric Surgery, 2006. **41**: p. 245-251.

140. Sixt SU, B.M., Jennissen HP, and Peters J, *Extracellular proteasome in the human alveolar space: a new housekeeping enzyme?* Am J Physiol Lung Cell Mol Physiol, 2007. **292**: p. L1280-L1288.

141. Lippert TH, S.H., Schieferstein G, *Immunoreactive Ubiquitin in Human Seminal Plasma.* J Andrology, 1993. **14**: p. 130-131.

142. Akarsu E, P.I., Selcuk NY, Tombul HZ, Cetinkaya R, *Relation between serum ubiquitin levels and KT/V in chronic hemodialysis patients.* Nephron, 2001. **88**: p. 280-282.

143. Okadu M, M.S., Hirasawa Y, *Increase in plasma concentrations of ubiquitin in dialysis patients: possible involvement in beta 2-microglobulin amyloidosis.* Clin Chem Acta, 1993. **5**: p. 135-144.

144. Daino H, M.I., Takada K et al, *Induction of apoptosis by extracellular ubiquitin in human hematopoietic cells: possible involvement of STAT3 degradation by proteasome pathway in interleukin 6-dependent hematopoietic cells.* Blood, 2000. **95**: p. 2577-2585.

145. Akarsu E, P.I., Capoglu I, Deni O, Akcay G, Unuvar N, *Relationship between electroneurographic changes and serum ubiquitin levels in patients with type 2 diabetes.* Diabetes Care, 2001. **24**: p. 100-103.

146. Takagi M, Y.M., Toda G, Takadu K, Hirakawa T, Ohkawa K, *Serum ubiquitin levels in patients with alcoholic liver disease.* Alcohol Clin Exp Res, 1999. **23**: p. 76-80.

147. Asserman C, P.V., Delanoye A, Capron A, Auriault C, *A radioimmunoassay for the quantification of human ubiquitin in biological fluids: application to parasitic and allergic diseases.* J Immunol Methods, 1994. **173**: p. 93-101.

148. Baska KM, M.G., Feng D, Agca Y, Tengowski MW, Sutovsky M, Yi YJ, Sutovsky P, *Mechanism of extracellular ubiquitination in the mammalian epididymis.* J Cell Physiology, 2008. **215**: p. 684-96.

149. Lamerz J, S.H., Scapozza L, Crameri R, Schulz-Knappe P, Mohring T, Kellman M, Khamenia V, and Zucht HD, *Correlation-associated peptide networks of human cerebrospinal fluid.* Proteomics, 2005. **5**: p. 2789-2798.

150. Majetschak M, P.N., Hirsch T, *Targeting the monocytic system with extracellular ubiquitin.* Immunology and Cell Biology, 2006. **84**: p. 59-65.

151. Christensen, E.a.B.H., *Megalin and Cubulin: Multifunctional Endocytic Receptors.* Mol Cell Bio, 2002. **3**: p. 258-268.

152. Zheng G, B.D., Stamenkovic I, Strickland DK, Brown D, Andres G, McCluskey RT., *Organ distribution in rats of two members of the low-density lipoprotein receptor gene family, gp330 and LRP/alpha 2MR, and the receptor-associated protein (RAP).* J Histo Cytochem, 1994. **42**: p. 531-542.

153. Bernadotte F, H.R., Juhlin C, Mattsson R., *Expression of a cell surface antigen with potential Ca2+-sensor/receptor function in rat placenta and uterus.* J Reprod Immunol, 1989. **16**: p. 199-205.

154. Sahali D, M.N., Chatelet F, Laurent-Winter C, Citadelle D, Roux C, Ronco P, Verroust P., *Coexpression in humans by kidney and fetal envelopes of a 280 kDa-coated pit-restricted protein. Similarity with the murine target of teratogenic antibodies.* Am J Pathol. 1992 Jan;140(1):33-44, 1992. **140**: p. 33-44.

155. Argraves WS, M.C., *Immunolocalization of cubilin, megalin, apolipoprotein J, and apolipoprotein A-I in the uterus and oviduct.* Mol Reprod Dev, 2004. **69**: p. 419-427.

156. Christensen EI, V.P., *Megalin and cubilin, role in proximal tubule function and during development.* Pediatric Nephrol, 2002. **17**: p. 993-999.

157. Chun JT, W.L., Pasinetti GM, Finch CE, Zlokovic BV, *Glycoprotein 330/Megalin (LRP-2) Has Low Prevelance as mRNA and Protein in Brain Microvessels and Chroid Plexus.* Experimental Neurology, 1999. **157**: p. 194-201.

158. Nielsen R, C.P., Jacobsen C, Dom G, Lima WR, Jadot M, Willnow TE, Devuyst O, Christensen EI., *Endocytosis provides a major alternative pathway for*

lysosomal biogenesis in kidney proximal tubular cells. PNAS, 2007. **104**: p. 5407-12.

159. Lundstrom M, O.R., Saedi MS, Woodward L, Kurihara H, Farquhar MG., *Immunocytochemical and biochemical characterization of the Heymann nephritis antigenic complex in rat L2 yolk sac cells.* Am J Pathol, 1993. **143**: p. 1423-1435.

160. Orlando RA, F.M., *Identification of a cell line that expresses a cell surface and a soluble form of the gp330/receptor-associated protein (RAP) Heymann nephritis antigenic complex.* PNAS, 1993. **90**: p. 4082-4086.

161. Marino M, Z.G., Chiovato L, Pinchera A, Brown D, Andrews D, McCluskey RT, *Role of Megalin (gp330) in Transcytosis of Thyroglobulin by Thyroid Cells.* J Biol Chem, 1999. **275**: p. 7125-7137.

162. Buttle DJ, M.M., Knight CG, Barrett AJ., *CA074 methyl ester: a proinhibitor for intracellular cathepsin B.* Arch Biochem Biophys, 1992. **299**: p. 377-80.

163. Stachowiak K, T.M., Karpińska A, Sosnowska R, Wiczk W., *Fluorogenic peptide substrates for carboxydipeptidase activity of cathepsin B.* Acta Biochim Pol., 2004. **51**(1): p. 81-92.

164. Zhou Y, V.V., Brown RP, Zhang J, Rosenzweig BA, Thompson KL, Miller TJ, Bonventre JV, Goering PL., *Comparison of kidney injury molecule-1 and other nephrotoxicity biomarkers in urine and kidney following acute exposure to gentamicin, mercury, and chromium.* Toxicol Sci., 2008. **101**: p. 159-70.

165. Gibbs, A., *Comparison of the specificity and sensitivity of traditional methods for assessment of nephrotoxicity in the rat with metabonomic and proteomic methodologies.* J Appl Toxicol, 2005. **25**: p. 277-295.

166. Laurent G, C.M., Rollman B, Van Hoof F, Tulkens P., *Mechanism of aminoglycoside-induced lysosomal phospholipidosis: in vitro and in vivo studies with gentamicin and amikacin.* Biochem Pharmac, 1982. **31**: p. 3861-3870.

167. Ramsammy LS, J.C., Lane B, Kaloyanides GJ., *Effect of gentamicin on phospholipid metabolism in cultured rabbit proximal tubular cells.* Amer J Physiol, 1989. **356**: p. C204-213.

168. Abdel-Gayoum AA, A.B., Ghawarsha K, Bashir AA., *Plasma lipid profile in rats with gentamicin-induced nephrotoxicity.* Human and Exp Toxicol, 1993. **12**: p. 371-375.

169. Murphy RC, H.J., Barkley RM., *Imaging of lipid species by MALDI mass spectrometry.* J Lipid Res, 2008. **Dec 2**: p. Epub ahead of print.

170. Aronson NN, a.B.A., *The specificity of cathepsin B. Hydrolysis of glucagons at the C-terminus by a peptidylpeptidase mechanism.* Biochem J, 1978. **171**: p. 759-765.

171. Nagler D, S.A., Portaro F, Carmona E, Juliano L, Menard R, *Major increase in endopeptidase activity of human cathepsin B upon removal of occluding loop contacts.* Biochemistry, 1997. **36**: p. 12608-15.

172. Nixon, R., *A "protease activation cascade" in the pathogenesis of Alzheimer's disease.* Ann NY Acad Sci, 2000. **924**: p. 117-31.

173. Matrisian, C.L.-O.a.L., *Emerging roles of proteases in tumour suppression.* Nat Rev Cancer, 2007(7): p. 800-8.

174. Pohl J, D.S., Blaha I, Strop P, Kostka V, *Chromophoric and fluorophoric peptide substrates cleaved through the dipeptidyl carboxypeptidase activity of cathepsin B.* Anal Biochem, 1987. **95**: p. 228-35.

175. Chaurand P, L.J., Lane KB, Mobley JA, Polosukhin VV, Wirth PS, Nanney LB, Caprioli RM *Imaging Mass Spectrometry of Intact Proteins from Alcohol-Preserved Tissue Specimens: Bypassing Formalin Fixation.* J Proteome Research, 2008. **7**(8): p. 3543-3555.

176. Burnum KE. Transguch S, D.M., Daikoku T, Dey SK, Caprioli RM, *Imaging mass spectrometry reveals unique protein profiles during embryo implantation.* Endocrinology, 2008. **149**(7): p. 3274-8.

177. Puolitaival SM, B.K., Cornett DS, Caprioli RM, *Solvent-free matrix dry-coating for MALDI imaging of phospholipids.* J Am Soc Mass Spectrom, 2008. **19**(6): p. 882-6.

178. Andersson M, G.M., Deutch AY, Caprioli RM, *Imaging mass spectrometry of proteins and peptides: 3D volume reconstruction.* Nat Methods, 2008. **5**(1): p. 101-8.

179. Cornett DS, F.S., and Caprioli RM, *MALDI-FTICR imaging mass spectrometry of drugs and metabolites in tissue.* Anal Chem, 2008. **80**(14): p. 5648-53.

180. Reyzer ML, H.Y., Ng K, Korfmacher WA, and Caprioli RM, *Direct analysis of drug candidates in tissue by matrix-assisted laser desorption/ionization mass spectrometry.* Journal of Mass Spectrometry, 2003. **38**(10): p. 1081-92.